ADDIS ABABA UNIVERSITY

ADDIS ABABA INSTITUTE OF TECHNOLOGY

AFRICAN RAILWAY CENTER OF EXCELLENCE

OPTIMIZATION OF CONCRETE SLEEPERS SUBJECTED TO STATIC AND IMPACT LOADINGS

A Thesis in Railway Engineering (Civil Infrastructure)

By NDABAMENYE Theogene

July, 2019

Addis Ababa

A Thesis

Submitted in Partial Fulfillment of the Requirements for the Degree of Master of Science in Railway Engineering (Civil Infrastructure)

APPROVAL

The undersigned have examined the thesis entitled '**Optimization of concrete sleepers subjected to static and impact loadings**' presented by **NDABAMENYE Theogene**, a candidate for the degree of **Master of Science in Railway Engineering (Civil Infrastructure)** and hereby certify that it is worthy of acceptance.

Dr. Abrham Gebre		
Advisor	Signature	Date
Dr. Bedilu Habte		
Internal Examiner	Signature	Date
Dr. Esayas G/Yohannes		
External Examiner	Signature	Date
Mr. Zewdie Moges		
Chair person	Signature	Date

UNDERTAKING

I certify that research work titled "**Optimization of concrete sleepers subjected to static and impact loadings**" is my own work. The work has not been presented elsewhere for assessment. Where material has been used from other sources it has been properly acknowledged.

……

NDABAMENYE Theogene

Id No: GSR/5016/10

theogene.ndabamenye@aait.et.edu.et

ninitha2020@yahoo.com

ABSTRACT

Prestressed concrete sleepers (PCSs) play an essential role in the track's performance and safety responses. PCS's most important function is to transfer and distribute loading from the track's superstructure to ballast bed. Loadings on sleeper are static and impact. Impact loadings originating from wheel or rail abnormalities is one of the main causes of cracks on the PCS's thus the excessive railway track maintenance cost. Previously, the effect, behavior and optimization of different prestressed sleeper shape subjected to static and impact loadings and the effect of prestressing steel horizontal spacing on sleeper loading capacity, has not been well investigated. The objective of this research was to optimize concrete sleeper shape subjected to static and impact loadings. Finite element package, ANSYS 16 was used in PCSs to analyze the static and impact loading responses on sleepers. A three-dimensional solid element, SOLID 65 was used to model concrete part of the sleeper. To simulate the behavior of pre-stressing wires, truss elements, LINK180, were used to withstand the initial strain attributed to pre-stressing forces. Validation of FE results was done using existing experimental data with a comparison of force-deflection diagrams of the experimental and FEM results. It was found that the quality of FE results is good. Conclusions to this research revealed that irregular hexagon sleeper shapes were safe as far as static and impact loadings are concerned. The sleeper SVII3 (sleeper 40), was found to be the best geometrical sleeper shape in terms of sleeper safety and volume. Furthermore, the best geometrical sleeper shape has a 1.75% volume reduction compare to the existing sleeper (in Addis-Djibouti railway track). In terms of the best geometrical irregular shaped sleeper safety, upon application of impact loading, 60% of sleepers were safe as compared to 40% of trapezoidal sections. However, in the case of rectangular shaped sleepers, none was safe. Static analysis of all modelled sleepers showed that all the three shapes used, were safe. Horizontal prestressing wire spacing had no effect on the sleeper loading capacity and deformation. Recommendations from this research thus points out to irregular hexagonal shape sleepers are economical and safe. Therefore, sleeper model SVII3 that has an irregular hexagon shape is proposed for use on future extension of the line or in the construction of new lines in Ethiopia.

KEYWORDS: Prestressed concrete sleepers, static and impact loadings, sleeper shape, FEM, optimization.

ACKNOWLEDGMENTS

I would like to express my deepest appreciation to Dr. Abrham Gebre, my research advisor for his constant motivation, assistance and direction, advice, guidance, support, supervision and constructive suggestions he offered in this thesis work.

Special thanks to Wold Bank through African Railway Center of Excellence (ARCE) for all the given financial supports during my study of Master of Science program in Addis Ababa University.

Particularly, I would like to express my thanks to the Government of Rwanda through Rwanda Polytechnic (RP) with the Integrated Polytechnic Regional College (IPRC) Huye for granting my study leave for the whole two years.

Thanks to my colleagues: WANTONO Francis, Duncan MWANGI, BIZIMUNGU Gaspard, Ivan NYAKANA, Morris MUGYEMA and NTAKIYEMUNGU Mathieu for moral, social, academic support and spiritual support during my studies and my stay in Ethiopia, may God bless you for me.

Unlimited gratitude goes to my family, especially my wife MANIKUZWE Marthe and my son MUNEZERO HIRWA Ivan for the unlimited support, encouragements for being on my side.

Finally, I would like to thank Almighty God for helping me and being with me during my studies and my stay in Ethiopia.

Thank you all!

TABLE OF CONTENTS

ABSTRACT ..... **III**

ACKNOWLEDGMENTS ..... **IV**

TABLE OF CONTENTS ..... **V**

LIST OF TABLES ..... **VIII**

LIST OF FIGURES ..... **X**

LIST OF ABBREVIATIONS ..... **XIII**

LIST OF NOTATION AND DEFINITIONS ..... **XIV**

CHAPTER 1 INTRODUCTION **1**

1.1 Background 1

1.2 Statement of the Problem 3

1.3 Research objectives 3

1.3.1 Main Objectives 3

1.3.2 Specific objectives 3

1.4 Methodology 4

1.5 Scope and limitations of the Thesis 6

1.6 Organization of the Thesis 6

CHAPTER 2 LITERATURE REVIEW **7**

2.1 Railway track structure 7

2.1.1 Introduction 7

2.1.2 Track superstructure components 7

2.1.3 Track substructure components 9

2.2 Forces exerted on track 9

2.3 Concrete sleepers 12

2.3.1 Introduction 12

2.3.2 Prestressed concrete sleepers 12

2.4 Failure Mechanisms of PCSs 14

2.4.1 Rail Seat Abrasion (RSA) 15

2.4.2 Flexural Cracking (Center-Binding) 15
2.5 Sleeper shape 16
2.6 Design consideration of PCSs 16
2.6.1 Rail seat load 16
2.6.2 Ballast pressure 17
2.7 Modelling track behaviour 18
2.7.1 Beam on Elastic Foundation (BOEF) 18
2.7.2 Vehicle-track models 19
2.7.3 Discrete component models 19
2.8 Concrete sleeper modelling 20
2.9 Behaviour of PCSs 21
2.9.1 Static behaviour of PCSs 21
2.9.2 Impact behaviors of PCSs 21
2.10 Modelling of ballast layer in railway track analysis 25
2.10.1 Derivation of ballast layer stiffness by using pyramid model 25
CHAPTER 3 OPTIMIZATION FORMULATION AND FINITE ELEMENT MODELLING 27
3.1 OPTIMIZATION FORMULATION 27
3.1.1 Introduction 27
3.1.2 Structural optimization 28
3.1.3 Multiobjective optimization 28
3.1.4 Weighted sum method 28
3.2 Finite Element Modelling 30
3.2.1 Validation of the FEM 30
3.2.2 Geometric shape and dimensions of modelled sleeper 38
3.2.3 Prestressed concrete sleeper modelling 54
CHAPTER 4 ANALYSIS RESULTS AND DISCUSSION 61
4.1 Static and impact behaviour of prestressed concrete sleeper 61
4.1.1 Static analysis of prestressed concrete sleeper 61

4.1.2 Impact behavior of prestressed concrete sleepers 72
4.2 Selection of the best geometrical sleeper shape 79
4.2.1 Static and Impact results 79
4.2.2 The total volume of the selected sleeper 84
4.2.3 Selection of the best geometrical sleeper shape 85
4.3 Effect of prestressing wire spacing on prestressed concrete sleepers 87
CHAPTER 5 CONCLUSION AND RECOMMENDATION 92
5.1 Conclusion 92
5.2 Recommendation 93
REFERENCES 94
APPENDICES 102
APPENDIX A: SKETCH OF SLEEPER TYPE A9P 103
APPENDIX B: EXCEL SHEET USED TO DETERMINE THE EXISTING SLEEPER VOLUME AND SOFFIT AREA 104
APPENDIX C: EXCEL SHEET USED TO DETERMINE THE VOLUME AND SOFFIT AREA FOR THE SLEEPER TO MODEL. 106
APPENDIX D: SLEEPER BALLAST STIFFNESS 110
APPENDIX E: MAXIMUM NUMBER OF CYCLES 112
APPENDIX F: STATIC ANALYSIS RESULTS 113
APPENDIX G: EXPLICIT DYNAMICS RESULTS 117

LIST OF TABLES

Table 2-1 Impact load characteristic in the soft track with rail pad [47] 23
Table 2-2 Impact load characteristics in the hard track with rail pad [47] 23
Table 2-3 Recommended relationship for dynamic coefficient factors [9], [17], [52] 24
Table 2-4 Typical range of values of Es for selected soils [56] 26
Table 2-5 Ballast and sub-ballast properties [58] 26
Table 3-1 Concrete material properties [24], [63] 30
Table 3-2 Pre-stressing reinforcement material properties [24], [63] 30
Table 3-3 Force Vs deformation 37
Table 3-4 detailed sleeper shape and dimensions selections 48
Table 3-5 General parameters 51
Table 3-6 Material properties of concrete and prestressing steel 52
Table 3-7: maximum permissible stresses in concrete under working conditions as per AREMA [35] 53
Table 3-8: Maximum permissible stresses in concrete under working conditions as per AS 1085.14-2003 [39] 53
Table 3-9 Allowable value of controlled stress for stretching [69]. 53
Table 3-10 Impactor properties 58
Table 4-1: Results from Static simulations 66
Table 4-2 Bending stress for static results 71
Table 4-3 Results from Impact Simulations 77
Table 4-4 Bending stress from impact results 78
Table 4-5 Permissible stress according to AS 1085.14-2003 79
Table 4-6 Impact results for sleeper SII3 with both modified and non-modified impact mass 80
Table 4-7 Multiplication factor on impact results 81
Table 4-8 impact results according to the modified impact mass 81
Table 4-9 Ratio of permissible and bending stresses according to impact results 82
Table 4-10 Safety ranking per sleeper case 83
Table 4-11 Overall ranking for impact simulations 83
Table 4-12 Ratio of permissible and bending stress according to static results 83
Table 4-13 safety ranking and overall ranking as per static results 84

Table 4-14 Safety ranking according to both static and impact results 84
Table 4-15 Total volume of the selected sleepers and their ranking 85
Table 4-16 safety and total volume ranking 85
Table 4-17 Best geometrical sleeper shape selection..... 86
Table 4-18 Static results with a variation of wire spacing for sleeper SVII3. 88
Table B-1 Existing sleeper volume calculation 104
Table B-2 Existing sleeper soffit area calculation 105
Table C-1 Rectangular sections with or without different width at rail seat and center section..... 106
Table C-2 Rectangular sections with a varying width, from center section to end section. 106
Table C-3 Rectangular sections with wing sections 107
Table C-4 Trapezoid and Irregular hexagon sections with or without different width.. 108
Table C-5 Trapezoid and Irregular hexagon sections with a varying width 109
Table D-1: Selected sleeper ballast stiffness 110
Table E-1 Maximum number of cycles..... 112

LIST OF FIGURES

Figure 1-1 Methodology flow chart 5
Figure 2-1 Typical ballasted track system components [12]. 7
Figure 2-2 an illustration of uplift force occurrences [20] 10
Figure 2-3 Typical wheel load distribution into the track structure [13] 11
Figure 2-4 Stages of pre-tensioning [24] 12
Figure 2-5 Center-binding support and void configuration [25] 16
Figure 2-6 Distribution of load from single axle along track [25] 17
Figure 2-7 Beam on an elastic foundation [37] 18
Figure 2-8 Model of interaction between wheel and track [42]. 19
Figure 2-9 Impact forces at different drop height [47] 22
Figure 3-1 Test set-up used in the test done by Rikard, 2000 31
Figure 3-2 Static structural model with fixed support 31
Figure 3-3: The load-vertical displacement relation for the six tested half-sleepers [63].32
Figure 3-4 SOLID65 Three-dimensional Element [64] 33
Figure 3-5 LINK180 bar element displayed with local and global axis [64] 34
Figure 3-6 Concrete body and prestressing wire with four supports. 34
Figure 3-7 Meshed sleeper model 35
Figure 3-8 Applied load 35
Figure 3-9 Compressive stress-strain graph for 52 MPa concrete 36
Figure 3-10 Sleeper directional deformation 36
Figure 3-11 Force –deformation graph with FEM results in blue color and experimental results in red color. 37
Figure 3-12 Estimated distribution of load (D.F) [35] 40
Figure 3-13 Estimated distribution factor (D.F) [39] 40
Figure 3-14 60-kg rail [67] 41
Figure 3-15 Type II sleeper drawing (a) Elevation (b) Plan [68] 43
Figure 3-16 Rectangular sleeper sections (a) winged sections, (b) without wing sections 45
Figure 3-17 Trapezoid sleeper sections with a varying width 46
Figure 3-18 Trapezoid sleeper sections with different width at rail seat and center sections 46

Figure 3-19 Irregular hexagon sleeper sections with different width at rail seat and center sections 47
Figure 3-20 Irregular hexagon sleeper sections with a varying width 47
Figure 3-21: The compressive stress-strain diagram of concrete, fc' =60 Mpa 52
Figure 3-22 Sleeper geometry and symmetry region at centre for SIV2 (SL-28). 55
Figure 3-23 Hex dominant mesh method for SIV2 (SL-28) 56
Figure 3-24 Model geometry and symmetry region for sleeper SIII1 (SL-19) 58
Figure 3-25 Model meshing for SIII1 (SL-19) 59
Figure 4-1 Critical sleeper sections 61
Figure 4-2 total deformations in concrete and probe tool for sleeper SV1 62
Figure 4-3 Equivalent (von-mises) stress for SV1 (SL-33) 62
Figure 4-4 Shear stress for SV1 (SL-33) 63
Figure 4-5 Sleeper SV1 Total deformation 63
Figure 4-6 Sleeper SV1 (a) equivalent stress at top section at top section 64
Figure 4-7 Shear stress (in red) and maximum shear stress (in black) at top section 64
Figure 4-8 Sleeper SV1 equivalent stress at bottom section 65
Figure 4-9 Total deformation for SVII3 (SL-40) 73
Figure 4-10 Equivalent (von-mises) stress for SVII3 (SL-11) 74
Figure 4-11 Total deformation 74
Figure 4-12 Sleeper SVII-3 equivalent stress at top section 75
Figure 4-13 Sleeper SVII-3 equivalent stress at bottom section 75
Figure 4-14 Sleeper SVII-3 Shear stress (in black) and maximum shear (in red) stress at bottom section 76
Figure 4-15 Best geometrical sleeper shape 87
Figure 4-16 Total deformation for SVII3 sleeper with a variation of wire spacing 89
Figure 4-17 Equivalent stress at top of SVII3 sleeper with a variation of the wire spacing 89
Figure 4-18 Equivalent stress at bottom of SVII3 sleeper with a variation of the wire spacing 90
Figure A-1 Sketch of sleeper type A9P, Rikard (2000) 103
Figure F-1 Static results for sleeper SI7 (a) equivalent stress (b) shear stress 113
Figure F-2 Static results for sleeper SII3 (a) deformation (b) equivalent stress 114
Figure F-3 Static results for sleeper SIII8 (a) deformation (b) equivalent stress 115
Figure F-4 Static results for sleeper SIV4 (a) equivalent stress (b) shear stress 116

Figure G-1 Impact results for sleeper SIII8 (a) deformation (b) equivalent stress 117
Figure G-2 Impact results for sleeper SIV4 (a) deformation (b) equivalent stress..... 118
Figure G-3 Impact results for sleeper SVI2 (a) deformation (b) equivalent stress..... 119
Figure G-4 Impact results for sleeper SVIII2 (a) deformation (b) equivalent stress 120

LIST OF ABBREVIATIONS

Term	Meaning
AALRT	Addis Ababa Light Rail Transit
ARCE	African Railway Center of Excellence
AREA	American Railway Engineering association
AREMA	American Railway Engineering and Maintenance-of-Way Association
AS	Australian Standard
CAD	Computer Aided Design
ERC	Ethiopian Railway Corporation
FEA	Finite Element Analysis
FEM	Finite Element Method
FFU	Fiber-reinforced foamed Urethane
IPRC	Integrated Polytechnic Regional College
LRT	Light Rail Transit
LST	Livermore Software Technology
PC	Prestressed Concrete
PCSs	Prestressed Concrete Sleepers
RSD	Rail Seat Deterioration
RP	Rwanda Polytechnic
UK	United Kingdom (Great Britain and Northern Ireland)
USA	United State of America

LIST OF NOTATION AND DEFINITIONS

Notation	Definitions
μ_c	Concrete Poisson's ratio
μ_s	Steel Poisson's ratio
φ_c	Concrete Density
α_c	Concrete Thermal expansion
f_{plk}	Characteristic strength of steel
$f_c{}'$	Characteristic strength of concrete
$f_{ct}{}'$	Tensile Strength on concrete
A_{pw}	Prestressing wires cross section area
A_{1pw}	Area of one prestressing wire
F_p	Prestressing force
E_s	Steel Young's modulus
E_c	Concrete Young's modulus
B	Sleeper width
R	Rail seat load
DF	The sleeper distribution factor
$L-g$	Effective length
P_{ab}	Average ballast pressure
E	Young's modulus of rail
I	Moment of inertia of rail
w	Deflection of rail
a	Sleeper spacing
K	Foundation coefficient
L	characteristic length
V_d	Drop velocity

Notation	Definitions
g	Gravity acceleration
h	Drop height
D	Wheel diameter
V	Vehicle speed
L_s	The distance between sleepers
L_b	Sleeper width
h_b	Ballast layer depth
α_1	Stress distribution angle at top ballast layer
α_2	Stress distribution angle at middle ballast layer
α_3	Stress distribution angle at bottom ballast layer
L_e	Effective support length of half sleeper
h_1	The thickness of top ballast layer
h_2	The thickness of middle ballast layer
h_3	The thickness of bottom ballast layer
E_1	The elastic modulus for top ballast layer
E_2	The elastic modulus for middle ballast layer
E_3	The elastic modulus for bottom ballast layer
$\emptyset$	dynamic impact coefficient factor
k	track modulus
E_o	Secant modulus of elasticity at ultimate stress, f_o
f	Axial stress in the concrete specimen
f_o	Ultimate stress in compression
ε	Unit strain in concrete caused by the “f” stress
ε_o	Unit strain in concrete at ultimate stress, f_o

CHAPTER 1 INTRODUCTION

1.1 Background

Railway transportation is one of the best and safest long distance, heavy haul transportation systems for both passenger and freight transport across the world. Durable track components are critical to railway networks. Sleepers form an integral part of the railway superstructure track components that help in transmission of rail vertical loads to the substructure.

As reported by D. Li et al. [1], the most important functions of railway sleeper include the transfer and distribution of vertical loads from superstructure to foundation, restrain of lateral, longitudinal and vertical movement of rails thus further providing a cant to the rails to help proper rail-wheel development, receiving of load from the rail and distributing it over the supporting ballast and holding the fastening system to maintain proper track gauge.

Cracks in concrete sleepers are due to impact loading caused by wheel/rail interaction with or without wheel/rail irregularities. Kaewunruen and Remennikov [2], [3], [4] noted that impact loads appear in short duration but of very high magnitude wheel loads due to abnormalities on the wheels and or on the railhead surface.

In Sweden, Australia, North America and many other countries, non-destructive methods were applied to inspect railway sleepers. Visual inspection and Engineers judgments were then applied to decide sleepers' conditions. However, to prevent sleeper damages and improve track performance, more reliable and accurate experimental and numerical analysis was necessitated on concrete sleepers under different support conditions due to the insufficiency of visual inspection. As pointed out by Ferdous [5], the critical concrete sleeper problems are rail seat deterioration (RSD), longitudinal cracking, cracking due to impact loading and chemical attack.

In Ethiopia, prestressed concrete sleeper has been analyzed numerically and analytically by different researchers. Haftom G. Michel [6], focused on numerically analyzing PCSs with sleeper-ballast support conditions and the worst case have been identified. The analytical method and numerical method have been conducted by Desalegn Fisseha [7],

to analyse and optimize a PCS. The optimization has been done based on PCSs capacity by varying one shape dimensions of the existing sleeper, concrete grade, and tendon (wire) type and profile. Only static loading has been applied during the analysis. Bethel Lulu Gebeyeliu [8], conducted a capacity analysis of PCS considering both static and dynamic loads. The optimization was focused on increasing the capacity of existing sleeper design through the investigation of prestressing wire type, quantity, configuration, stress level and other material properties.

Optimization of PCS and impact loads due to wheel / rail interaction and / or irregularities were not considered by [6], only quasi-static wheel loading was used in numerical analysis. In addition to this, [7] did not consider impact loading in the design and only one trapezoidal cross section shape was considered and many other shapes like rectangular, hexagonal, or any other shape may be analyzed. Non-linear behaviour of PCS was not taken into account by [8], as well as possible crack condition. Bethel Lulu Gebeyeliu [8] recommended for future works to focus on producing an efficient and reliable transportation mean of transportation by upgrading the existing track structure and making them economical and durable.

In Iran, B70 prestressed concrete sleeper have been optimized by Sadeghi and Babaee [9] in 2006; considering different dimensions and pressure distribution beneath the sleeper. Comparison between B70 and the proposed sleeper were done with regard to the structural strength and the construction cost. In the analysis, only one cross section shape has been used, others cross section shape at both rail seat and center of sleeper were not considered. Only bending moment at both rail seat and center of sleeper were considered, the other mechanical behaviors such as displacements, stresses, strain and forces were overlooked in selection of the most effective sleeper as far as safety is concerned.

In Japan, the optimization of prestressed concrete sleeper has been conducted by Minoura et al. [10] using sensitivity analysis with different sleepers so as to determine the number and position of rebars, hence obtaining an optimized structural sleeper. The selected sleeper was analyzed and the results like dimensions, number of tendons were determined using the prestressed concrete design method.

Therefore, the sleeper shape optimization and wire horizontal placements formed the back bone of this study.

1.2 Statement of the Problem

Prestressed Concrete sleepers (PCSs) are a vital track superstructure but unfortunately previous studies have achieved little in examining the effect and behavior of different prestressed concrete sleeper shape subjected to both static and impact loading, and prestressing wire spacing on loading capacity of PCSs.

Previous Prestressed Concrete (PC) design has utilized the permissible stress principle taking into account only the static and quasi-static loads used in the design of PC sleepers, thus not tolerating the small sleeper cracks resulting due to large spikes from track loading. Theoretically, cracked sleepers must be replaced by new ones, that make the design conservative, and railway maintenance very costly. Hence, the research efforts are required to perform comprehensive studies of both static and impact loading conditions, and the impact resistance of the prestressed concrete sleepers [11]**.** The concrete sleeper not well designed, may raise consequences and create serious problems. Therefore, there is a need in investigating sleeper shape behavior under impact loading. A well-designed concrete sleeper may increase the track maintenance efficiency, thereby gaining rail capacity. This research focused on determination of static and impact responses of different concrete sleeper shapes, and their corresponding volume so as to identify the best geometrical sleeper shape.

1.3 Research objectives

1.3.1 Main Objectives

The main objective of this study is to numerically investigate the behavior of concrete sleeper and optimize sleeper shape subjected to static and impact loadings.

1.3.2 Specific objectives

1. To identify the geometry parameters and material properties for PCSs.
2. To analyze the effect of concrete sleeper geometrical shape under static and impact loadings.
3. To select the best geometrical sleeper shape based on sleeper safety and volume.
4. To investigate the effect of prestressing wire horizontal spacing in PCSs.

1.4 Methodology

The existing literature on related topics in the library, internet and reports, books, journals and other publications, research paper and sources available in electronic media were reviewed. The basic design parameters and input data were identified and conducted from Ethiopian Railway Corporation (ERC) as some input data; and from different foreign standards like AS1085.14, AREMA, Chinese Standard and other acknowledge publications used in the design of pre-stressed concrete sleeper. Generally, the following was followed in this research.

- Input parameters which are obtained from ERC, AREMA, Chinese standard, Australian Standard (AS) and other acknowledged publications.
- Three dimensional prestressed concrete sleeper models in ANSYS commercial software package.
- Static structural analysis was conducted to study the concrete sleeper response (stresses and deformations)
- Impact simulations were employed by conducting explicit dynamic analysis.

The detailed methodology was shown in figure 1-1

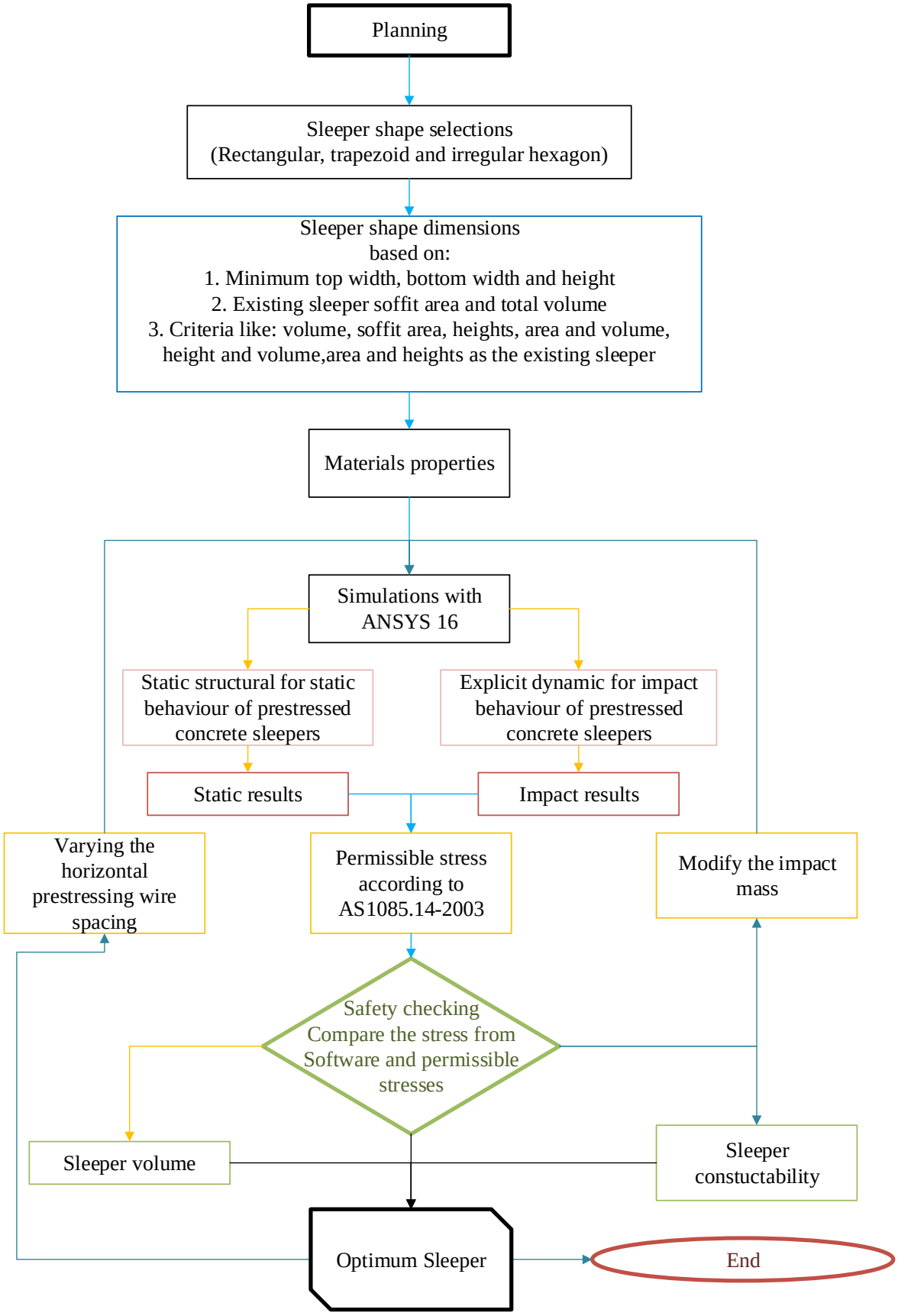

Figure 1-1 Methodology flow chart

1.5 Scope and limitations of the Thesis

Due to the time and budget constraint, the research was focused on optimizing a prestressed concrete sleeper under static and impact loadings with an investigation of prestressing wire horizontal spacing effect on PCSs behaviours. Both numerical static and impact simulations was developed as a suitable way to develop an understanding of the static and impact behaviour of PC sleepers. Only, the vertical wheel load was considered, the other track loadings were not considered. The effect of other track components, like rail pads, ballast bed and subgrade, and the experimental investigations were not conducted in this research. Therefore, only numerical simulations were conducted.

1.6 Organization of the Thesis

This Thesis is presented in 5 chapters as follows:

- Chapter 1 gives a brief background and the problem statement of the research. The objective, the scope, and the research methodology and limitations to the research are found in this chapter.
- Chapter 2 Literature Review the behaviour of prestressed concrete sleepers (PCSs) under both static and impact loading. Some numerical modelling using finite element packages of PCSs were also reported. Factors affection impact behaviour of a prestressed concrete sleeper is discussed in this chapter.
- Chapter 3 describes the optimization formulation and Finite Element Modelling as methodology used. The validation of FEM, geometrical shape and dimensions of sleepers are discussed in this chapter. Both static and impact simulations were also discussed.
- Chapter 4 presents the Analysis results and discussion: this part contains the numerical analysis result of studied sleepers. The behavior of concrete sleeper in times of deformation and stresses was presented and discussed.
- Chapter 5 Conclusion and recommendations. In the final chapter, the research thesis has been concluded and further research areas have been suggested.

CHAPTER 2 LITERATURE REVIEW

Before performing this research thesis, fundamental knowledge and previous work needs to be learned and reviewed. Existing knowledge and ideas are based on, to develop researches. Therefore, a literature review is extremely important to the research thesis.

2.1 Railway track structure

2.1.1 Introduction

A track is divided into two main parts; superstructure and substructure. Track superstructure consists of rails, rail pads, sleepers and fastening system [11]. Track substructure is composed of the ballast, sub-ballast and the subgrade (Figure 2-1).

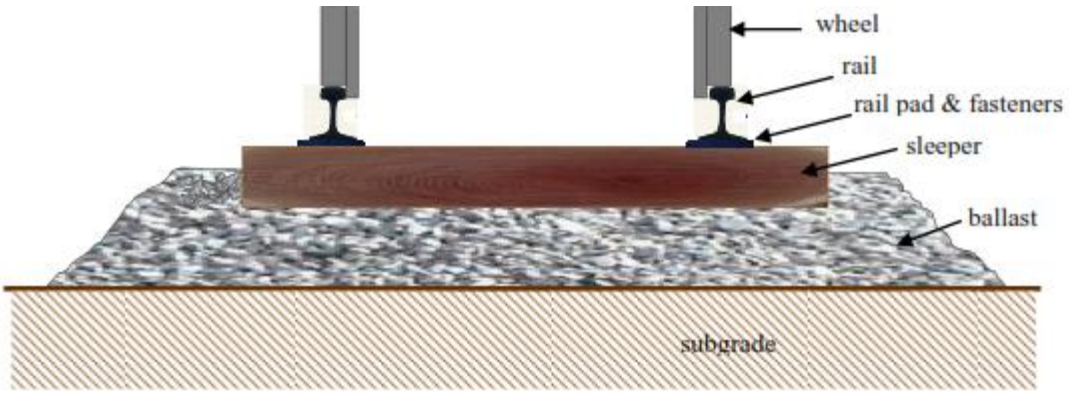

Figure 2-1 Typical ballasted track system components [12].

Rail track's main function is to support the vehicle and guide its steering; it should also carry the load of the train and distribute it over an area that is as large as possible.

2.1.2 Track superstructure components

Rails: These are the longitudinal steel members that are in contact with the train wheels, that directly guide the rolling stock wheels evenly and continuously [13]. The function of the rails is to guide the train and steer the wheel by conicity and the flange, provide a smooth-running surface and transfer wheel loads to the sleepers. Rails distribute the acceleration and braking forces by means of adhesion, acting as an electric conductor on electrified line and conduct signal currents to detect trains [13].

Rail pad: In a railway track with concrete sleepers, rail pads are placed between the steel rails and the sleepers. The rail pads protect the sleepers from wear and dynamic loads from the rails by absorbing shocks and vibrations, and they provide electrical insulation for track circuits. It also prevents abrasion of the rail and the sleeper, resists lateral movements of the rail, provide a conforming element between the steel rail and concrete surface and transfer the rail load to the sleeper [14]**,** [15]. Rail pads with a dynamic stiffness of between 100 and 200MN/m and static pad stiffness between 50 and 100MN/m are commonly used.

The fastening system: The fastening system is used to hold rails onto the sleepers, keep the track gauge and transversal inclinations of rails on sleeper's constant, attenuate and dampen vibrations caused by train traffic, secure the rail position and resist vertical, lateral, longitudinal, and overturning movements of the rails [15].

Sleeper: The word sleeper is defined as transverse beams laying on ballast and support. Sleepers may be made of wood, concrete and steel [3]. Concrete sleepers require resilient pads in the fastening system to provide resiliency and damping for the superstructure; they also allow high speeds and keep track gauge within satisfactory tolerances.

Functions of sleepers include distribution and transmission of forces to the ballast bed or slab track and restrain rail movement by anchorage of the superstructure in the ballast. Sleepers secure the track, dampen rail vibration and reduce the influence of sound and impact waves on the environment, hold the rails to proper gauge, distribute the load from the rails over large area of ballast underneath it or to the girders in case of bridge, provide elastic medium between the rails and ballast, maintain proper alignment of the track, support the rails at a proper level in straight tracks and proper super elevation on curves.

Sleepers also provide means to rectify track geometry during service life. They also add to the longitudinal and lateral stability of the permanent track on the whole and provide the general stability and the permanent way throughout, insulation of track for the electrified tracks for signaling and easy replacement of the rail fastenings without any traffic disturbances [16]**,** [17].

2.1.3 Track substructure components

Ballast: Seling and Waters [13] defined ballast as the selected crushed granular material placed as the top layer of the substructure in which the sleepers are embedded [13]. Important functions of ballast are to retain track position by resisting vertical (including uplift), lateral and longitudinal forces applied to the sleepers. Ballast reduces the sleeper bearing pressure for the underlying materials and provides large voids for storage of fouling material. Train vibrations and noise absorption are attenuated with a provision of some resiliency and energy absorption material such as ballast. Water falling onto the track is easily drained with the use of ballast materials [13], [16]. According to Tutumluer et al. [18], ballast is the most important component of the substructure because it is the only external constraint applied to the track in order to restrain it.

Subgrade: As reported by Fong [16], subgrade is the foundation for the track structure. Subgrade can be the existing natural or placed soil. Subgrade's main function is to provide a stable foundation for the track structure.

2.2 Forces exerted on track

Longitudinal forces

The forces in longitudinal direction act on the track structure, parallel to the rails. It is usually due to acceleration and braking of trains and thermal expansion or contraction of the rails [13].

Lateral force

The forces in lateral direction act on the track structure, parallel to the long axis of the sleepers, usually comes from the lateral wheel force due to the friction between the rail and wheel especially when a train goes around corners. It also comes from the buckling reaction force of the rail which is usually caused by a high longitudinal force in the rail [19].

Vertical force

The vertical forces act perpendicularly to the plane of the track and are due to the vertical wheel and uplift forces [13].

Vertical wheel force: The vertical wheel force is often simplified as a static component equal to the vertical weight divided by the number of wheels. On moving trains, combining this vertical wheel force with track geometry, vehicle dynamic and/or rail and wheel conditions can produce variety of dynamic forces [20].

Uplift force: figure 2-2 illustrates the reaction to the vertical load on a rail at the wheel contact points; the rail tends to lift up, moving away from the wheel. If this uplift force is not countered by the weight of the sleeper and rail together with ballast confinement (frictional force), the sleeper will lift momentarily. This movement causes a pumping action on the track bed which, if it sits on cohesive soils or fully fouled ballast, can cause track component to deteriorate.

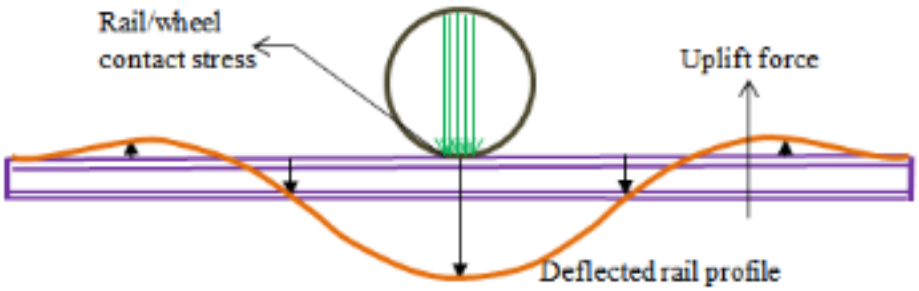

Figure 2-2 an illustration of uplift force occurrences [20]

The forces in vertical direction act on the track structure that can be subdivided into the downward and upward force. The upward force induced by the rail depends on the wheel loads and self-weight of the superstructure, whereas the downward force is a combination of a static load and a dynamic component and ends to lift up the rail and sleeper some distance away from the contact point (as shown in figure 2-3). The static component is the weight of the train while the dynamic component is a function of track conditions, train characteristics, operating conditions, train speed, and environmental conditions. According to [13], the magnitude of the dynamic component can be up to 2-3 times the static load as it causes an adverse effect to the track.

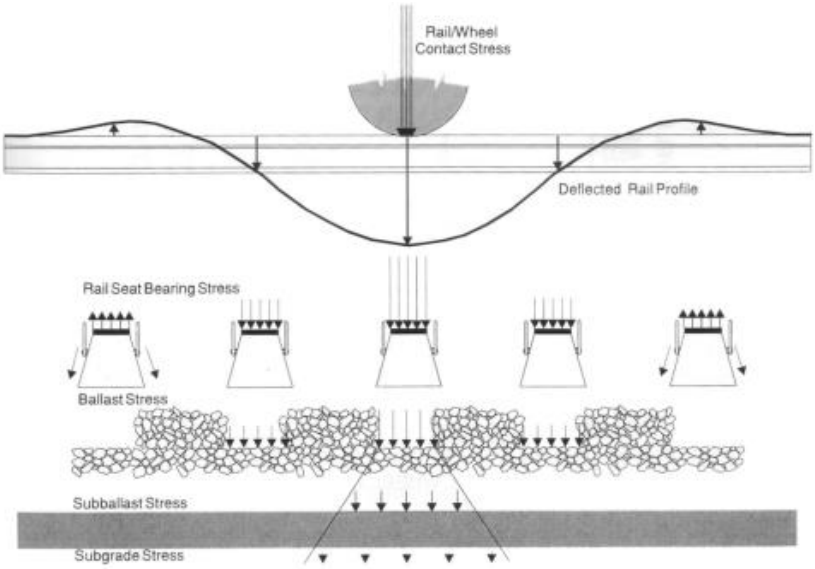

Figure 2-3 Typical wheel load distribution into the track structure [13]

Impact forces

Construction imperfections or transitions and damaged on rails and wheels generate impact forces causing track deterioration, noise and vibration. The main sources of impact forces are dipped rails, turnouts, crossings, insulated joints, and expansion gap between two segments, imperfect rail welds, rail corrugation, wheel-flats, wheel-shells and worn wheels [20]**,** [21].

The effect of train speed on impact force was studied by Leong and Murray 2008 [22], which led to a conclusion that doubling the speed of a train would increase impact forces by approximately 140%. This agrees with the conclusion of Priest and Powrie 2009 [23] that for constant sleeper support stiffness, the apparent dynamic loads increase with train speed.

As the wheel advances, the lifted sleeper is forced downwards causing an impact load, which increases with increasing train speed. This movement causes a pumping action in the ballast, which increases the ballast settlement by exerting a higher force on the ballast and causing “pumping up” of fouling materials from the underlying materials in the presence of water [13]. It is also noted that the impact load increases with the increase in track irregularity or differential settlement. The track geometry tends to degrade in an accelerating manner due to the increase of impact load would then lead to an increase in ballast settlement and lead to a larger gap underneath the sleeper [19].

2.3 Concrete sleepers

2.3.1 Introduction

Concrete sleepers are more generally used because they are not severely influenced by either atmosphere or climate. Furthermore, they provide anchorage for fastening system and limit longitudinal, parallel and vertical movement by implanting itself onto the substructure [4]. As pointed out by Li [24], concrete sleeper does not rot like wooden sleeper thus it has longer life. Less maintenance is needed on concrete sleepers as compared to other types of ties, hence it's worldwide use. Concrete sleeper advantages include longer life, cheaper construction, and low maintenance cost of fastening and smaller lateral displacement on account of large weight. According to Lutch [25], the most critical parameters needed to be captured are crushing and cracking of sleeper whereby maximum tensile stress and strain analysis is paramount.

2.3.2 Prestressed concrete sleepers

Generally, prestressed monoblock concrete sleepers are commonly used as reported by Hwang et al. [26], and Wolf [27] in many countries such as North America, Europe, Asia, etc. According to Li [24], pre-stressing technology has been developed for many years, and it is divided into pre-tension and post-tension. For railway sleepers, pre-tensioning is widely used where tension is applied to tendons before casting of concrete. The stages of pre-stressing include anchorage of tendons against the end abutments, placing jacks, applying tension to the tendons, casting of concrete; and cutting of tendon as shown in Figure 2-4 below.

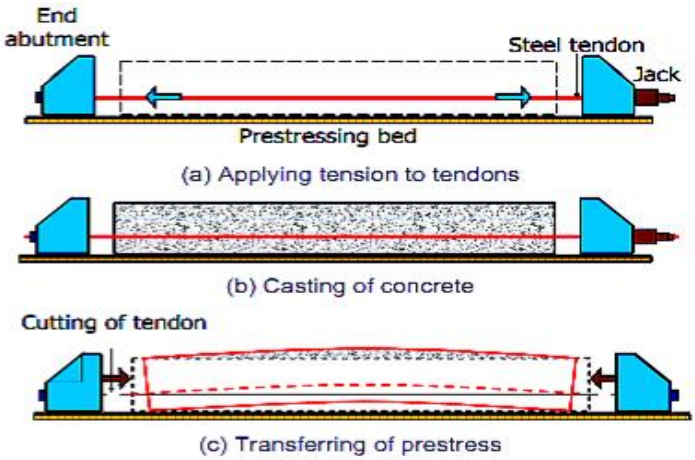

Figure 2-4 Stages of pre-tensioning [24]

2.3.2.1 Concrete

Concrete is strong in compression, but weak in tension. The concrete material behaves as elastic material and more as a plastic material. The ultimate strain for most structural concretes tends to be a constant value of approximately 0.0035, irrespective of the strength of the concrete [28].

Literatures provide empirical formula for numerical approximation of the stress-strain diagram. Among them, the value of E/E_o ratio is a fixed number regardless of the concrete strength. This ratio varies from 4 for normal concretes of 1,000 psi to about 1.3 for concretes of 100,000 psi [28]. According to Popovics [29], formulas with variable E/E_o ratios are more flexible because they can take the composition of the concrete into consideration directly or indirectly, such as through the concrete strength. Such a formula is the following:

$$f = E\varepsilon \frac{n-1}{(n-1)+(\frac{\varepsilon}{\varepsilon_0})} \qquad \textbf{2-1}$$

Considering that at $\varepsilon = \varepsilon_0$, $E = \frac{f}{f_0}\frac{n}{(n-1)}$

$$f = f_0 \frac{\varepsilon}{\varepsilon_0} \frac{n}{n-1+(\frac{\varepsilon}{\varepsilon_0})^n} \qquad \textbf{2-2}$$

Where;

E = initial modulus of elasticity (psi)

E_0 = secant modulus of elasticity at the f_0 ultimate stress, that is, $E_0 = \frac{f_0}{\varepsilon_0}$

f = axial stress in the concrete specimen (psi)

f_0 = ultimate stress; in compression (psi)

ε = unit strain in concrete caused by the f stress, and

ε_0 = unit strain in concrete at the f_o ultimate stress

Where; the n power can be expressed as an approximate function of the compressive strength of normal-weight concrete as follows:

$$n_{concrete} = 0.4 * 10^{-3} f_0 + 1.0 \quad \textbf{2-3}$$

The value of ε_0 can be estimated from one of the available formulas in the literature, and then this value used with Eq. 2-2.

$$\varepsilon_0 = k * 10^{-4} \sqrt[4]{f_0} \quad \textbf{2-4}$$

k = experimental parameter ($k = 2.12in^{1/2}Ib^{1/4}$) for normal-weight concrete).

2.3.2.2 Advantages and disadvantages of PCSs

Advantages of PCSs : According to Li [24], PCSs offers both technical and economic advantages. Sleeper cross-sections are kept fully in compression under design service loads to ensure that tension cracks do not occur. Prestressed concrete members possess improved resistance to shearing forces due to the effect of compressive prestress and are stiffer than reinforced concrete member of the same depth under working load. PCSs provide better load distribution to the underlying ballast bed, good longitudinal, lateral resistance, give stabiliity to the track and maintain track gauge in a good manner due to their heavy weight.

Disadvanatages of PCSs: As reported by Li [24], PCSs are difficult when handling, lying and maintaining due to their heavy weight. Transport, laying and maintenance of PCSs require superior technology which is not readily available in the manufacturing sectors of many developing countries.

2.4 Failure Mechanisms of PCSs

PCSs are expected to withstand high magnitude loads and hence have failure modes like other concrete elements and structures. Hwang et al. [26], noted that PC's often encounter concrete damage in the form of cracks. Those problems shorten the service life of PCSs hence some research have to be undertaken to fully understand their behaviors and their interaction with other components of track. As reported by Wolf [27], rail seat abrasion (RSA), flexural cracking from centre binding and rail fastener failure are the three primary failure mechanisms of PCSs. It should be noted that the Rail Seat Abrasion (RSA) is a common type of failure in North America, ranked as the most important problem.

2.4.1 Rail Seat Abrasion (RSA)

AREMA defines RSA as the gradual wearing away of the cement paste from the concrete, resulting in an uneven aggregate bearing surface beneath the tie pad [30]. However, RSA may degrade the concrete uniformly across the entire interface depending on the mechanism causing the deterioration. Factors contributing to RSA include: the presence of water, high tonnage, steep track grades, and especially track curves greater than two degrees [27].

According to Thun et al. [31], RSA was reported not to be a main problem except in North America. Consequently, cracking was noted to be the most important failure of PCSs in the world. However, other failures such as spalling, crashing, splitting and slippage between matrix and strands have been reported, especially under events like derailment. Cracking of PCSs is a crucial behaviour, not only in terms of mechanical and load carrying capacity, but also for durability and fatigue properties. Rail seat and mid-span static bending tests and impact tests have been used previously to identify cracking mechanism and propagation in concrete sleepers [32].To prevent RSA and prolong the tie life; manufacturers investigated different methods to protect concrete in the rail seat region. Lutch [25] focused on the application of abrasion resistant materials applied in the rail seat region and found out the following methods: epoxy or polyurethane materials applied to rail seat shortly after casting, cast-in-place plates or use abrasion resistant pad assembly.

2.4.2 Flexural Cracking (Center-Binding)

Negative moments affect cracking at the top centre location due to inadequacy of tie flexural capacity and have been observed on mainline tracks [31]. Concrete develops uniform ballast support in response to ballast consolidation negative moment that commonly occurs at the tie center. Over time, cyclic loading applied to the track causes ties to oscillate and deform vertically within the track structure.

Deformation produced results to pumping action which ultimately allows ballast to abrade the bottom of the tie and pulverize the ballast beneath the tie. The extent of ballast deterioration is unique to concrete ties when compared to that observed with wood ties resulting from the difference in the tie material strength and hardness [25]. Figure 2-5 below shows a flexural crack at the top center of tie.

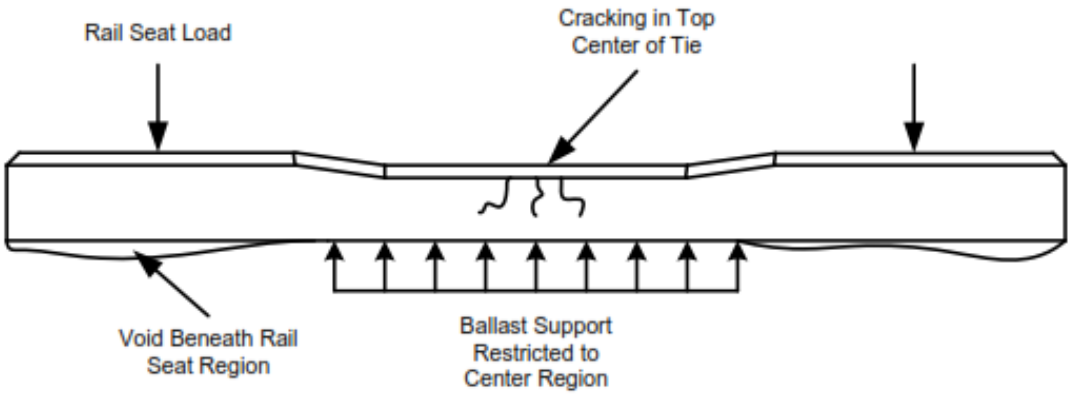

Figure 2-5 Center-binding support and void configuration [25]

2.5 Sleeper shape

As pointed out by Ungureanu and Maris [33], a Y-shape from Fiber-reinforced foamed urethane (FFU) was proposed to increase lateral stability. According to Koike et al. [34], different shapes have been used to numerically analyze the lateral resistance of sleepers though their research did not consider the loading capacity of those different shapes. The study done by Ungureanu and Maris [33], the effect of Y FFU composite sleepers truss gives lateral displacement stiffness of 2.5 times than classical FFU sleepers. Railways using Y FFU sleepers present viable and effective solutions for bridges, tunnels, railway switching and crossing and main line, a preferred solution of increasing the resistance to lateral displacement, recommended for use in high-speed lines, trams and metro lines, without danger of loss of track stability.

2.6 Design consideration of PCSs

An evaluation of loads being transferred to sleeper is essential in sleeper design. Required flexural capacity is determined based on the ballast support encountered during the life of the sleeper and the applied rail seat loads.

2.6.1 Rail seat load

As pointed out by Lutch [25], a single tie carries 45 to 55 percent of an axle load directly above it as a train moves along the track due to its rigidity. According to AREMA, typical track design with concrete ties utilizes tie spacing between 19 and 27 inches [35].

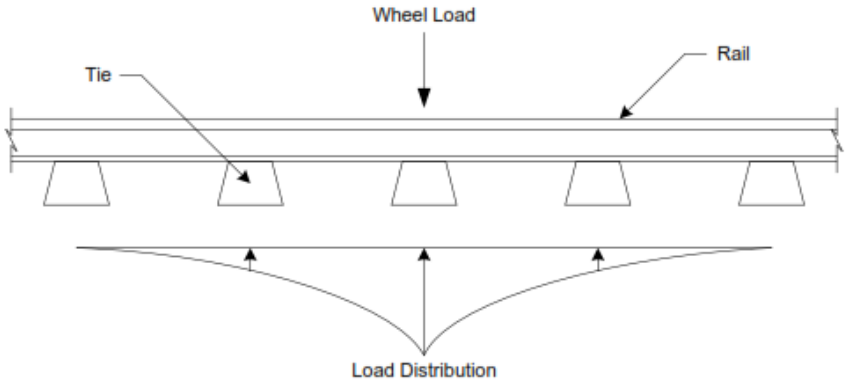

Figure 2-6 Distribution of load from single axle along track [25]

As reported by Jeffs and Tew [36], the rail seat load is dependent on a number of factors including: the weight of the rail, spacing of the sleepers, the stiffness of the sleeper, the track modulus per rail, the amount of play between the rail and the sleeper, and the amount of play between the sleeper and the ballast.

The rail seat force is the load on sleeper, it is the wheel-rail force transferred through rail and rail pad, as shown at upper part in Figure 2-6. The rail seat force causes the sleeper bending moment. So, the sleepers are deformed under the force on rail seat.

2.6.2 Ballast pressure

Ballast support is crucial to a tie's ability to support load. Therefore, once the wheel loads are applied to the tie, wheel loads must be transferred to the ground through the ballast and the sub-ballast material. In reality, pressure between the tie and ballast is not uniform across the bottom of the tie though an approximation is used to limit bearing pressures to prevent excessive depression of the track. Average ballast pressure is a function of the applied axle loads, impact factors, and the bearing area of the tie per AREMA [35]**.** It is also stated that while tie-to-ballast pressure is not uniformly distributed across or along the bottom of a cross tie, an approximate calculation can be made of "average" pressure at the bottom of the tie. The average pressure at the tie bottom is equal to axle load, modified by distribution and divided by the bearing area of the tie.

2.7 Modelling track behaviour

Track dynamic behaviour is classified into different categories, that representing the beam on elastic foundation, vehicle track model and discrete component models.

2.7.1 Beam on Elastic Foundation (BOEF)

The beams of two parallel rails, the track structure, and the sleepers, rail pads and ballast bed forming are a track structure are assumed as elastic foundation as presented in figure 2-7.

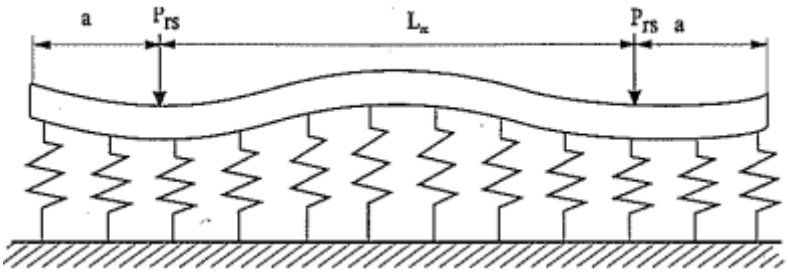

Figure 2-7 Beam on an elastic foundation [37]

As pointed out by Jian Bian [38], the length of the beam is considered as an infinite with a unit width and bending stiffness EI which is continuously supported by an elastic foundation with foundation modulus C and a single load is Q. Transformed to the railway structure, it is expressed by:

$$EI\frac{d^4w}{dx^4} + kw = p(x) \qquad \textbf{2-5}$$

Where:

E-Young's modulus of rail;
I-Moment of inertia of rail;
W-deflection of rail and
K-foundation coefficient and expressed by $\frac{C*A}{a}$ (A is the effective surface area of load exerted on the half sleeper, a is the sleeper spacing).
The necessary results are stress and bending moment in rails and they are based on vertical deflections [38]. The achieved result of vertical deflection is expressed by:

$$w(x) = \frac{QL^3}{8EI}\mu(x) = \frac{Q}{2EI}\mu(x) \quad \textbf{2-6}$$

Where L-so-called characteristic length determined by: $= (\frac{4EI}{k})^{0.25}$;

$$\mu(x) = e^{-x/L} * [\cos(x/L) + \sin(x/L) \quad \textbf{2-7}$$

According to the equations above, the load under the rail can be expressed by equation 2.8, which is transformed according to the Australian standard of concrete sleeper [39].

$$Q(x) = \frac{Qa}{2I}\mu(x) \quad \textbf{2-8}$$

2.7.2 Vehicle-track models

The studies on vehicle/track interaction have been performed and the historical background of modelling of railway vehicle/track interaction has been reviewed by Knothe & Grassie [40], and Timoshenko [41]**.** Studies on both static and dynamic stress in rail caused by vehicle/track interaction have been done by [40]**,** [41]. Xie and Iwnicki [42]**,** developed a model based of wheel-rail system assuming the rail as a beam, the rail pads and ballast as springs and dampers, and the sleepers locate between those equivalent springs and dampers as shown in figure 2-8 below.

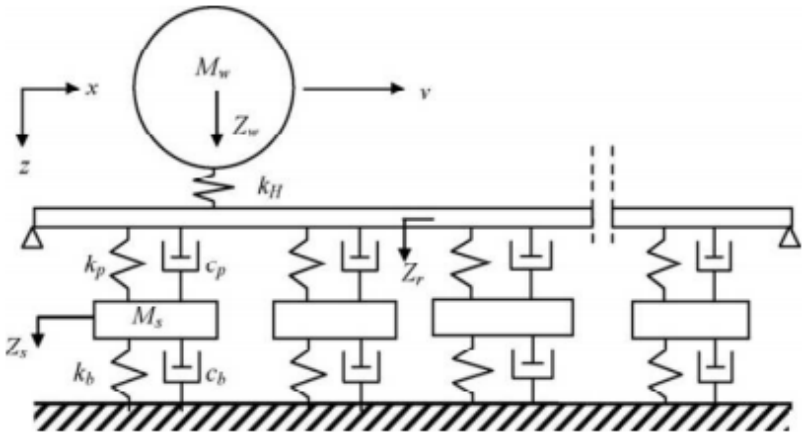

Figure 2-8 Model of interaction between wheel and track [42].

2.7.3 Discrete component models

The simulations are based on relevant models and mainly used to analyze the dynamic forces in track structures. The principle function of a railway track dynamic analysis model is to couple the components of the vehicle and track structure to each other so that

their complex interaction is properly represented when determining the defect of traffic load on stresses, strains and deformations in the components of the railway system. There have been several benchmarking exercises in the past that compared the results of various computer models of railway track [43], [44]. In each of these benchmarking exercises, results for comparative analysis when provided with a set of rigorously stipulated parameters were provided by the participants. A benchmark test which allows the railway track engineers to see whether the calculations of one model of track dynamic behaviour agreed with the calculations of others with the accurate inputs was described by [45].

2.8 Concrete sleeper modelling

Numerical modelling using finite element package was employed by researchers includes ANSYS, ABUQUS, LS-DYNA, etc. Remennikov and Kaewunruen [46] investigated the dynamic responses of railway concrete sleeper using experimental and numerical studies in the University of Wollongong. It was found that the static testing procedure could not test the impact behaviour of railway concrete sleeper. In addition, the ultimate capacities of concrete sleepers under static and impact loads have been conducted by Kaewunruen and Remennikov [4]. Finite element model using ANSYS was used for static analysis which was later extended to the use of LS-DYNA for impact analysis, to predict impact responses. For impact resistance, the sleeper is most likely to split due to lack of bonding between prestressing wires and concrete under dynamic circumstances [2], [47].

The performance of prestressed concrete sleeper under impact loading with holes of varying size was investigated by Hong et al. [48] using ABUQUS. The results of load-deflection relationship, von misses stress distribution and crack propagation was presented and one shape has been used in the analysis. Behaviour of different PCS shape was not considered. LS-DYNA was also used by Taherinezhad et al., Kaewunruen and Remennikov [49], [50] to investigate the impact responses and load capacity of prestressed concrete sleeper respectively. The effect of bottom wear, prestressing force and rebar corrosion on the loading capacity of the PC sleeper were evaluated quantitatively even in an environment where the impact force act on PC sleepers for both static and dynamic analysis.

2.9 Behaviour of PCSs

2.9.1 Static behaviour of PCSs

Static behaviour of railway concrete sleeper can be depicted by their hogging and sagging behaviour, usually presented by either numerical or experimental analysis. Bending mode of failure could be observed for hogging behaviour while sagging behaviour causes sudden failure. Within static behaviour, the combining major shear diagonal cracks and some bending cracks were detected in previous analysis. Sagging and hogging behaviors and cracks are always due to flexures.

2.9.2 Impact behaviors of PCSs

2.9.2.1 Impact loading

Railway track suffers from impact loads caused by the wheel-rail interactions associated with abnormalities in the wheels or rails [4], [51]. As reported by Leong and Murray [22], impact forces could be up to four to six times of the wheel loads. The magnitude of impact loads on rail seat of concrete sleeper exceeds the static wheel load and it is not only related to the train speed but also depend on causes of such loads in times of wheel tread irregularities [3]. The range of impact was reported to be from 100 to 750 KN with duration of 1 to 12 ms having a frequency of 2000Hz [50].

2.9.2.2 Impact behaviour of railway concrete sleepers

The impact behaviour of railway concrete sleeper is presented by the relationship between impact force and time from either numerical or experimental results. However, the falling mass, drop height and falling velocity have to be specified accordingly. Drop height, that is directly associated with the drop velocity was reported to play a vital role on the magnitude of impact load. The ballast support affects exclusively the contact pressures between sleeper and ballast and the ballast strength does not contribute much to increase the system contact stiffness so that the contact forces are slightly influenced [46], [47].

2.9.2.3 Factor affecting impact load

2.9.2.3.1 Drop height and or drop velocity

The higher the drop height the higher the impact load and the higher the drop velocity the higher the impact load. Kaewnruen [47] established an equation relating to both drop velocity and drop velocity.

$$0.98 * V_d = \sqrt{2gh} \qquad \textbf{2-9}$$

Where V_d = the drop velocity, g = gravity acceleration and h = drop height.

The low impact velocity is defined as the model having a drop velocity less than 100 m/s. In the research done by Kaewnruen [47], drop heights from 0.1 m to 0.8 m have been used as far as experiments are concerned. Numerically, the corresponding velocity have been computed and used. In his thesis [47], sensitivity analysis has been made to see how the drop height and drop velocity affect the impact load.

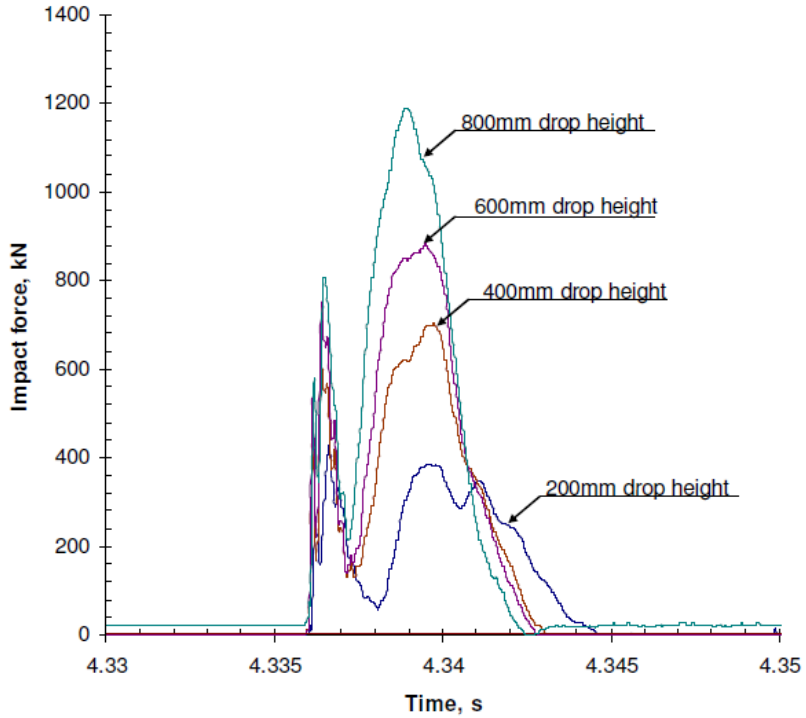

Figure 2-9 Impact forces at different drop height [47]

2.9.2.3.2 Ballast elasticity

The contact forces increase dramatically during the low range whilst the effect of ballast elastically becomes insignificantly when the stiffness is large. It was discovered that the ballast stiffness has little effect on the impact responses in terms of bending curvatures of railway concrete sleeper [47].

2.9.2.3.3 Rail pads

The rail pads tend to reduce the impact force from the rail foot and help attenuate the flexural responses in prestressed concrete sleeper. The impact reduction is calculated from the difference between the contact impact force at rail interface and the load burden that is distributed to rail seat of the sleeper [47].

2.9.2.3.4 The type of railway track

According to the results from [47], soft track and hard track were considered. The results showed that the impact load for hard track is greater than the impact load produced when the soft track is considered, see table 2-1 and 2-2.

Table 2-1 Impact load characteristic in the soft track with rail pad [47]

Softening media	Drop height			
	0.2 m		0.4 m	
	Impact characteristics		Impact characteristics	
	Magnitude, kN	Durations, ms	Magnitude, kN	Durations, ms
Direct contact	426	7	700	7
1 mm Neoprene	362	9	611	8
3 mm Neoprene	327	9	466	9
5 mm Neoprene	300	11	419	10

Table 2-2 Impact load characteristics in the hard track with rail pad [47]

Softening media	Drop height			
	0.2 m		0.4 m	
	Impact characteristics		Impact characteristics	
	Magnitude, kN	Durations, ms	Magnitude, kN	Durations, ms
Direct contact	441	8	761	6.5
1 mm Neoprene	429	8.5	622	8
3 mm Neoprene	386	9	563	8.5
5 mm Neoprene	313	11	363	10

2.9.2.3.5 Use of softening media (neoprene)

The experiments shown in his thesis [47], the thickness of this layer have been varied and the results showed that, when its thickness increases, the impact load decreases as shown in table 2-1 & 2-2.

2.9.2.4 Dynamic coefficient factor

As reported by Sadeghi and Barati [52]; the dynamic impact factor is a corrective factor for compensating the dynamic as well as impact effects of wheel load resulted from wheel and rail irregularities. According to Sadeghi and Babaee [9], in the current practices wheel load is static, considering a dynamic coefficient factor. Researchers all over the world have recommended several formulae and values for the calculation of the dynamic coefficient. Table 2-3 presents a summary of the main recommendations for the dynamic coefficient factors.

Table 2-3 Recommended relationship for dynamic coefficient factors [9], [17], [52]

Recommender	Relation
AREMA	$\phi = 1 + 5.21\frac{V}{D}$
DB	$\phi = 1 + \frac{V^2}{30000}$ for $V \leq 100\ km/hr$ $\phi = 1 + \frac{4.5V^2}{10^5} - \frac{1.5V^3}{10^7}$ for $V > 100\ km/hhr$
India	$\phi = 1 + \frac{V}{58.14k^{0.5}}$
South Africa	$\phi = 1 + 4.92\frac{V}{D}$ for narrow gauge
CA	$\phi = 1 + \frac{19.65V}{Dk^{0.5}}$
WMMTA	$\phi = (1 + 3.86 * 10^{-7}V^2)^{0.67}$
SADEGHI	$\phi = 1.098 + 8 * 10^{-4}V + 10^{-6}V^2$
Parameters are defined in the nomenclature list.	

Where,

ϕ	dynamic coefficient factor
V	velocity (km/h)
D	wheel diameter (mm)
k	track modulus (MPa)

2.10 Modelling of ballast layer in railway track analysis

According to Jabbar and Seyed [53], the ballast layer is to be considered as mass spring model under the sleeper in order to evaluate the effect on the railway track analysis. Therefore, many models are using the dynamic analysis of railway structures. Three categories are considered under the rail as lumped masses, beam on condition foundation and beam on elastic discrete supports.

2.10.1 Derivation of ballast layer stiffness by using pyramid model

The stiffness of a ballast layer under the sleepers can be measured using the pyramid model [54]. Ballast can be divided into three layers and then the stiffness of each layer can be derived based on the developed pyramid model.

2.10.1.1 Derived stiffness at the top of ballast layer

The assumption made is that there is no overlap between layers and one of the three layers is the top ballast layer. The corresponding layer stiffness is calculated as follows:

$$K_1 = \frac{2E_1(L_e - L_b)\tan(\alpha_1)}{\ln[\frac{L_e}{L_b} * \frac{L_b + 2h_1\tan(\alpha_1)}{L_e + 2h_1\tan(\alpha_1)}]} \quad \textbf{2-10}$$

2.10.1.2 Derived stiffness at the middle layer of ballast layer

The ballast layer corresponding stiffness to the middle layer is given in equation 2.11 as follows:

$$K_2 = \frac{2E_2(L_e - L_b)\tan(\alpha_2)}{\ln[(\frac{L_e + 2h_1\tan(\alpha_1)}{L_b + 2h_1\tan(\alpha_1)}) * (\frac{L_b + 2h_1\tan(\alpha_1) + 2h_2\tan(\alpha_2)}{L_e + 2h_1\tan(\alpha_1) + 2h_2\tan(\alpha_2)})]} \quad \textbf{2-11}$$

2.10.1.3 Derived stiffness at the bottom layer of ballast layer

The ballast layer corresponding stiffness to the bottom layer is given in equation 2.12 as follows:

$$K_3 = \frac{2E_3(L_e - L_b)\tan(\alpha_3)}{\ln[(\frac{L_e + 2h_1\tan(\alpha_1) + 2h_2\tan(\alpha_2)}{L_b + 2h_1\tan(\alpha_1) + 2h_2\tan(\alpha_2)}) * (\frac{L_b + 2h_1\tan(\alpha_1) + 2h_2\tan(\alpha_2) + 2h_3\tan(\alpha_3)}{L_e + 2h_1\tan(\alpha_1) + 2h_2\tan(\alpha_2) + 2h_3\tan(\alpha_3)})]} \quad \textbf{2-12}$$

The equation 2-10 to 2-12 present the stiffness derived by authors based pyramid model for each ballast layer without overlap. L_e and L_b are the effective support length of half

sleeper, and the sleeper width, respectively; h_1, h_2 and h_3 are the thickness of the top, middle and bottom ballast layers, respectively. E_1, E_2 and E_3 are the elastic moduli for the top, middle and bottom ballast layers, respectively; α_1, α_2 and α_3 are stress distribution angles at top, middle and bottom ballast layers. The ballast layer distribution angles could range from 25 to 37 degrees with an increase in the ballast layer depth [55]. The values of different soils elastic moduli including the ballast have been reviewed by Bowles [56] as shown in table 2-4.

Table 2-4 Typical range of values of Es for selected soils [56]

Type of soil	Es (MN/m2) or (Mpa)
Very soft clay	0.3-3
Soft clay	2-4
Medium clay	4.5-9
Hard clay	7-20
Sandy clay	30-42.5
Glacial till	10-16
Loess	6-15
Silt	2-20
Silty sand	5-20
Loose sand	10-25
Dense sand	50-100
Loose and gravel	50-140
Dense sand and gravel	80-200
shale	140-1,400
Ballast	**200-280** [55] **105-245** [57]

As reported by James Alan [58], the young's modulus, unit weight and internal angle of friction for ballast and sub-ballast are shown in table 2-5.

Table 2-5 Ballast and sub-ballast properties [58]

Ballast material	Young's modulus (Mpa)	Unit weight (KN/m3)	Internal angle of friction (^{0})
Ballast	200	20	50
Sub-ballast	150	18.5	40

CHAPTER 3 OPTIMIZATION FORMULATION AND FINITE ELEMENT MODELLING

3.1 OPTIMIZATION FORMULATION

3.1.1 Introduction

Optimization is defined as the selection of the best element which can be cost, profit, quality, safety or environment impact; from some set of available alternatives. It consists of maximization or minimization a real function and can include a wide range of problems with the aim of searching for certain optimality. According to [59], optimization can mean many different things. However, mathematically speaking, it is possible to write an optimization problem in the generic form:

$$\text{Maximize / minimize } f_i(x), i = 1,2,....,M \quad \textbf{3-1}$$

$$\text{Subjected } \begin{matrix} \phi_j(x) \le 0,\ j = 1,2,....,M \\ \vartheta_k(x) = 0, k = 1,2,....,M \end{matrix} \quad \textbf{3-2}$$

Where, $f_i(x)$, $\phi_i(x)$ and $\vartheta_i(x)$ are functions of the design vector

$$x = (x_1, x_2, ..., x_n)^T \quad \textbf{3-3}$$

The components x_i of x are called design or decision variables, and they can be real continuous, discrete or a mixture of these two. The functions $f_i(x), i = 1,2,\dots,M$ are called the objective functions, and in case of M=1, there is only a single objective.

The objective functions can be either linear or non-linear. The equalities for $\vartheta_k(x)$ and inequalities for $\emptyset_j(x)$ are called constraints. It is worth pointing out that we can also write the inequalities in the other way ≥ 0, and we can also formulate the objectives as a maximization problem. This is because the maximization of *f(x)* is equivalent to the minimization of *–f(x)*, and any inequality $g(x) \leq 0$ is equivalent to $-g(x) \geq 0$. For constraints, the simplest case for a decision variable x_i is

$$x_{i,\min} \le x_i \le x_{i,\max} \quad \textbf{3-4}$$

The above expression (equation 3-4) is called bounds.

3.1.2 Structural optimization

According to Peter and Anders [59], a structural optimization is the subject dealing with optimal design of an assemblage of materials to sustain loads in the best way. The objective might be to minimize the total weight of the structure to constraints on displacements and stresses in the structure under the given loads.

3.1.3 Multiobjective optimization

In this thesis, optimization was conducted to ensure the safety of the sleeper and minimize the total volume of the sleeper that is affecting the sleeper total weight. In this case, two objective functions are analyzed. According to Yang [60], multiobjective optimization consists of multiple objective functions that be written as:

$$\text{Maximize / minimize } f(x) = [f_1\{x\}.f_2\{x\},....., f_p\{x\}] \quad \textbf{3-5}$$

$$\text{Subjected } \begin{matrix} g_j(x) \le 0, j = 1,2,....,M \\ h_k(x) = 0, k = 1,2,....,M \end{matrix} \quad \textbf{3-6}$$

Where $x = (x_1, x_2,....., x_n)^T$ present a vector of decision variables.

The inequalities $g_j(x), j = 1,2,...,M$ can also include any equalities because an equality $g(x) = 0$ can be converted into two inequalities $\phi(x) \le 0$ and $\phi(x) \ge 0$.

Multiobjective optimization problems solution unlike a single objective optimization problem, do not necessarily have an optimal solution that minimizes all the multiobjective functions simultaneously. For example improving the sleeper safety and minimize the cost at the same time. As reported by Yang in 2010 [60]; to transform a multiobjective optimization problem into a single objective; weighted sum method could be used.

3.1.4 Weighted sum method

Many solution algorithms intend to combine all the multi-objective functions into one scalar objective using weighted sum [60].

$$F(x) = \alpha_1 f_1(x) + \alpha_2 f_2(x) + ... + \alpha_p f_p(x) \quad \textbf{3-7}$$

The important issue arises in assigning the weighting coefficients $\alpha_1, \alpha_2,....., \alpha_p$ because the solution strongly depends on the chosen weighting coefficients having a sum of 1.

In this thesis, two objective functions such as sleeper safety and sleeper cost in times of sleeper total volume are given as $f_1(x)$ and $f_2(x)$ respectively**.** Combining the two, the following scalar objective is given as:

$$F(x) = \alpha_1 f_1(x) + \alpha_2 f_2(x) \quad \textbf{3-8}$$

Where, α_1 and α_2 are the weighting coefficients with $\alpha_1 + \alpha_2 = 1$, α_1 and α_2 are from literatures.

Railway design have to consider safety over the whole project from development to maintenance as the safe by design principles actively eliminate risk during design development and maintenance activities [61]. This shows that the safety has to have a percentage greater than 50%. According to Jonan Backman in 2002 [62] , in his study; a rail safety of 59% was reported with 41 % cost. The sleeper safety and total volume of 59 % and 41% were used in this report.

The sleeper safety is based on the way the sleepers behave under both static and impact loading. Both bending stress at top and bottom have to be considered and compared to the permissible stress provided by AS 1085.14. The sleeper cost is taken into account by considering only the sleeper volume. The other elements that are affecting the sleeper cost were not considered in the analysis.

The weighted sum method was used to select the best geometrical sleeper shape. The sleeper safety as one of the objective function that is constrained by the permissible stress in compression and tension, sleeper total volume constrained by the sleeper shapes and dimensions are discussed in this thesis report.

The two objective functions (safety and volume) are formulated from ANSYS software after importing some parameter into the software. For sleeper safety, both static simulations and impact simulation were taken into account with a comparison with the obtained values with the permissible ones. The following discusses in detail sleeper modelling, static and impact simulations in section 3.2, sleeper safety and rankings and the sleeper total volume and their corresponding rankings in chapter 4.

3.2 Finite Element Modelling

To investigate and analyze the behaviour of concrete sleeper (such as deformations and stresses), a finite element model was developed using ANSYS software package under static and impact loadings.

3.2.1 Validation of the FEM

In the case of FEM validation, only static structural analysis was conducted. The following sections outline the properties of concrete and prestressing steel wires used as input values in finite element analysis.

3.2.1.1 Concrete and prestressing wires materials

3.2.1.1.1 Concrete material

The railway sleeper is made of concrete material. The typical properties of normal strength concrete C55/67 used as input data are shown in table 3-1.

Table 3-1 Concrete material properties [24], [63]

Density, ρ_c (kg / m3)	Poisson's ratio: v_c	Fc, cube (MPa)	Fc, cyl (MPa)	Young's modulus E_c (MPa)	Compressive strength, σ_{cc} (MPa)	Tensile strength: σ_{ct} (MPa)	GF (N/m)
2400	0.2	67	55	34,400	52	2.85	154

3.2.1.1.2 Pre-stressing steel wire material

Typical properties of reinforcement are indicated in table 3-2.

Table 3-2 Pre-stressing reinforcement material properties [24], [63]

Diameter, ∅ (mm)	Density, ρ_c (g / cm3)	Poisson's ratio, v_c	Thermal expansion: α (/°C)	Young's modulus, E_s (GPa)	Yield strength, σ_{tt} (MPa)	Tangent modulus, E_{st} (MPa)	Initial strain, ε_0 (mm/m)
7	7.8	0.3	1.1×10^{-5}	200	1750	20000	5

The quality assessment of FE model and validation according to [63]. Static full-scale test is next discussed below.

3.2.1.2 Static full-scale test done by Rikard

The hydraulic jack, used by Rikard was mounted in a set-up as shown in figure 3-1.

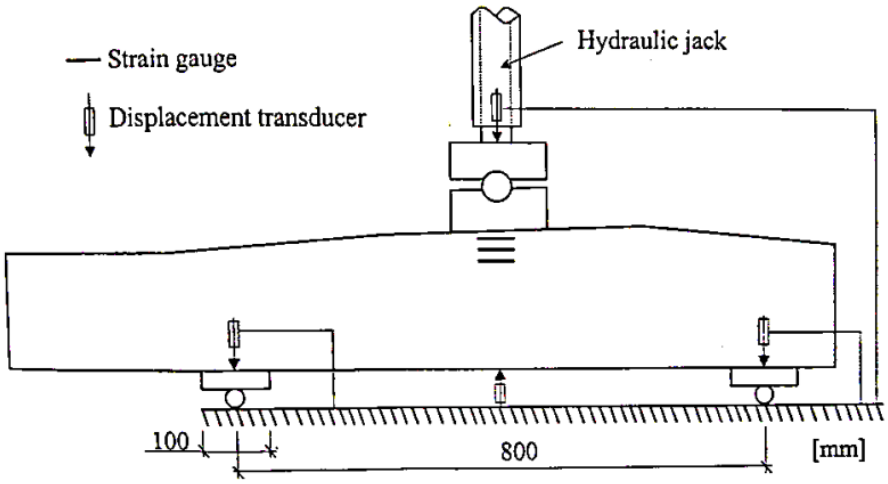

Figure 3-1 Test set-up used in the test done by Rikard, 2000

According to the figure above, sleepers have been supported. Six sleepers, manufactured by Abetong Teknik AB, of type A9P were cut at the middle perpendicular to the line of the sleeper. Each half-sleeper was subjected to a bending moment that produced the same principal deflections shape of the sleeper as if the sleeper were placed in a track system. The static test is carried out using a hydraulic jack as [63]; the load is applied to the rail seat area varying from 0 to 237.5 KN. The support condition in this case is fixed where sleeper is tied on the ground on four locations as shown in figure 3-2.

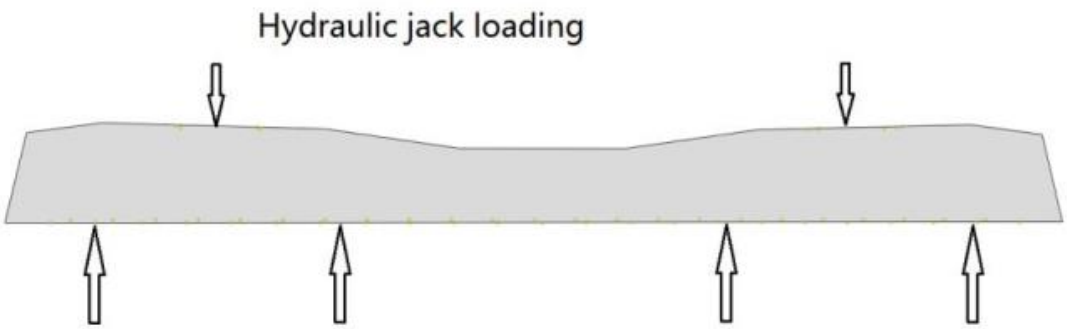

Figure 3-2 Static structural model with fixed support

Sleeper of type A9P was studied, and detailed dimensions are shown in appendix A (figure A-1). All tested half-sleepers had similar load-vertical displacement relations according to figure 3-3.

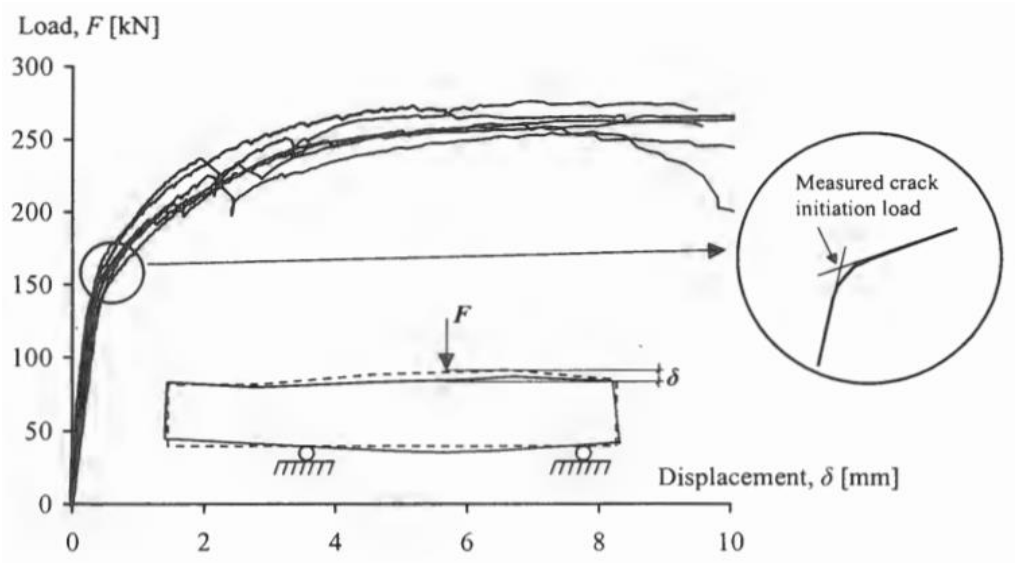

Figure 3-3: The load-vertical displacement relation for the six tested half-sleepers [63].

3.2.1.3 Sleeper modelling and validation

3.2.1.3.1 Element types

A variety of element types exists for both steel and concrete materials because the purpose and desired output may vary from model to model. The following summarizes the elements used in modelling prestressed concrete sleeper. These recommended elements are based on the commercially available in ANSYS software.

3.2.1.3.1.1 SOLID65 Element

The concrete section is modelled using a three-dimensional solid element, SOLID65, which has the material model to predict the failure of brittle elements. This element has eight nodes with three degrees of freedom at each node-translation in the nodal x, y and z directions. This element is capable of plastic deformation, cracking in tension, and crushing in compression due to build in algorithms which are dependent on user input of material parameters [25]**.**

In the current practice, the concrete sleeper is designed to resist prestressing force fully throughout the whole cross-section as the force / moment redistribution. This makes the smeared crack unsuitable for the replacement of prestressing tendons in fully prestressed concrete sleeper [64]**.**

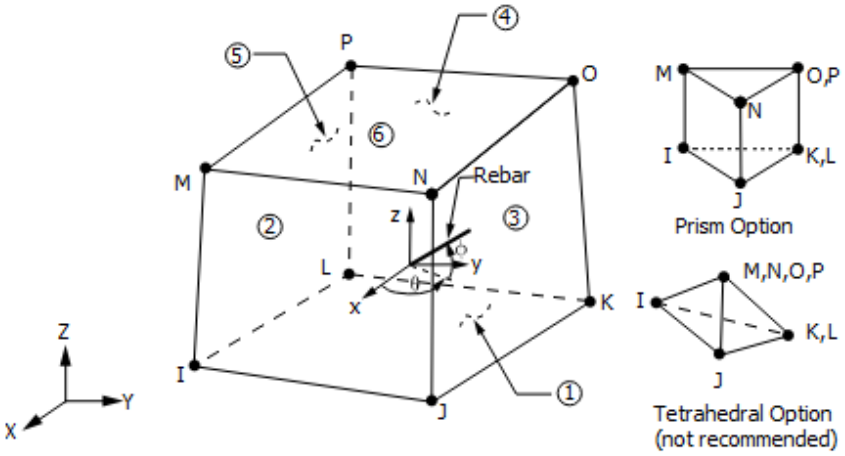

Figure 3-4 SOLID65 Three-dimensional Element [64]

3.2.1.3.1.2 LINK180 Element

To simulate the behaviour of prestressing wire, LINK180, is used to withstand the initial strain attributed to prestressing forces, as a typical truss element cannot resist neither bending moments nor shear forces. Truss elements are capable of compression and tension with three degrees of freedom at each node: translation in the nodal x, y, and z directions and, also capable of plastic deformation. Each end node is modelled as a pin connection, so no bending of the element is considered.

LINK180 requires users to input 'real constants' to define reinforcement geometry, material behaviour, and prestressing strain. However, the perfect bonding between concrete and prestressing wires has to be assumed [64]. An advantage of using LINK180 is that, it is possible to specify an initial strain for the element. This is useful for defining the initial prestressing force. LINK 180 further allows a change in cross-sectional area as a function of axial elongation. By default, the cross-sectional area changes such that the volume of the element is preserved, even after deformation. The default is suitable for elasto-plastic applications. LINK 180 offers compression-and-tension, tension-only, and compression-only options [64].

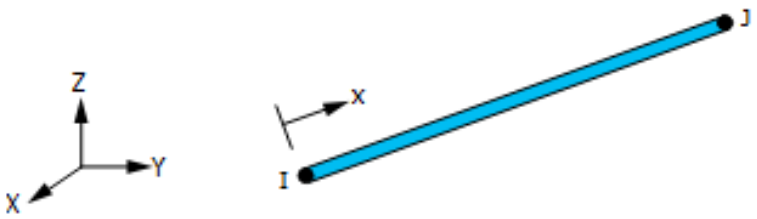

Figure 3-5 LINK180 bar element displayed with local and global axis [64]

3.2.1.3.2 Static modelling of sleeper type A9P

The sleeper is modelled having concrete as a three- dimensional solid element, SOLID 65 and with the prestressed wire as an embedded truss element, LINK 180 subjected to an initial prestrain of 5 mm/m. Bond slip between concrete and reinforcement is ignored. The sleeper's cross-section is simplified as rectangle. The model was composed of concrete body, prestressing wires and four fixed supports shown in figure 3-6 below. The sleeper model was modelled, analyzed and compared with Rikard results shown in figure 3-3.

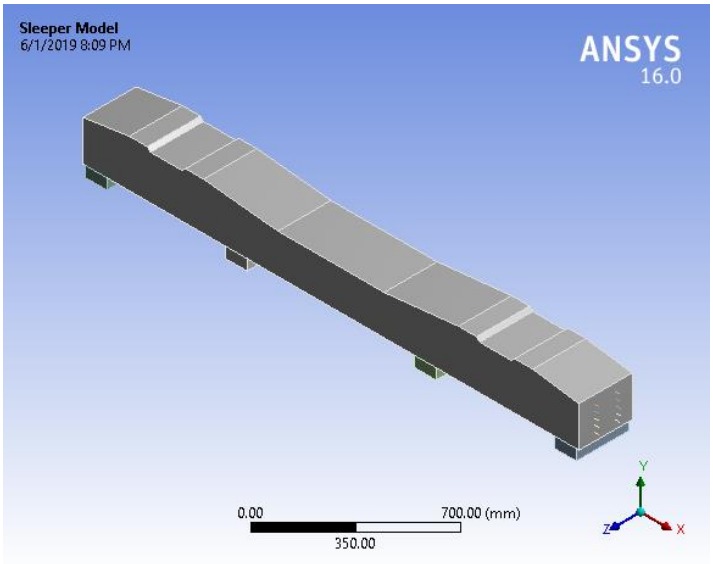

Figure 3-6 Concrete body and prestressing wire with four supports.

The sleeper was subjected to the same hydraulic jack loading as Rikard [63] and the load applied to the rail seat area is varying from 0 to 237.5 KN. The model was then meshed as shown in figure 3-7.

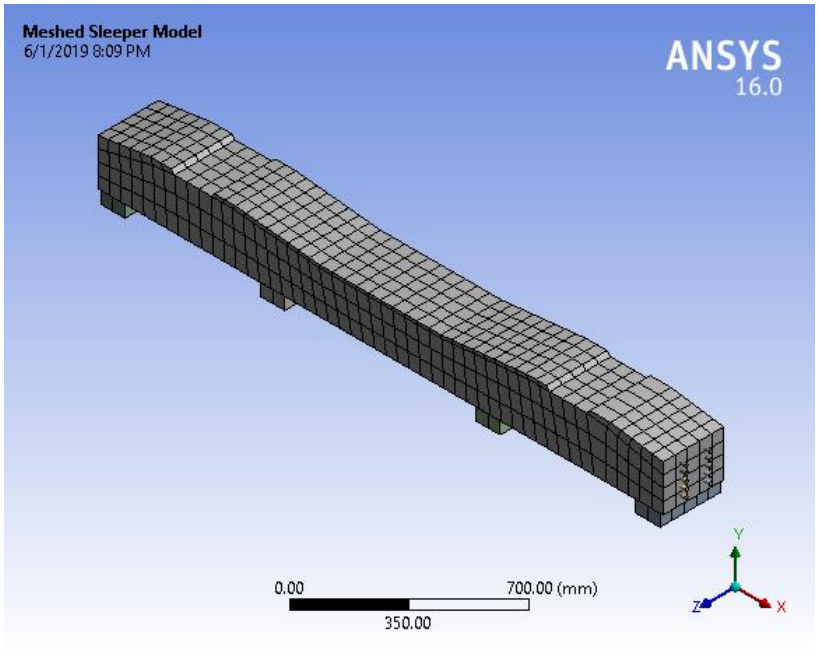

Figure 3-7 Meshed sleeper model

Figure 3-8 shows the FE model with the location of the area where the load was applied.

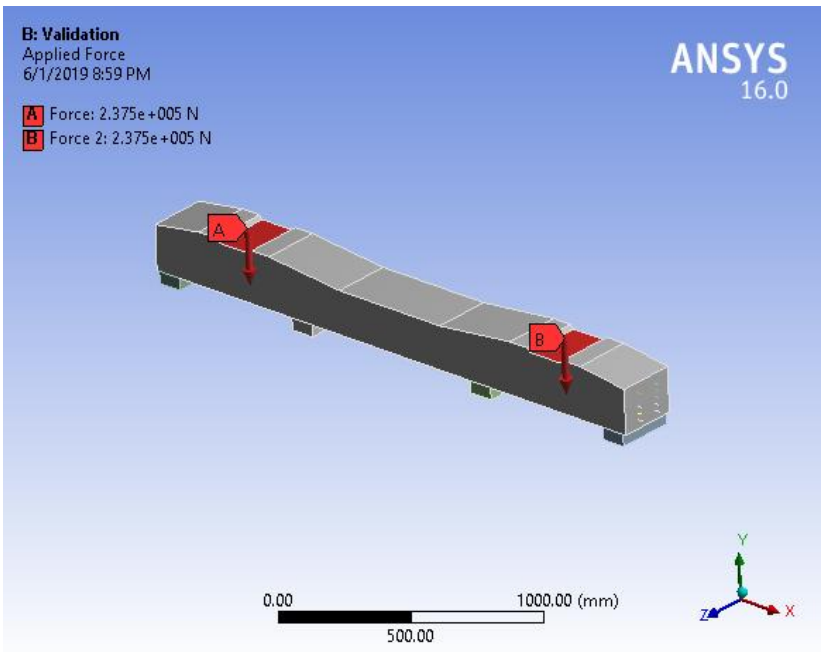

Figure 3-8 Applied load

3.2.1.4 Numerical results

Validation of the FE-model was conducted by comparing the structural response in the experimental tests and numerical analysis results. The structural response of the concrete sleeper is studied by examining the load-vertical displacement relationship. In this FEM

model concrete was modelled as an elastoplastic material, however in Rikard's model concrete is modelled as elastoplastic and brittle cracking material. The stress-strain relationship of the concrete used by Rikard is shown in figure 3-9. The total sleeper deformations were shown in figure 3-10.

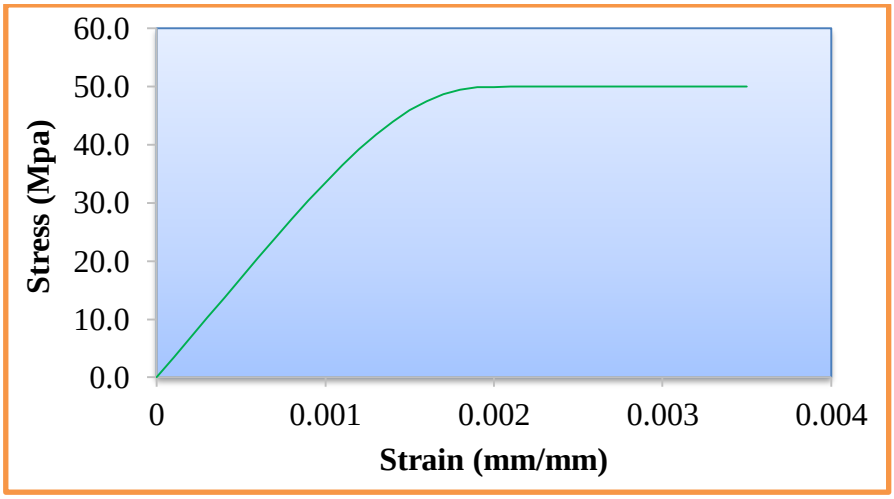

Figure 3-9 Compressive stress-strain graph for 52 MPa concrete

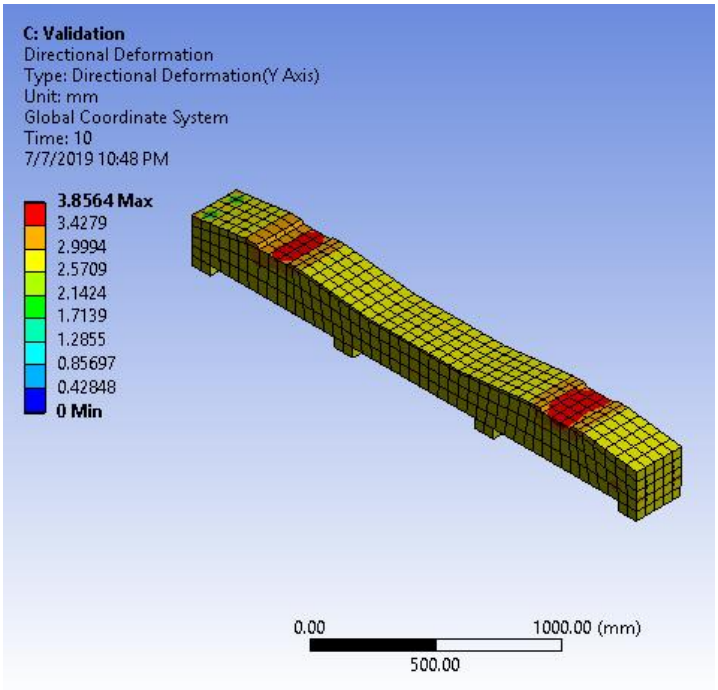

Figure 3-10 Sleeper directional deformation

The maximum directional deformation (y-axis) of the sleeper was obtained at 237.5 KN. The ANSYS Software gave the deformation in Table 3-3 with the corresponding applied force varying from 0 to 237.5 KN. The force-deformation curve is shown in figure 3-11.

Table 3-3 Force Vs deformation

Force	deformation
0	0.000
50	0.357
150	1.087
200	2.089
237.5	3.856

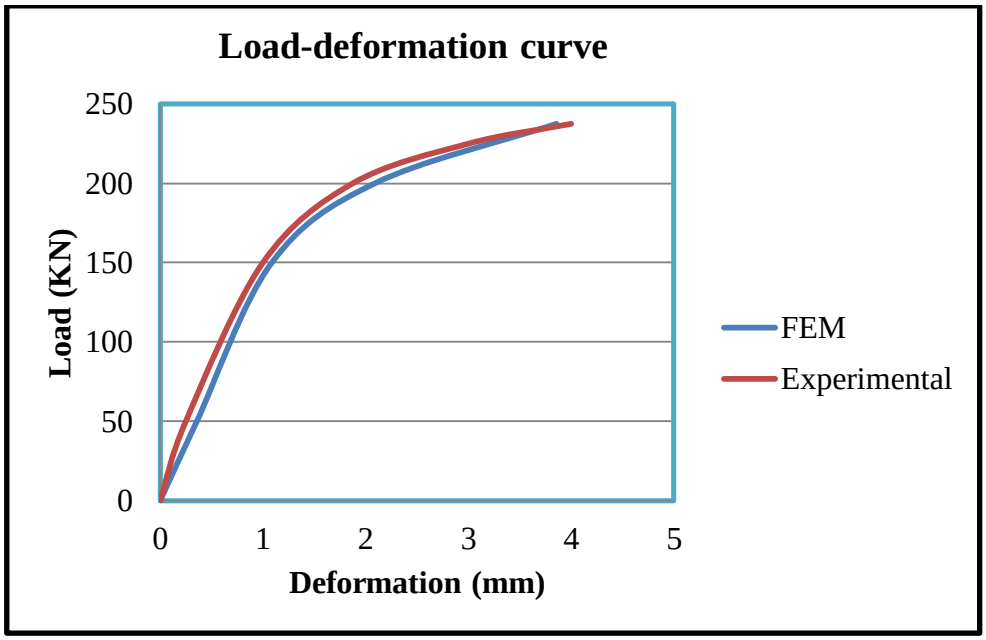

Figure 3-11 Force –deformation graph with FEM results in blue color and experimental results in red color.

The force and vertical displacement diagram match Rikard 2000, proving that the quality of FE model is good as shown in figure 3-11 above. Once the model is validated with respect to the test results, further analysis using this FE-model can proceed. Static analysis isn't sufficient as most severe damage mainly come from impact loading. Therefore, it is imperative that both static and impact sleeper models are studied in order to get a reliable critical deformation and stress responses. Since the static results match experimental results, ANSYS software can be used to conduct static simulations. Impact validation of the FEM was not conducted in this research due to the fact that, experimental results (time varying contact forces) reported in literatures; were not available in ANSYS workbench explicit dynamics used in this research.

3.2.2 Geometric shape and dimensions of modelled sleeper

3.2.2.1 Sleeper cross-section

As reported by Doyle [65], the condition of the ballast underneath the sleeper, affects the bending moment subjected to vertical loads. The performance of a sleeper to withstand lateral and longitudinal loading is dependent upon the sleeper's size, shape, surface geometry, weight and spacing.

Different cross sections of sleeper at both rail seat and center were selected: trapezoidal cross section, rectangular, and irregular hexagon sections, taking into account the variation in shape and size of sleeper. The sleeper is symetric in shape and size about its centre portion. The total length of sleeper is 2,500 mm. The central distance between the rail seats (standard gauge distance) is 1.435 m.

The selections of sleeper dimensions were first based on the minimum values of bottom and top width at both rail seat and center section and the corresponding minimum heights. The existing sleeper that was used by ERC was considered as baseline, where its corresponding volume, soffit area and dimensions at both rail seat and center section were computed.

3.2.2.2 Computation of minimum values

The maximum ballast pressure

Ballast pressure, based on the uniform pressure beneath each rail seat is limited to 750 KPa for high ballast quality according to AS 1085-14 and AREMA 2010 [35]**,** [39]. The maximum ballast pressure helps to get the minimum value of the base width.

3.2.2.2.1 The minimum bottom width

For standard gauge, the average ballast pressure is computed as;

$$P_{ab} = \frac{R}{B*(L-g)} \qquad \textbf{3-9}$$

Where:

R = Rail seat load; B = Sleeper width and $L-g$ = Effective length

This formula is valid for standard and broad gauge where, g is greater than 1.5 m [39]**.** The bottom width can be limited from equation 3-9 when the maximum ballast pressure is limited to 750 KPa.

In this case, the required minimum sleeper width is computed based on the equation 3-9. This equation is also constrained by the rail seat load and the effective length.

Rail seat load

According to AS1085.14 **[40]**, the rail seat load is computed as

$$R = \frac{Q}{2} * DF * \frac{I}{100} \qquad \textbf{3-10}$$

R = Rail seat load, Q = Axle load DF = Distribution factor, I = Impact factor in %

Axle load is taken as 25 tones.

Impact factor

According to Karkik et al. [66] the magnitude of impact loads due to wheel irregularities were limited to the range of 200-300% of static load. AREMA manual, in chapter 30, [35] suggests the use of an impact factor of 200% over the expected loads for the design of track components to account for the irregularities in wheel and rail. The manual does not make a distinction between dynamic and impact factors. In the case of tangent and curved section, a factor of 1.2 and 1.6 were applied respectively.

The formula in table 2-3 was reviewed for a speed of 80 km/h with a wheel diameter of 920 mm [50] and a track modulus of 40 MPa. It was found that all coefficients are all less than 1.5. As per [66], the impact factor including all quasi-static factors is said to be 250%; (2.5); this minimum impact factor has been reported by [47] and the same value was proposed by Australian Standards [39].

Distribution Factor: The distribution factors are obtained from figure 3-12 and 3-13 shown below.

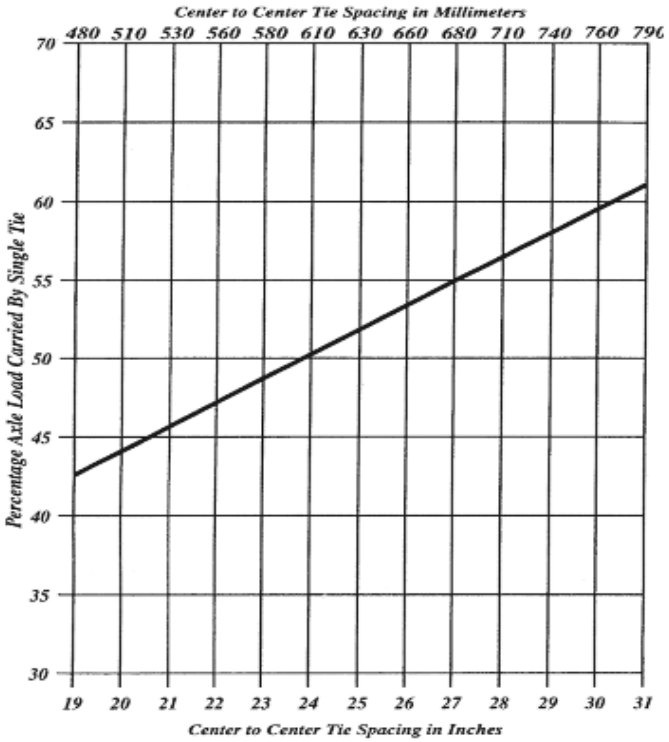

Figure 3-12 Estimated distribution of load (D.F) [35]

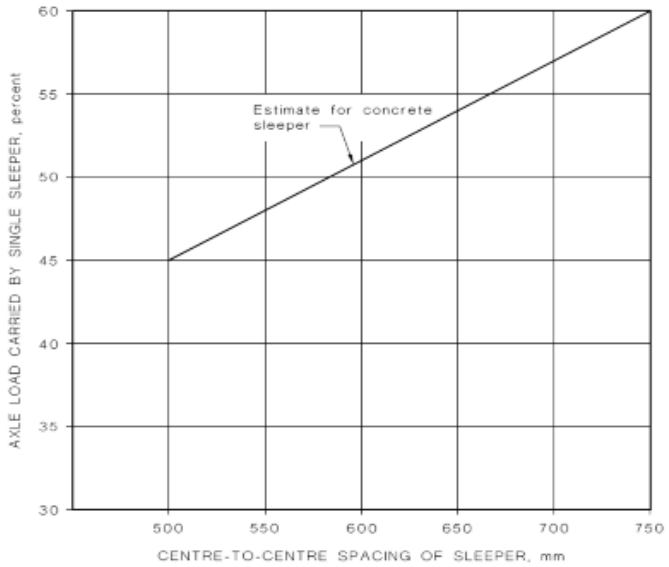

Figure 3-13 Estimated distribution factor (D.F) [39]

The DF was 0.5 as per figure 3-12 and 0.51 as per figure 3-13. For the sake of this research, the value of 0.51 was used as per figure 3-13 for a sleeper spacing of 60 cm. Therefore, the rail seat load was computed as

$$R = \frac{250}{2} * 0.51 * \frac{250}{100} = 159.375KN$$

Ballast pressure

The limiting ballast pressure is 750 KPa. According to [39], the ballast pressure is computed as follows;

$$P_{ab} = \frac{R}{B*(L-g)} = 750$$

Where;

L = 2.5 m

g (equal to standard gauge + the top width of rail) = 1435+74.3 = 1509.3 mm (≈1510mm) since standard gauge, G = 1435 mm, according to UIC 60 and the corresponding top width is 74.3 mm as per figure 3-14.

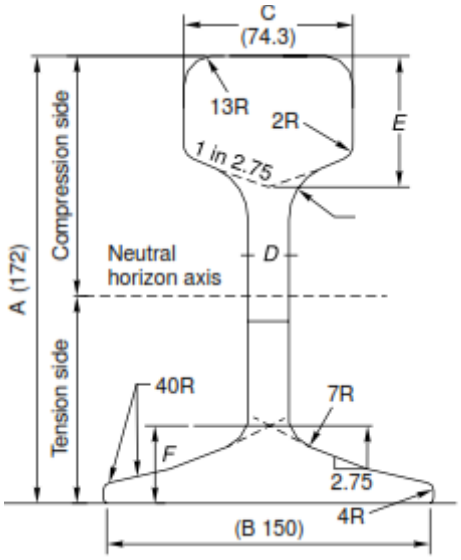

Figure 3-14 60-kg rail [67]

L-g is said to be the effective support length = 2,500 mm – 1,510 mm = 990 mm.

So, $B \geq \frac{159.375}{750*(2.5-1.51)}$, $B \geq 0.210375m$

According to AREMA 2010, the ballast pressure is given by

$$P_a = \frac{2Q_0}{A_B} = \frac{2Q_0}{\frac{2}{3}L*B} = \frac{3}{L*B}Q_0$$

The limiting ballast pressure is 750 KPa, thus $\frac{3}{L*B}Q_0 \leq 750$

$$B \geq \frac{3*159.375}{750*2.5},\ B \geq 0.255m$$

The minimum base width is 255 mm**.** Therefore the assumed minimum ballast-sleeper contact area (considering a uniform base) is

$$A_{c,\min} = B*L = 0.255*2.5m^2 = 0.6375\,m^2$$

3.2.2.2.2 The minimum top width and height

The top width of the sleeper is determined by the fastening requirements and the reinforcement's accommodation with adequate concrete cover. The following dimensions thus applied;

- Minimum clear concrete cover at the soffit of sleeper = 35 mm.
- Minimum clear cover to tendons = 25 mm with the exception where the tendon may be exposed at end faces [35]
- Minimum clear tendon covers to insert hole of fitting = 12 mm.

3.2.2.2.2.1 Minimum top width

One layer of four prestressing wires was used with a minimum spacing of 25 mm each. The clear distance for both ends $=25*2=50mm$. Assuming 7 mm wire diameter and the maximum size of aggregate (MSA) was 25 mm. The minimum spacing between the pre-stressing wires is $1.5*MSA=1.5*20mm=30mm$; the minimum top width was computed as $30*3+7*4+50=168mm$. The minimum top width was thus selected as 168 mm.

3.2.2.2.2.2 Minimum height

The minimum height was computed by assuming three layers of prestressing wires. As highlighted above, the minimum clear concrete cover at the soffit of sleeper was 35 mm while the minimum clear cover to tendons was considered as 30 mm. The wire diameter was assumed to be 7 mm and the maximum size of aggregate (MSA) was 25 mm. The minimum spacing between the pre-stressing wires is equal to 30 mm. Assuming the top and bottom cover of 35 mm, considering three layers of prestressing wires, the minimum height was computed as $35mm+35mm+2*30mm+7mm*3=151mm$. The minimum sleeper height was therefore fixed to 160 mm**.**

3.2.2.3 Computation of the existing sleeper volume and soffit (breadth) area

The reference sleeper used is Chinese Type II sleeper, currently used on the Ethiopian national railway. The detailed drawing and dimensions are shown in figure 3-15 below.

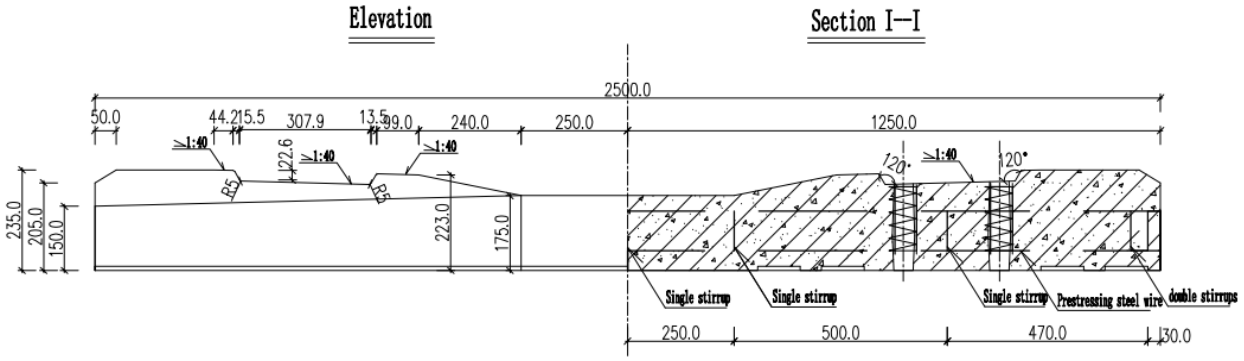

(a) Elevation

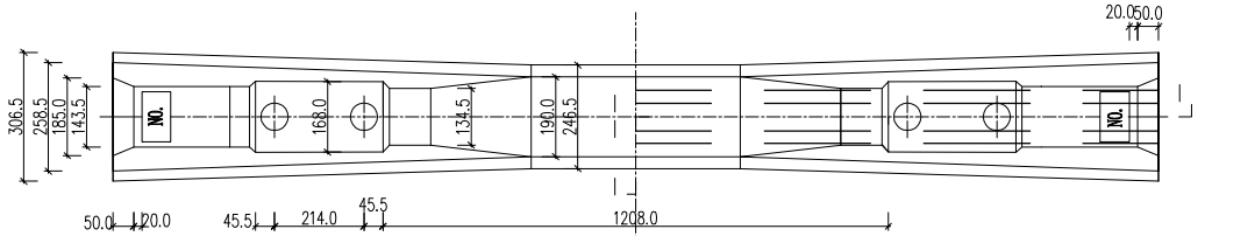

(b) Plan

Figure 3-15 Type II sleeper drawing (a) Elevation (b) Plan [68]

3.2.2.3.1 Total volume

The existing sleeper is complex in shape thus to analyses the total volume, it was divided into elements whose corresponding segment volume were computed and summed up to find the total volume. The detailed calculations are found in appendix B, table B-1. The total volume for the existing sleeper was calculated as **0.1139 m^3**.

3.2.2.3.2 Total soffit area / breadth area

The soffit/ breadth area of the existing sleeper was computed to **0.68 m^2**. The detailed calculations are found in appendix B, table B-2.

Variation of different cross section shapes and dimensions resulted to the following elements being taken into account in their selection; sleeper volume, sleeper soffit area, soffit area and volume, soffit area and height, and the volume and heights as the existing

sleeper. For every case, the sleeper volume, soffit area and height at both rail seat and center section were computed using Microsoft Excel as shown in Appendix C, from C-1 to C-5.

3.2.2.4 Selection of sleeper shape and dimensions

Criteria like sleeper having the same volume, soffit area, heights, volume and soffit area, volume and heights, soffit area and heights as the existing sleeper were considered as constraints. In addition to this, sleeper shapes were considered with various dimensions to meet the minimum requirements.

Different sleeper shapes were first selected as discussed above and their corresponding figure are shown in figure 3-16 to figure 3-20. The excel randonbetween functions between the minimum (bottom) and the maximum (top), was used to generate the random geometrical parameters. In addition to this, the moment of inertia at both sleeper rail seat section and center section was taken also as the basis of the sleeper selections. The moment of inertia affect the sleeper's bending resistance in time of stresses and defection, the higher the moment of inertia the better the bending resistance. Therefore, fifty one models with their corresponding dimensions were selected with respect to the criteria highlighted above, as shown in table 3-4.

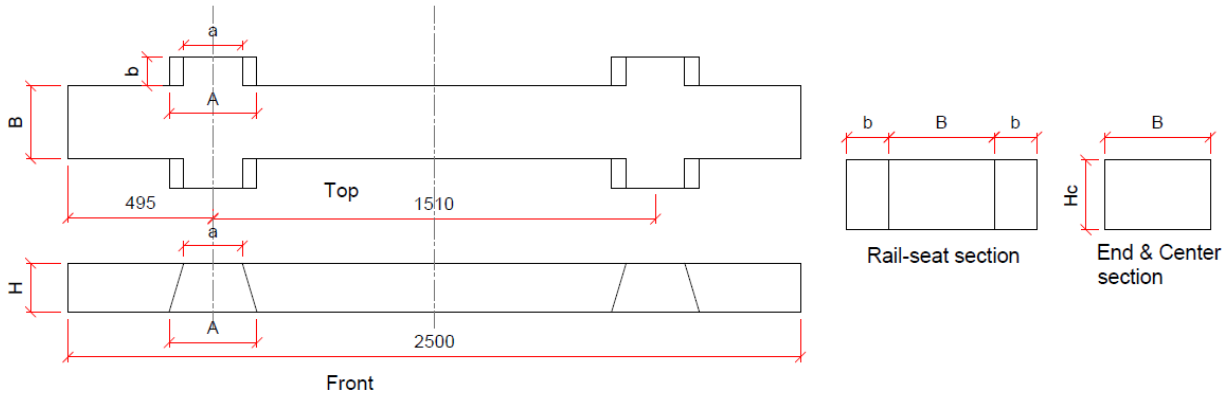

(a)

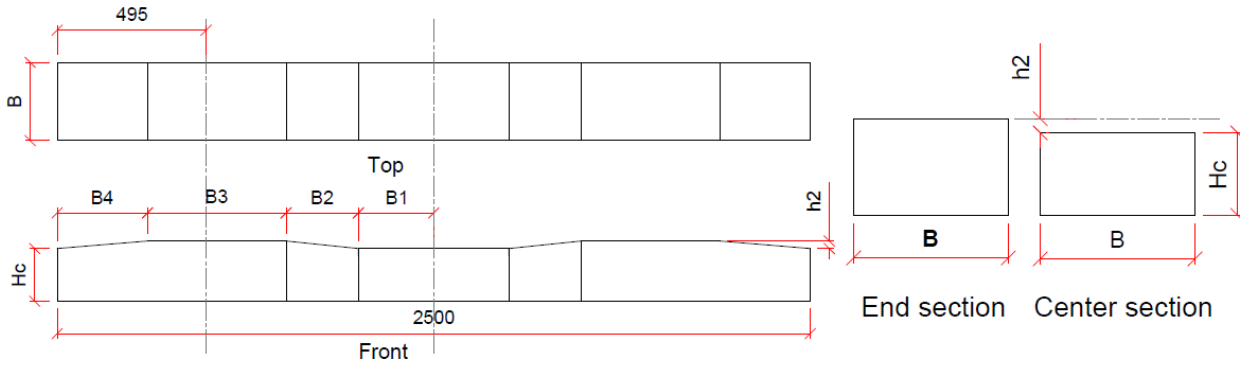

(b)

Figure 3-16 Rectangular sleeper sections (a) winged sections, (b) without wing sections

The rectangular with wing sections shown in figure 3-16 (a), corresponds to sleeper SI4, SI5, SII4 and SII5. The corresponding values of A, a, b are not shown in table 3-4. Therefore, the following are:

1. For SI4, A = 200 mm, a=200 mm and b=125 mm
2. For SI5, A = 290 mm, a=200 mm and b=100 mm
3. For SII4, A = 250 mm, a=250 mm and b=100 mm
4. For SII5, A = 300 mm, a=200 mm and b=100 mm

For the rectangular sleeper without wing sections as shown in figure 3-16 (b); when the value of h2 = 0 mm; the sleeper is a full rectangular sections having a length of 2,500 mm. As shown in figure 3-4 below, for all rectangular sleeper sections shown in figure 3-16 (a) and (b), the width B is the same as Bc, and H as Hc.

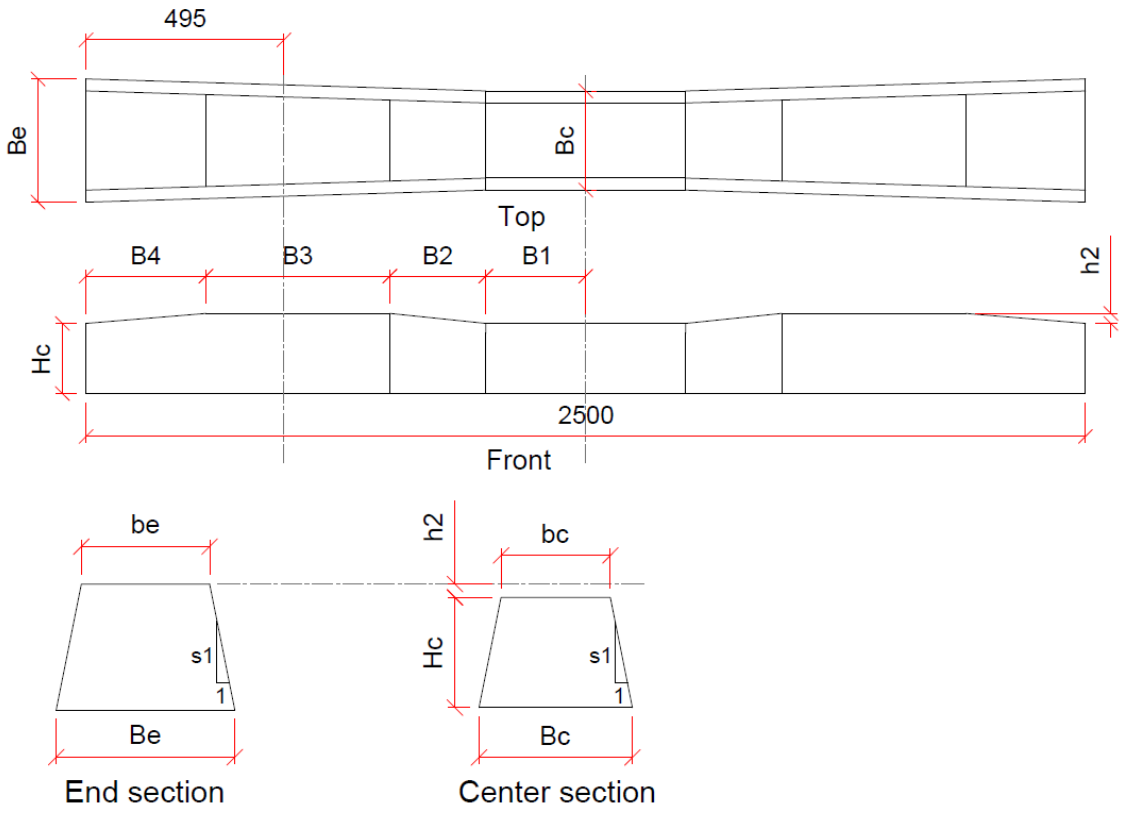

Figure 3-17 Trapezoid sleeper sections with a varying width

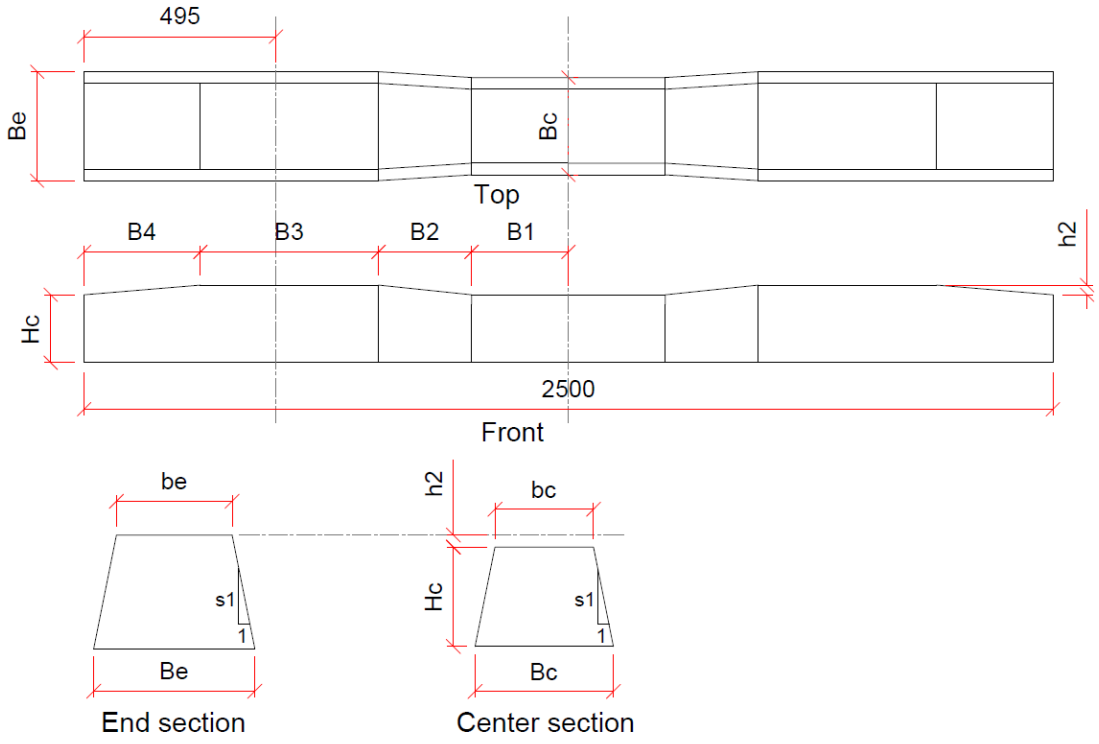

Figure 3-18 Trapezoid sleeper sections with different width at rail seat and center sections

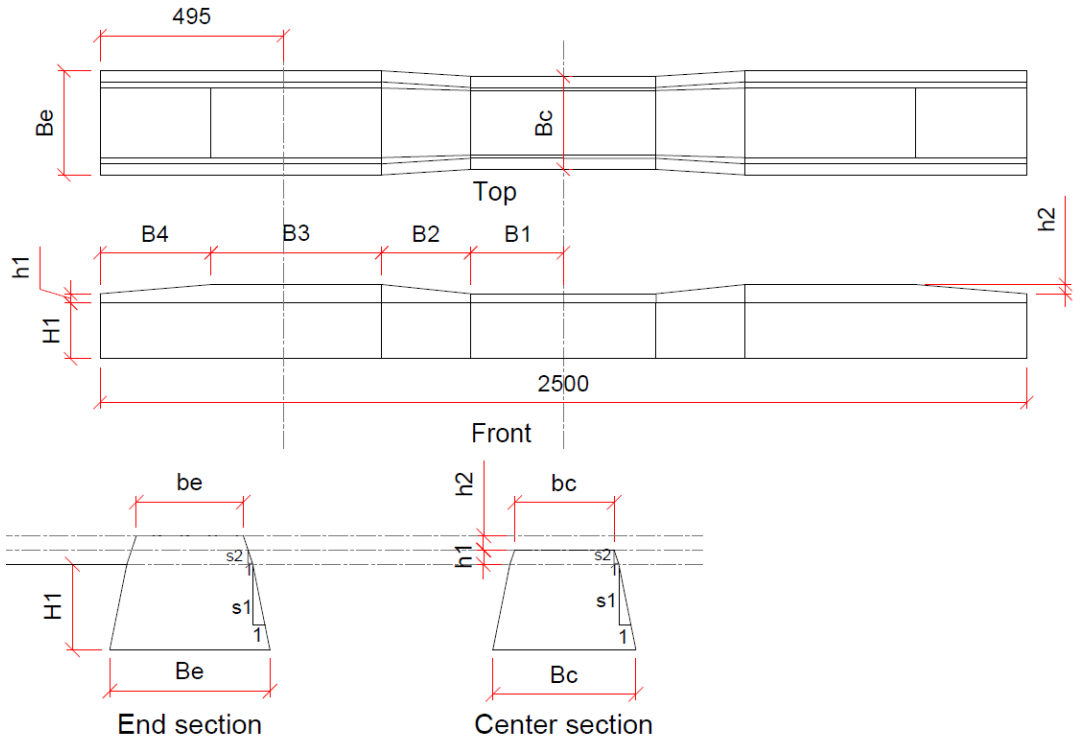

Figure 3-19 Irregular hexagon sleeper sections with different width at rail seat and center sections

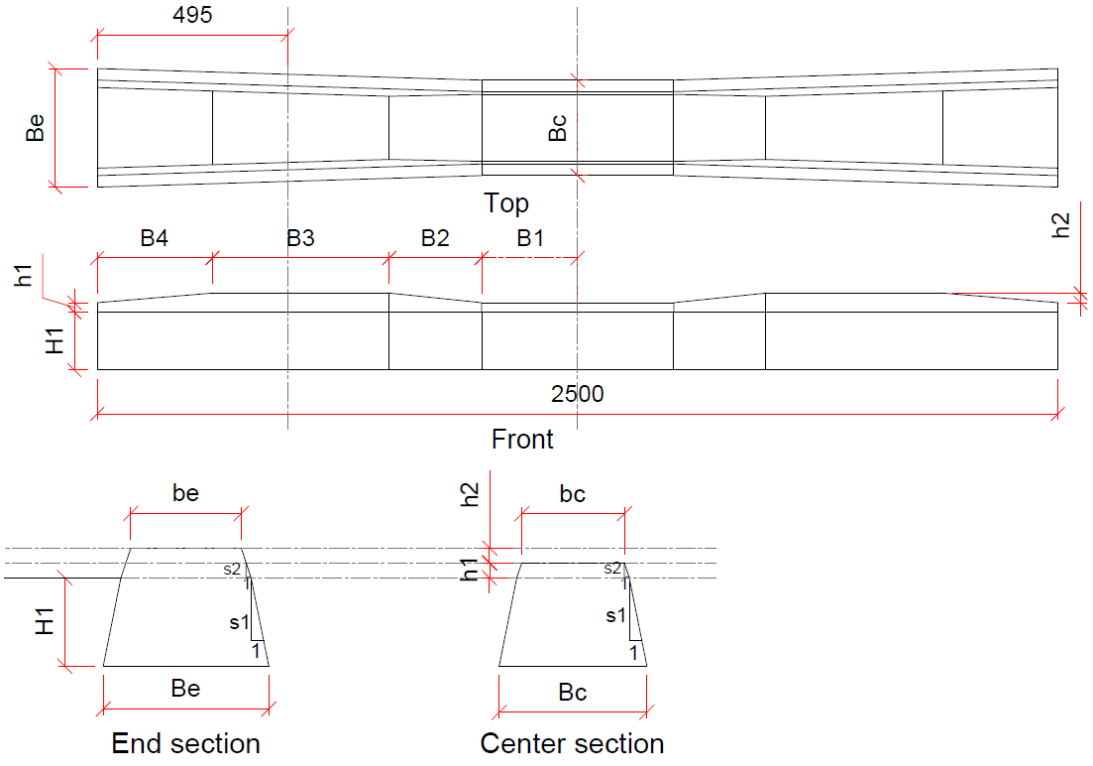

Figure 3-20 Irregular hexagon sleeper sections with a varying width

Table 3-4 below, shows the selected sleeper shapes and dimensions.

Table 3-4 detailed sleeper shape and dimensions selections

Cases	Criteria	Sleeper name	Shape	Sleeper dimensions																	
				Be	be	He	Br	br	Hr	Bc	bc	Hc	H1	h1	h2	S1	S2	B1	B2	B3	B4
				Mm	mm	mm	mm	mm	mm	mm	mm	mm	mm	mm	mm			mm	mm	mm	mm
1	Same volume as existing sleeper	SI-1	Rect.	260.0	260.0	175.3	260.0	260.0	175.3	260.0	260.0	175.3									
2		SI-2		265.3	265.3	175.9	265.3	265.3	175.9	235.0	235.0	175.9									
3		SI-3		236.2	236.2	165.0	486.2	486.2	165.0	236.2	236.2	165.0									
4		SI-4		221.2	221.2	175.0	421.2	421.2	175.0	221.2	221.2	175.0									
5		SI-5	Trap.	263.3	181.3	205.0	263.3	181.3	205.0	263.3	181.3	205.0				5					
6		SI-6		305.0	225.5	198.8	275.3	195.8	198.8	245.0	165.5	198.8				5					
7		SI-7		315.0	239.4	208.9	285.3	201.7	208.9	255.0	179.4	188.9			20.0	5		250	240	760	
8		SI-8	Ir. Hex.	285.0	183.7	201.6	285.0	190.6	201.6	255.0	181.0	171.0	150	21	30.6	5	2.5	250	240	760	
9		SI-9		310.0	213.2	199.2	280.3	174.9	199.2	250.0	164.0	175.0	135	40	24.2	5	3.0	250	240	760	
10	Soffit area as the existing sleeper	SII-1	Rect.	272.0	272.0	175.0	272.0	272.0	175.0	272.0	272.0	175.0									
11		SII-3		272.0	272.0	160.0	272.0	272.0	180.0	272.0	272.0	160.0			20.0			250	240	710	50
12		SII-4		252.0	252.0	164.0	452.0	452.0	164.0	252.0	252.0	164.0									
13		SII-5		248.0	248.0	166.5	448.0	448.0	166.5	248.0	248.0	166.5									
14		SII-6	Trap.	272.0	192.0	200.0	272.0	192.0	200.0	272.0	192.0	200.0				5					
15		SII-7		308.0	230.0	195.0	278.3	200.3	195.0	248.0	170.0	195.0									
16		SII-8		281.0	207.0	185.0	281.0	207.0	185.0	251.0	177.0	185.0									

Cases	Criteria	Sleeper name	Shape	Sleeper dimensions																	
				Be	be	He	Br	br	Hr	Bc	bc	Hc	H1	h1	h2	S1	S2	B1	B2	B3	B4
				Mm	mm	mm	mm	mm	mm	mm	mm	mm	mm	mm	mm			mm	mm	mm	mm
17	**Soffit area**	SII-9	Ir. Hex.	308.0	214.7	200.0	278.3	183.9	200.0	248.0	174.7	170.0	150	20	30.0	5	3.0	250	240	760	
18		SII-10	Trap.	280.0	190.0	180.0	280.0	172.5	215.0	250.0	160.0	180.0			35.0	4		300	320	310	320
19	**Volume and area**	SIII-1	Rect.	272.0	272.0	167.5	272.0	272.0	167.5	272.0	272.0	167.5									
20		SIII-3		281.0	281.0	178.0	281.0	281.0	178.0	251.0	251.0	160.0			18.0			250	240	760	
21		SIII-4	Trap.	272.0	193.7	195.7	272.0	193.7	195.7	272.0	193.7	195.7				5					
22		SIII-5		284.0	201.0	207.5	284.0	201.0	207.5	244.0	170.8	183.0			24.5	5		250	240	760	
23		SIII-6		308.0	229.8	207.2	278.3	195.4	207.2	248.0	174.0	185.0			22.2	5		250	240	760	
24		SIII-7	Ir. Hex.	281.0	182.3	208.0	281.0	195.7	208.0	251.0	177.7	170.0	150	20	38.0	5	3.0	250	240	760	
25		SIII-8		308.0	209.5	207.8	278.3	179.8	207.8	248.0	177.2	171.0	150	21	36.8	5	3.0	250	240	760	
26		SIII-9	Trap.	282.0	192.0	180.0	282.0	174.5	215.0	255.0	165.0	180.0			35.0	4		300	320	310	320
27	**Volume and Heights**	SIV-1	Trap.	275.0	205.0	175.0	275.0	195.0	200.0	275.0	205.0	175.0			25.0	5		250	240	710	50
28		SIV-2		312.7	242.7	175.0	283.0	203.0	200.0	252.7	182.7	175.0			25.0	5		250	240	560	200
29		SIV-3	Ir. Hex.	285.1	191.8	200.0	285.1	191.8	200.0	255.1	178.4	175.0	150	25	25.0	5	3.0	250	240	760	
30		SIV-4		312.3	219.0	200.0	282.6	182.6	200.0	252.3	172.3	175.0	150	25	25.0	5	3.0	250	240	760	
31		SIV-5	Trap.	291.7	211.7	200.0	291.7	211.7	200.0	251.7	181.7	175.0			25.0	5		250	240	760	
32		SIV-6		309.0	221.5	175.0	309.0	209.0	200.0	250.5	163.0	175.0			25.0	4		300	320	310	320
33	**Heights**	SV-1	Trap.	284.0	214.0	175.0	284.0	204.0	200.0	244.0	174.0	175.0			25.0	5		250	240	435	325

Cases	Criteria	Sleeper name	Shape	Sleeper dimensions																	
				Be	be	He	Br	br	Hr	Bc	bc	Hc	H1	h1	h2	S1	S2	B1	B2	B3	B4
				Mm	mm	mm	mm	mm	mm	mm	mm	mm	mm	mm	mm	mm			mm	mm	mm	mm
34	Heights	SV-2	Ir. Hex.	307.9	235.9	200.0	278.2	188.2	200.0	247.9	170.4	175.0	20	155	25.0	1	5.0	250	240	760	
35		SVI-1	Trap.	270.0	200.0	175.0	270.0	190.0	200.0	270.0	200.0	175.0			25.0	5		250	240	610	150
36		SVI-2	Trap.	310.0	240.0	175.0	280.3	187.0	200.0	250.0	173.3	175.0			25.0	5		250	240	660	100
37		SVI-3		300.0	230.0	175.0	300.0	200.0	200.0	260.0	172.5	175.0			25.0	4		300	320	310	320
38	Area and Heights	SVII-1	Trap.	308.0	238.0	175.0	278.3	198.3	200.0	248.0	178.0	175.0			25.0	5		250	240	560	200
39		SVII-2		272.0	202.0	175.0	272.0	192.0	200.0	272.0	202.0	175.0			25.0	5		250	240	560	200
40		SVII-3	Ir. Hex.	281.0	187.7	200.0	281.0	187.7	200.0	251.0	174.3	175.0	150	25	25.0	5	3.0	250	240	760	
41		SVII-4		308.0	214.7	200.0	278.3	178.3	200.0	248.0	168.0	175.0	150	25	25.0	5	3.0	250	240	760	
42		SVII-5	Trap.	283.0	195.5	175.0	283.0	183.0	200.0	253.0	165.5	175.0			25.0	4		300	320	310	320
43		SVII-6		284.0	214.0	200.0	284.0	204.0	200.0	244.0	174.0	175.0			25.0	5		250	240	760	
44	Any Volume	SVIII-1	Ir. Hex.	308.0	231.3	175.0	278.3	178.3	200.0	248.0	168.0	175.0	150	25	25.0	5	3.0	250	240	460	300
45		SVIII-2		281.0	204.3	175.0	281.0	187.7	200.0	251.0	174.3	175.0	150	25	25.0	5	3.0	250	240	460	300
46		SVIII-3		310.0	229.3	175.0	280.3	174.9	199.2	250.0	164.0	175.0	135	40	24.2	5	3.0	250	240	560	200
47		SVIII-4		285.0	208.2	171.0	285.0	190.6	201.6	255.0	181.0	171.0	150	21	30.6	5	2.5	250	240	510	250
48		SVIII-5		308.0	234.0	171.0	278.3	178.1	207.8	248.0	177.2	171.0	150	21	36.8	5	3.0	250	240	460	300
49		SVIII-6	Trap.	284.0	214.0	175.0	284.0	204.0	200.0	244.0	174.0	175.0			25.0	5		250	240	460	300
50		SVIII-7	Ir. Hex.	308.0	234.7	170.0	278.3	183.9	200.0	248.0	174.7	170.0	150	20	30.0	5	3.0	250	240	510	250
51		SVIII-8	Trap.	308.0	234.0	185.0	272.0	192.0	200.0	248.0	192.0	185.0			22.2	5		250	240	460	300

The following are the abbreviations used in table 3-4.

1. Rect. = Rectangular
2. Trap. = Trapezoid
3. Ir. Hex. = Irregular hexagon
4. Be = the sleeper bottom end width; be = the sleeper top end width and He = the sleeper end height.
5. Br = the sleeper bottom rail seat width; br = the sleeper top rail seat width and Hr = the sleeper rail seat height.
6. Bc = the sleeper bottom center width; bc = the sleeper top center width and Hc = the sleeper center height.
7. Other abbreviations such as, H1, h1, h2, S1, S2, B1, B2, B3 and B4 are shown from figure 3-16 to 3-20.

3.2.2.5 Material properties

The elastic beam member of the prestressed concrete sleeper was assumed. General parameters are given such as:

Table 3-5 General parameters

Parameters	Values	Source
Axle load	25 t	ERC Feasibility Study [68]
Speed	80-120 km/h	ERC Feasibility Study [68]
Sleeper spacing	60 cm	ERC Feasibility Study [68]
Load distribution factor (DF)	51 %	[39]
Maximum ballast pressure	600-750 KPa	[35], [39]
Track modulus	20-40 MPa	[39]
Design life	30-40 years	ERC Feasibility Study [68]
Concrete grade	60 Mpa	ERC Design Department

Properties of concrete and prestressing wires

According to National Standard of People's Republic of China [69], the concrete strength grade for prestressed concrete structures shall not be less than C30. When strand, steel wires and heat-treated steel reinforcements are to be used as prestressed steel reinforcement and the concrete strength grade may not be less C40. The standard further recommends an intended stress-relieved prestressing steel wire of diameter of 5 or 7mm.

As reported by ERC design department, the concrete grade C60 was used. The stress-strain relationship is shown in figure 3-21 below.

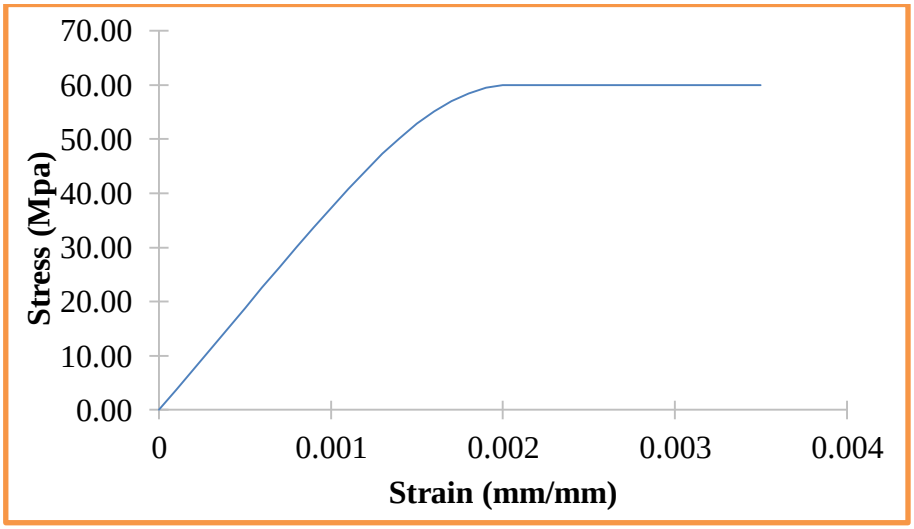

Figure 3-21: The compressive stress-strain diagram of concrete, fc' =60 Mpa

The values presented in figure 3-21 represent the behaviour of concrete and are taken as model inputs in SOLID65 and LINK 180. The table 3-6 summarizes the corresponding properties of concrete and prestressing wires used in Finite Element Analysis.

Table 3-6 Material properties of concrete and prestressing steel

S/N	Properties	Value
	Concrete	
1	Density (φ_c), kg/m3	2400
2	Young's modulus, (E_c), Mpa	37,720 Mpa
3	Poisson's ratio (μ_c)	0.2
4	Thermal expansion (α_c), /c	$1*10^{-5}$
5	Strain value	0.003
6	Yield strength	55 Mpa
7	Tensile strength	2.85 Mpa
8	Shear transfer	0.9
	Prestressing wires	
1	Density (φ_s), kg/m3	7,800
2	Young's modulus, (E_c), Mpa	200,000
3	Poisson's ratio (μ_s)	0.3
4	Characteristic strength (f_{plk}), Mpa	1,570
5	Strain value	0.00542
6	Yield strength	1,750 Mpa
7	Tensile strength	1,085 Mpa

AREMA and AS standards recommended maximum permissible stresses in concrete after allowing all losses of prestress (under working conditions) as shown in table 3-7 and 3-8.

Table 3-7: maximum permissible stresses in concrete under working conditions as per AREMA [35]

Types of stress	Maximum permissible stress
Compression	$0.45 * f_c^{'}$
Tension (flexure)	$0.62 * (f_c^{'})^{0.5}$
$f_c^{'}$ is the concrete strength	

Table 3-8: Maximum permissible stresses in concrete under working conditions as per AS 1085.14-2003 [39]

Types of stress	Maximum permissible stress
Compression	$0.45 * f_c^{'}$
Tension (flexure)	$0.4 * (f_c^{'})^{0.5}$
$f_c^{'}$ is the concrete strength	

The value of controlled stress for stretching prestressed reinforcement may not exceed the allowable value of controlled stress for stretching as stipulated in table 3-9 and shall be not less than $0.4 * f_{plk}$ [69].

In order to increase the crack resistance in the construction stage for the members, it is required that the prestressed reinforcement shall be provided in the compression zone at service stage. Prestressing reinforcement is required to offset a part of the loss of prestress caused by the factors such as stress relaxation, friction, batch stretching of steel reinforcement or the difference of temperature between the prestressed reinforcement and the stretching bed.

Table 3-9 Allowable value of controlled stress for stretching [69].

Type of steel reinforcement	**Method of stretching**	
	Pre-tensioned	Post-tensioned
Stress-relief steel wire, strand	$0.75 * f_{plk}$	$0.75 * f_{plk}$
Heat-treated steel bar	$0.70 * f_{plk}$	$0.65 * f_{plk}$
f_{plk} Characteristic strength of prestressed steel wire		

The value of stress for stretching prestressed reinforcement in the steel wire must be used, therefore the required stress was calculated as;

$$\sigma = 0.75 * 1570MPa = 1177.5MPa$$

The initial strain of tendons can be obtained from the formula

$$\varepsilon = \frac{\sigma}{E_S} \qquad \textbf{3-11}$$

$$\varepsilon = \frac{1177.5}{200{,}000} = 0.00058875m/m = 5.8875mm/m$$

The prestressing wire diameter was 7 mm and the total number of wires was 12 (12@7mm diameter). The initial strain applied on prestressing wires corresponding to the prestressing force was 5.8875 mm/m.

The cross-sectional area of the prestressing wires was computed as

$$A_{pw} = 12 * \pi * \frac{d^2}{4} \qquad \textbf{3-12}$$

$$A_{pw} = 12 * \pi * \frac{7^2}{4} = 461.58mm^2 \text{ and } A_{1pw} = \pi * \frac{7^2}{4} = 38.45mm^2$$

3.2.3 Prestressed concrete sleeper modelling

3.2.3.1 Overview

Finite element analysis (FEA) is a powerful tool which can be applied to the design of irregular shaped member, whose geometry causes standard analysis to be difficult or more importantly inaccurate. It provides a tool that can simulate and predict the responses of reinforced and prestressed concrete members. The FEM is a numerical method for approximating solution for the problem that is difficult to solve analytically. This numerical method is done when the problem domain is divided into small elements having a simple geometry.

ANSYS is an advanced linear and non-linear simulation package that has been previously used to solve many complex and real word problem. Model constructions were first done using SOLID works and then later imported in ANSYS Workbench.

Using ANSYS 16, a three-dimensional non-linear finite element model of railway prestressed concrete was developed.

3.2.3.2 Static analysis in ANSYS

In ANSYS Workbench, the static structural is used to analyze models under static loadings starting from renaming the project as such. In the case of engineering data, the values of material properties and their respective units are entered carefully as per table 3-6 above.

3.2.3.2.1 Sleeper geometry

The selected sleeper dimensions are shown in table 3-4. Drawings for the various sleeper shapes were first carried out using a Computer Aided Design; Solid Works. The sleeper geometries were saved in a file compatible to ANSYS Workbench. After importing the sleeper geometries, line bodies were created with a minimum concrete cover of 35 mm at soffit area and the spacing between prestressing wires was taken as 30.417 mm. The pre-tensioning process was next executed by applying an initial strain corresponding to the prestress. For analysis purposes, since the sleeper was symmetric, a half sleeper was considered as shown in figure 3-22.

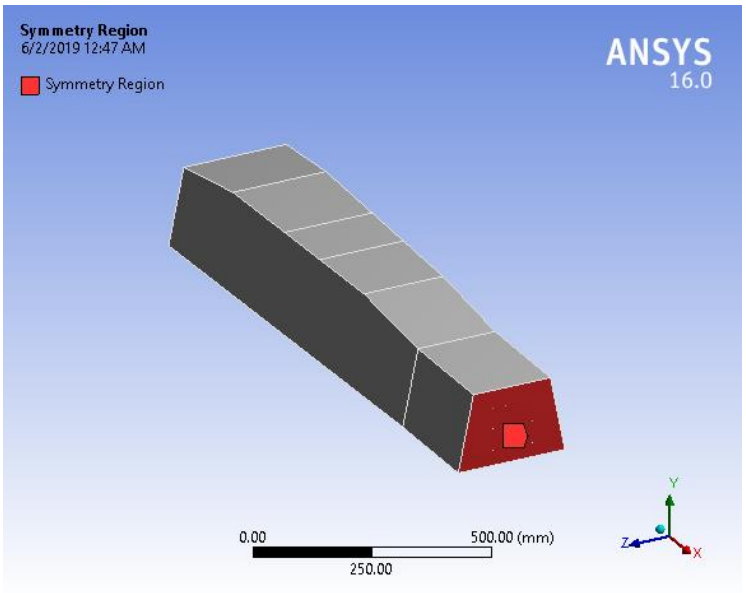

Figure 3-22 Sleeper geometry and symmetry region at centre for SIV2 (SL-28).

3.2.3.2.2 Meshing

The meshing shown in figure 3-23 was used. Hex dominant method was used for this model and mid-sized nodes set to "Dropped" to force the use of 8-nodes SOLID65 element instead of the default SOLID186. The hex-dominant meshing was preferred as it is both more efficient and accurate therefore producing a better (more uniform) mesh if a size control is placed on one or more edges. Hex meshing reduces element count therefore reducing the running time. The elements are aligned in direction of flow thus reducing the numerical error. The mesh size used was 25 mm for all models.

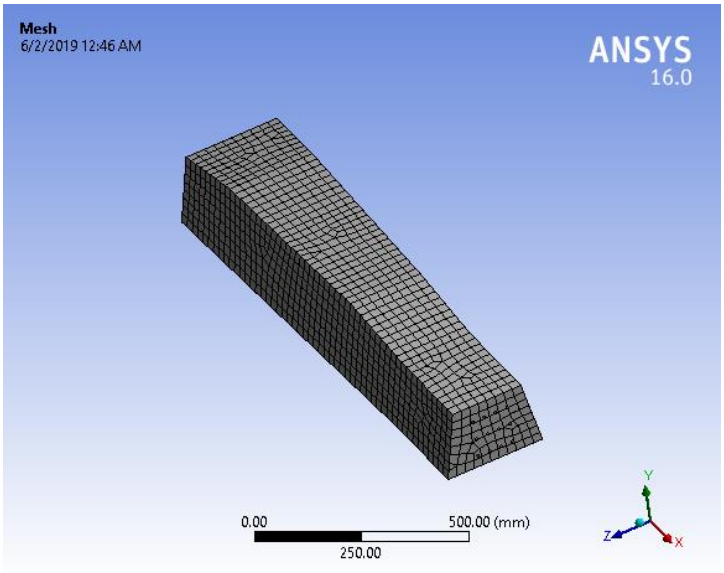

Figure 3-23 Hex dominant mesh method for SIV2 (SL-28)

3.2.3.2.3 Loading and boundary conditions

The loading applied to the sleeper was calculated based on the area in contact between the bottom rail and the sleeper. The rail seat load was computed as 159.375 KN. The support of the sleeper is modelled as a spring as done by Shan li [24] and recommended by [53] and Hong et al. [48]. For all cases, the ballast stiffness has been computed considering two layers; ballast and sub-ballast. As per Ahlbeck et al. [55]; the distribution angles for both ballast and sub-ballast are assumed to be 30 degrees and 35 degrees respectively for the two layers with 300 mm and 200 mm thickness respectively. The corresponding elastic moduli for the two thicknesses are 200 Mpa and 150 Mpa [53], [56], [57] respectively. The table below shows the detailed value of the ballast layer

stiffness calculated from the formula 2-10 and 2-11 outlined above. The detailed ballast stiffness was shown in appendix D (Table D-1).

3.2.3.2.4 Solutions in ANSYS Workbench static structural analysis

A set of solutions are available in ANSYS such as deformation (total or directional) and stresses (equivalent, shear, and normal, principal). The selected sleepers are modelled and analyzed to determine the respective deformations and stresses. The relationship between the three stresses such as equivalent stress, shear stress and bending stress was reported by Ivanov and Corves [70] in 2014 when the normal stress in times of bending stress was converted into an equivalent stress.

$$\sigma_V = \sqrt{(\sigma_b)^2} + 3*(\sigma_s)^2 \quad \textbf{3-13}$$

Where:

σ_V = Equivalent (Von-Mises) stress, σ_b = bending stress and σ_s = shear stress

$$\sigma_b = \sqrt{(\sigma_V)^2} - 3*(\sigma_s)^2 \quad \textbf{3-14}$$

3.2.3.3 Explicit dynamics in ANSYS

An explicit dynamics analysis is used to determine the dynamic response of a structure due to stress wave propagation, impact or rapidly changing time-dependent loads. The Explicit Dynamics system is designed to enable the user to simulate nonlinear structural mechanics applications involving one or more of the following: impact from low [1m/s to very high velocity 5000m/s]; high frequency dynamic response; large deformations and geometric nonlinearities; complex contact conditions; complex material behavior including material damage and failure; shock wave propagation through solids and liquids and rigid and flexible bodies [65].

Explicit dynamic in ANSYS Workbench was used to model impact loads so as to analyze impact analysis of prestressed concrete sleeper. The model is hammered by the impactor that generates an impact force when it is given an initial velocity. The velocity given to the impactor and its contact to the element to analyze, creates an impact force.

3.2.3.3.1 Impactor's mass and its properties

The mass of the impactor is taken as the mass of the wheel as reported by Hong et al. [48] and Kaewunruen [47]. It was assumed that the rail and the impactor are made of steel that bear similar properties as given in table 3-10.

Table 3-10 Impactor properties

Density, ρ_c (g / cm3)	Poisson's ratio, v_c	Young's modulus, E_s (GPa)	Yield strength, (MPa)	Ultimate yield strength (MPa)
7.85	0.3	205	250	460

The mass of 592 kg used by Kaewunruen was adopted in this thesis and the drop velocity of 1.373 m/s equivalent to 0.1 m [47]. The model showing the sleeper, rail and impactor is shown in 3-24.

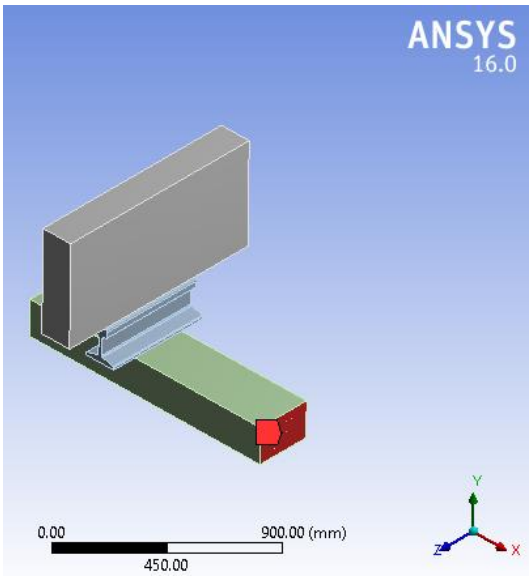

Figure 3-24 Model geometry and symmetry region for sleeper SIII1 (SL-19)

3.2.3.3.2 Materials properties

The multi-linear isotropic dynamic stress-strain for concrete and prestressing wires can be computed based on the effect of strain rate. The strain rate for static and impact simulations are different. Thus, the dynamic behaviour of concrete and prestressing wires is different from those static. In this thesis, the same properties used for static structural analysis are assumed to be same for explicit dynamic analysis corresponding to both concrete and prestressing wires.

3.2.3.3.3 Geometry and meshing

The geometry of the sleeper model was constructed using Computer Aided Design (CAD) solid works; saved in a format capable of being read by ANSYS Workbench. As in the previous static case, half of the sleeper geometry was used for analysis with the application of the symmetry tool in ANSYS as shown in figure 3-24 above.

The same meshing method and element size used in static structural analysis was maintained for explicit dynamics analysis. The mesh size used was 25 mm for all impact models under analysis as shown in figure 3-25.

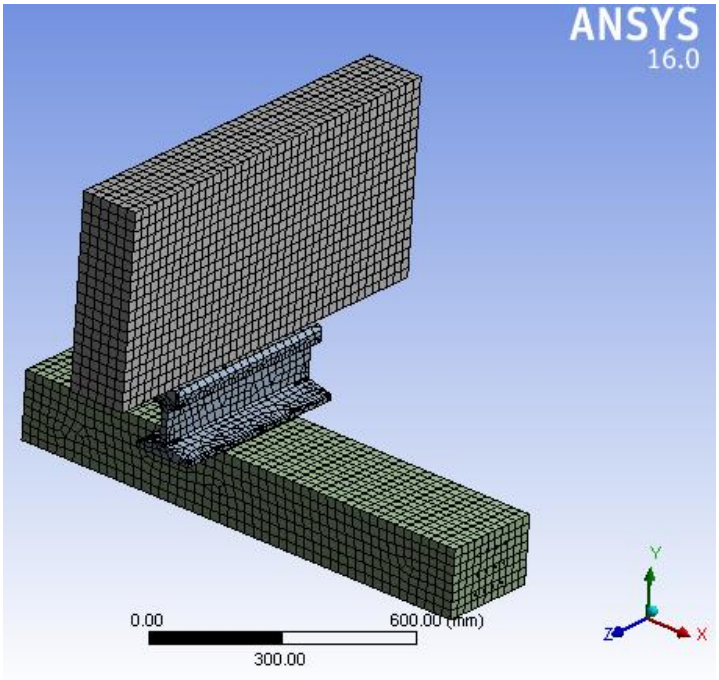

Figure 3-25 Model meshing for SIII1 (SL-19)

3.2.3.3.4 Loading and boundary conditions

The analysis model was selected in reference to the Kaewunruen model, the later model having been validated against the experiment impact testing. The drop velocity was 1.373 m/s equivalent to 0.1m drop height [47]**.** The initial velocity on the impactor was set so that the impact event on the sleeper is created. The ballast stiffness used to support the sleeper is not supported by explicit dynamics, hence, the fixed support was assumed for all models which don't affect the stress result.

3.2.3.3.5 Analysis settings

1. Maximum number of cycles

The maximum number of cycles indicates when the model will stop. In all models, the total number of cycles used was 11,300,400 cycles. Detailed calculation of the maximum number of cycles is shown in table E-1 Appendix E

2. Ending time

The ending time specifies the maximum length of time to be used by the explicit analysis. An end time of 0.005 sec (5 msec) was selected and thus used in the analysis.

3.2.3.4 Solution in ANSYS explicit dynamics

After solving the model, the equivalent stresses, total deformation and shear stresses were recorded at rail seat, center and end section.

The methods described under 3.2.3.2 and 3.2.3.3 above, were used for all the remaining sleepers.

CHAPTER 4 ANALYSIS RESULTS AND DISCUSSION

4.1 Static and impact behaviour of prestressed concrete sleeper

4.1.1 Static analysis of prestressed concrete sleeper

In chapter three, the sleeper shape and dimensions were selected and the corresponding rail seat and center sections dimensions, were also computed. The geometry, material property, elements and parameters used in modelling are highlighted in chapter three. The prestressed concrete sleeper was analyzed using ANSYS Workbench through static structural analysis. In this section, the analysis results of all models are presented and statically analyzed to obtain the deformation and stresses for different sleepers. Figure 4-1 shows the critical sections (rail seat, center and end) that have been considered on both top and bottom part of those critical sections. Stresses and deformations at those critical sections were recorded.

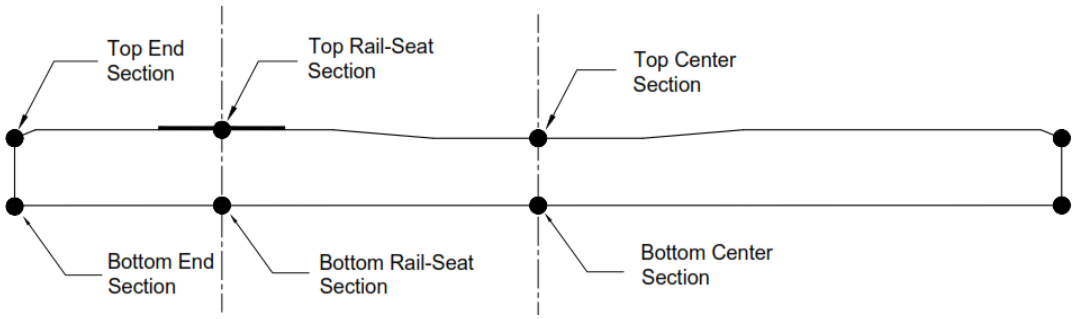

Figure 4-1 Critical sleeper sections

4.1.1.1 Deformation

In ANSYS Workbench; deformation results are generally obtained as either total deformation or directional deformation. The maximum deformation obtained in the sleeper occurs on the prestressing wires (line bodies) while the minimum deformation occurs on concrete part. In this thesis, the critical sections such as the rail seat, center and end sections have been emphasized and maximum deformation in concrete is located at rail seat section. The total deformations at critical sections have been recorded using a probe tool in ANSY workbench as shown in figure 4-2. The probe tool locates the maximum and minimum deformation of the model. In figure 4-2; the concrete part has

been selected and the deformations have been evaluated at rail seat, center and end sections.

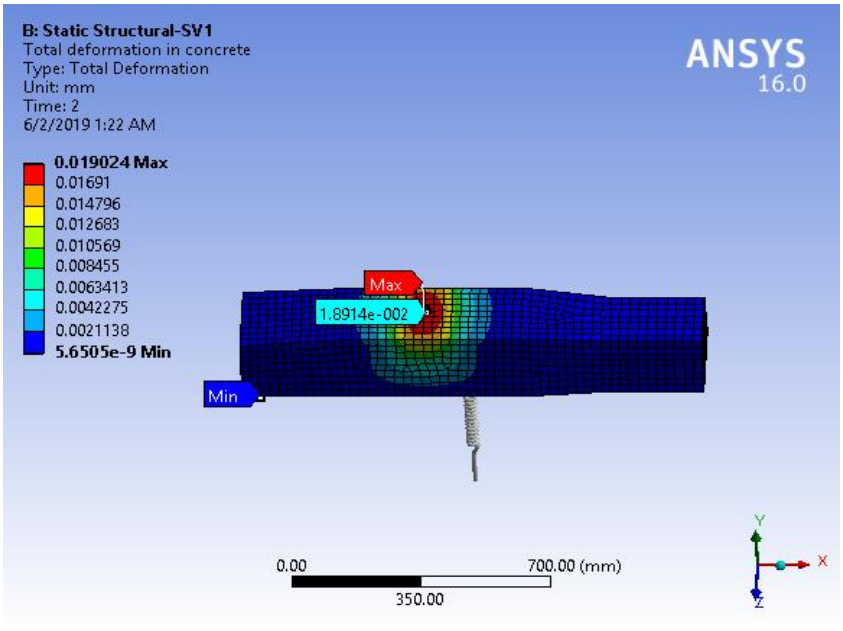

Figure 4-2 total deformations in concrete and probe tool for sleeper SV1

4.1.1.2 Equivalent (Von-Mises) stress

The von mises stress is a yielding criterion widely used for metals and ductile materials. The von mises stress in ANSYS was recorded as shown figure 4-3 for sleeper SV1.

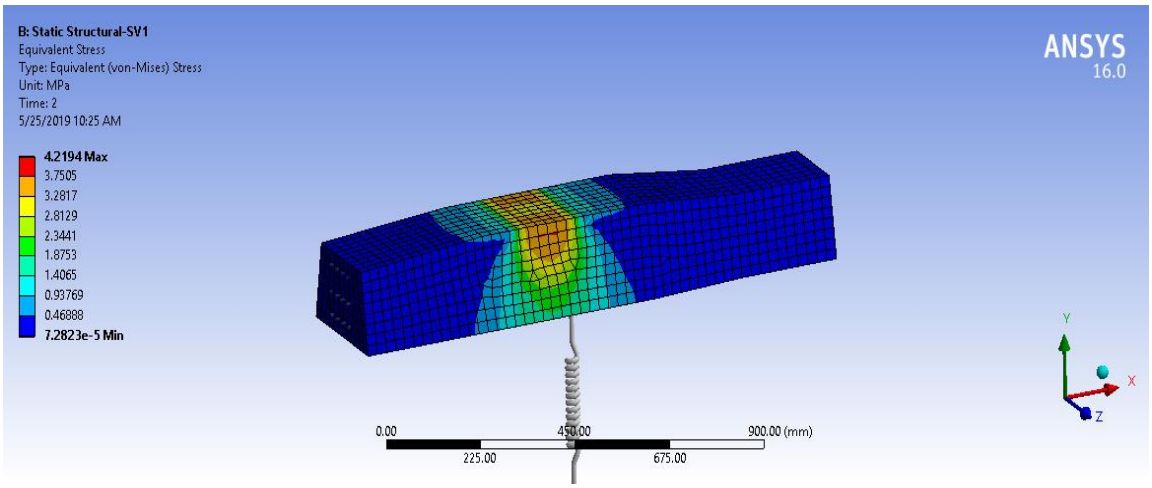

Figure 4-3 Equivalent (von-mises) stress for SV1 (SL-33)

4.1.1.3 Shear stress

Shear stress occurs when a load is applied parallel to its area and it equally varies across the cross sectional area. The shear stress in one of the selected sleepers is shown in figure 4-4 below.

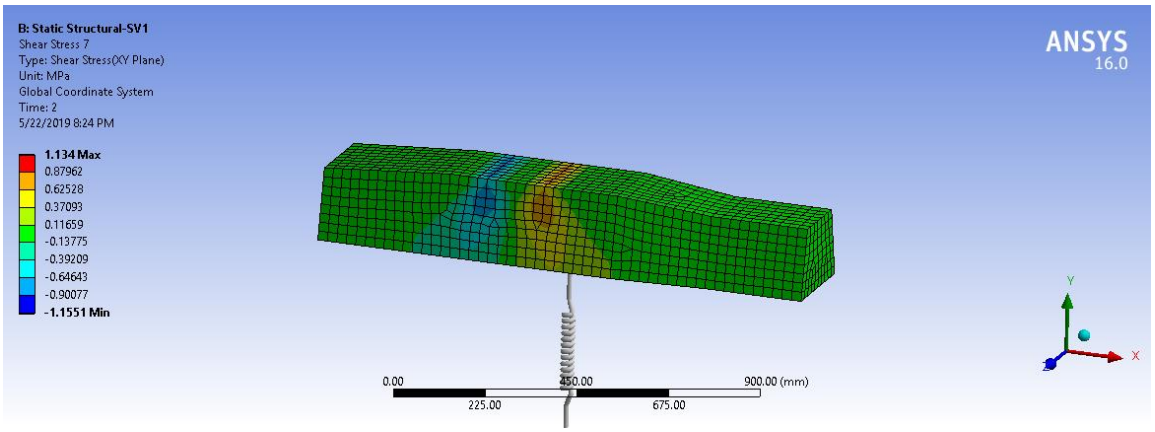

Figure 4-4 Shear stress for SV1 (SL-33)

The total deformation, equivalent stress and shear stress along the sleeper length (SL-33) at top and bottom section are shown in figure 4-5 to 4-6 and figure 4-7 to 4-8 respectively.

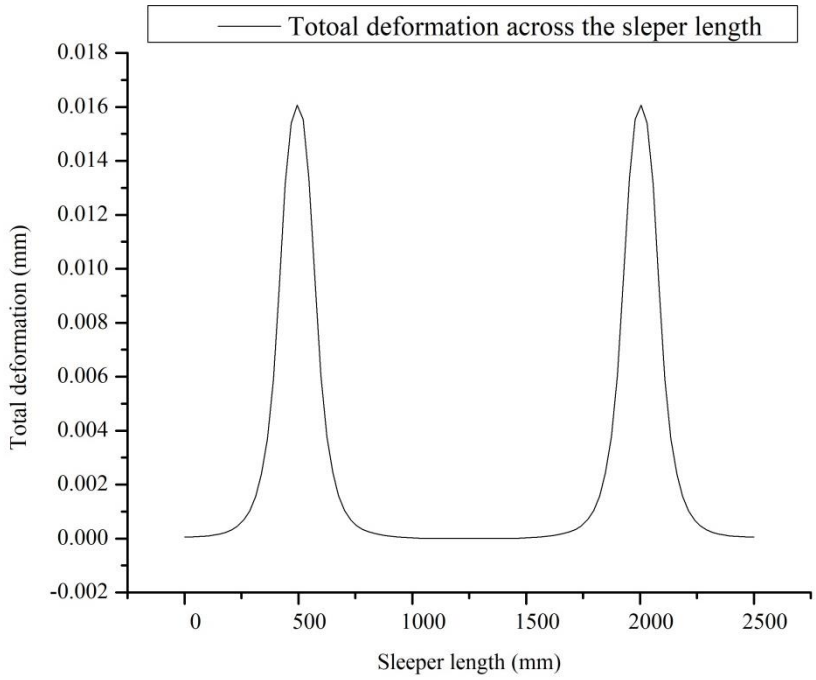

Figure 4-5 Sleeper SV1 Total deformation

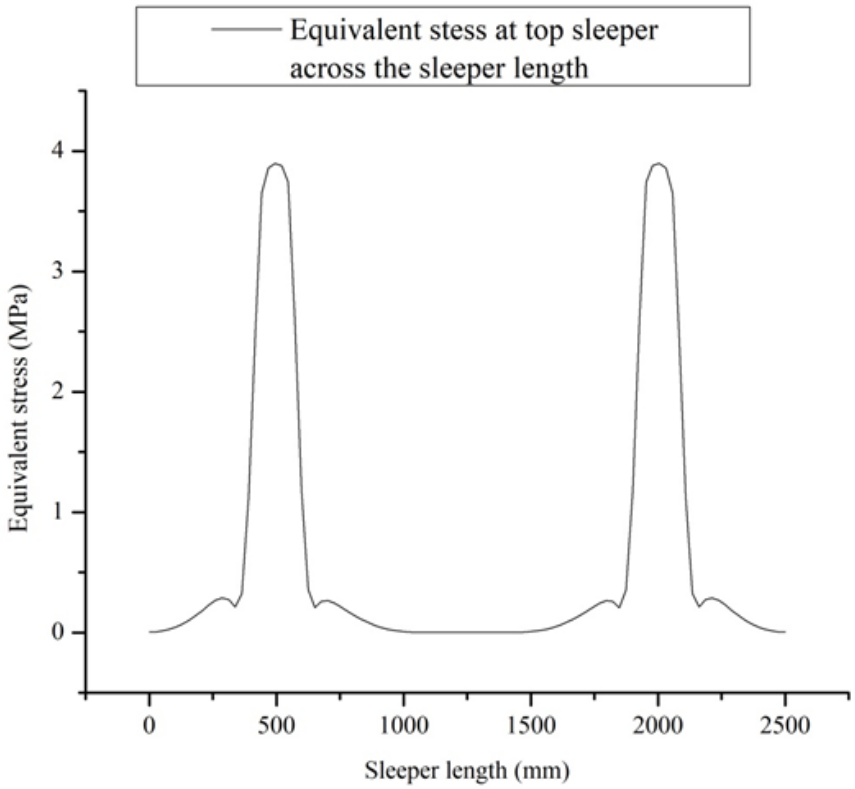

Figure 4-6 Sleeper SV1 (a) equivalent stress at top section at top section

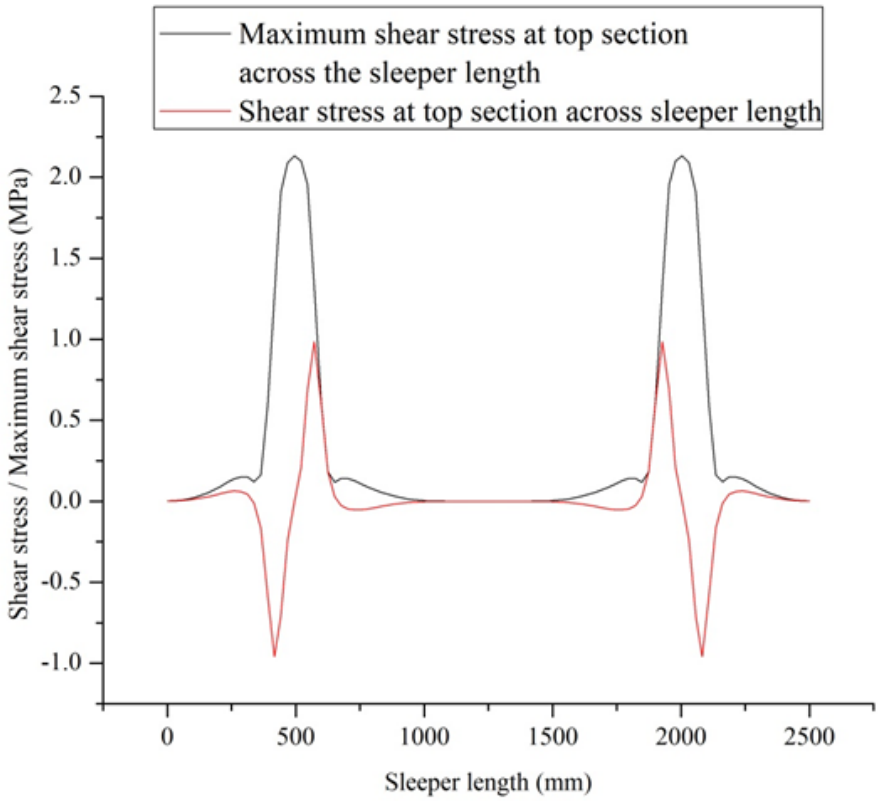

Figure 4-7 Shear stress (in red) and maximum shear stress (in black) at top section

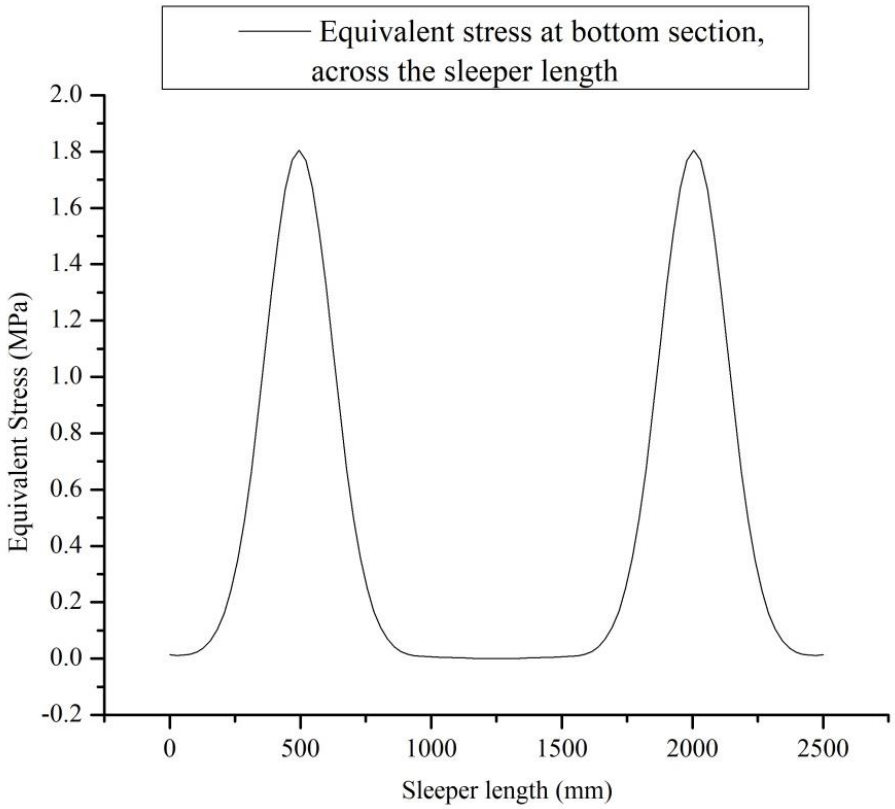

Figure 4-8 Sleeper SV1 equivalent stress at bottom section

The figures 4-5 to 4-8, the pick total deformation and stress (both equivalent and maximum shear) values are located at rail seat section and minimum values at center and end section. The results shown in figure 4-5 to 4-8, the considered through line was at the centre top section. Or, the maximum values may be located at any point at critical sections shown in figure 4-1. Therefore, the recording was based on the use of probe tool as it indicates the maximum values at those critical sections.

In this thesis, fifty-one sleepers have been modelled; the detailed total deformations and stresses for all the selected sleepers are clearly shown in table 4-1. Among the fifty-one sleepers modelled, numerical results of four of them are attached in Appendix F.

Table 4-1: Results from Static simulations

S/N	Sleeper Case	RAIL SEAT					CENTER SECTION					END SECTION				
		Total Displacement (mm)	Stresses (Von-Mises) (MPa)		Stresses (Shear) (Mpa)		Total Displacement (mm)	Stresses (Von-Mises)		Stresses (Shear) (Mpa)		Total Displacement (mm)	Stresses (Von-Mises)		Stresses (Shear) (Mpa)	
			Top	Bottom	Top	Bottom		TOP	Bottom	Top	Bottom		Top	Bottom	Top	Bottom
1	SL-1	0.016	3.64	2.67	0.83	0.55	4E-04	0.336	0.148	-6E-04	-0.009	0.003	0.15	0.769	-0.002	0.2
2	SL-2	0.016	3.76	2.49	0.83	0.56	6E-07	9E-04	5E-04	7E-06	-8E-05	8E-05	0.005	0.03	3E-05	0.01
3	SL-3	0.01	2.31	2.16	0.36	0.33	3E-05	0.002	0.104	7E-05	0.0005	3E-05	0.001	0.053	2E-05	0.03
4	SL-4	0.011	2.28	1.93	0.39	0.67	4E-04	0.445	0.156	0.0004	-0.014	8E-04	0.004	0.228	-2E-04	0.05
5	SL-5	0.021	4.11	1.98	0.97	0.31	1E-04	0.096	0.044	-4E-04	-0.003	0.003	0.036	0.69	-0.002	0.19
6	SL-6	0.019	3.78	2	0.93	0.47	2E-07	2E-04	4E-04	1E-05	-7E-05	1E-04	0.004	0.024	0.0004	0
7	SL-7	0.02	3.63	2.3	0.94	0.76	9E-06	0.013	0.006	4E-05	-5E-04	0.003	0.238	1.179	-0.005	0.42
8	SL-8	0.021	3.54	1.97	0.98	0.79	2E-04	0.18	0.088	-9E-04	-0.006	0.003	0.153	0.891	-0.002	0.26
9	SL-9	0.021	3.74	2.01	1.02	0.82	0.001	0.821	0.386	0.0599	-0.002	2E-04	0.006	0.048	0.0006	0.01
10	SL-10	0.016	3.71	2.46	0.84	0.54	9E-07	0.001	7E-04	3E-06	-9E-05	7E-05	0.005	0.026	8E-05	0
11	SL-11	0.016	3.49	2.43	0.8	1.09	0.001	1.023	0.428	0.0043	-0.017	0.005	0.798	2.402	-9E-04	0.89
12	SL-12	0.01	2.12	1.75	0.36	0.47	5E-06	0.003	0.013	-1E-06	0.0007	0.001	0.075	0.342	-3E-04	0.09
13	SL-13	0.01	2.12	1.76	0.44	0.4	3E-07	4E-04	2E-04	2E-06	-3E-05	2E-05	0.001	0.01	-5E-05	0

S/N	Sleeper Case	RAIL SEAT					CENTER SECTION					END SECTION				
		Total Displacement (mm)	Stresses (Von-Mises) (MPa)		Stresses (Shear) (Mpa)		Total Displacement (mm)	Stresses (Von-Mises)		Stresses (Shear) (Mpa)		Total Displacement (mm)	Stresses (Von-Mises)		Stresses (Shear) (Mpa)	
			Top	Bottom	Top	Bottom		Top	Bottom	Top	Bottom		Top	Bottom	Top	Bottom
14	SL-14	0.02	3.89	2.05	0.93	0.36	0.002	0.32	0.582	0.0032	0.0022	0.007	0.234	1.806	-0.006	0.58
15	SL-15	0.019	3.74	2.08	0.87	1.11	1E-03	0.49	0.306	0.0242	-0.012	4E-04	0.006	0.082	0.0004	0.02
16	SL-16	0.018	3.6	1.97	0.83	0.45	4E-07	8E-04	5E-04	8E-06	-8E-05	8E-05	0.003	0.02	0.0003	0
17	SL-17	0.021	3.76	1.86	1.04	0.96	0.001	0.846	0.331	0.0379	-0.01	0.002	0.086	0.619	-0.001	0.22
18	SL-18	0.022	4.1	1.98	1.07	0.35	4E-05	0.031	0.016	-5E-05	-7E-04	9E-04	0.022	0.198	0.0024	0.04
19	SL-19	0.015	3.5	2.8	0.77	0.49	2E-05	0.017	0.01	-6E-05	-6E-04	0.005	1.149	3	0.0096	0.96
20	SL-20	0.015	3.57	2.37	0.74	0.52	6E-07	0.001	5E-04	3E-06	-7E-06	8E-05	0.005	0.027	0.0001	0
21	SL-21	0.021	3.92	1.69	0.91	0.4	3E-06	9E-04	0.002	-1E-05	-2E-04	3E-04	0.006	0.03	0.0012	-0
22	SL-22	0.02	3.72	1.76	0.86	0.42	2E-07	1E-04	6E-04	2E-05	-1E-04	2E-04	0.004	0.025	0.0009	0
23	SL-23	0.02	3.8	1.82	0.96	0.43	4E-07	7E-04	3E-04	2E-05	-7E-05	2E-04	0.006	0.03	0.0008	0
24	SL-24	0.021	3.76	1.83	0.95	0.74	3E-04	0.266	0.129	-1E-04	-0.009	4E-04	0.006	0.077	0.0005	0.01
25	SL-25	0.022	3.81	1.97	1.09	1.08	0.001	1.076	0.484	0.0597	-0.01	8E-04	0.008	0.155	0.0002	0.03
26	SL-26	0.023	4.1	1.8	1.03	0.84	3E-04	0.323	0.13	-0.001	-0.01	0.004	0.427	1.557	-0.012	0.56
27	SL-27	0.02	3.8	1.88	0.89	0.66	0.001	0.874	0.482	0.0569	0.0378	2E-04	0.007	0.033	0.0018	0

S/N	Sleeper Case	RAIL SEAT					CENTER SECTION					END SECTION				
		Total Displacement (mm)	Stresses (Von-Mises) (MPa)		Stresses (Shear) (Mpa)		Total Displacement (mm)	Stresses (Von-Mises)		Stresses (Shear) (Mpa)		Total Displacement (mm)	Stresses (Von-Mises)		Stresses (Shear) (Mpa)	
			Top	Bottom	Top	Bottom		Top	Bottom	Top	Bottom		Top	Bottom	Top	Bottom
28	SL-28	0.019	3.65	1.83	0.89	0.44	1E-04	0.087	0.039	0.0027	-4E-04	1E-04	0.007	0.052	0.001	0
29	SL-29	0.02	3.55	1.91	1.08	0.47	0.002	1.345	0.741	0.0693	-0.055	0.007	0.265	2.352	-0.018	0.78
30	SL-30	0.021	3.6	2.41	1.04	1.25	0.001	0.828	0.416	0.0505	-0.003	6E-04	0.008	0.125	0.0008	0.03
31	SL-31	0.019	3.5	1.82	0.82	1.02	0.002	1.093	0.39	0.0419	0.0002	0.005	0.302	2.231	-3E-04	0.82
32	SL-32	0.018	3.39	1.78	1.01	0.7	0.001	0.863	0.335	0.0401	-0.013	0.003	0.198	0.753	-0.002	0.23
33	SL-33	0.019	3.64	1.81	0.85	0.42	3E-07	2E-04	4E-04	2E-05	-8E-05	6E-05	0.004	0.013	0.0007	0
34	SL-34	0.02	3.78	1.87	0.97	0.44	4E-07	5E-04	1E-04	2E-05	-5E-05	1E-04	0.005	0.027	0.0006	0
35	SL-35	0.019	3.97	2.4	0.97	0.15	5E-05	0.071	0.033	-4E-04	-0.003	0.005	0.6	2.261	-0.007	0.81
36	SL-36	0.019	3.69	1.84	0.92	0.45	7E-05	0.082	0.019	0.0004	-0.001	1E-04	0.008	0.029	0.0016	0
37	SL-37	0.019	3.54	1.88	0.89	0.4	0.001	0.946	0.469	0.0576	-0.011	0.007	0.881	2.72	-0.003	0.97
38	SL-38	0.019	3.73	1.84	0.92	0.44	4E-07	4E-04	2E-04	2E-05	-3E-05	1E-04	0.007	0.026	0.001	0
39	SL-39	0.02	3.87	1.9	0.89	0.44	3E-07	2E-04	0.003	2E-05	-1E-04	0.006	0.027	0.023	0.0011	0
40	SL-40	0.02	3.66	2.13	1.11	1.12	0.003	3.1	0.921	0.022	-0.007	0.006	0.08	1.395	-0.001	0.41
41	SL-41	0.021	3.7	2.21	0.97	1.14	0.003	1.998	0.8	0.045	-0.008	0.004	0.147	1.079	-0.001	0.34

S/N	Sleeper Case	RAIL SEAT					CENTER SECTION					END SECTION				
		Total Displacement (mm)	Stresses (Von-Mises) (MPa)		Stresses (Shear) (Mpa)		Total Displacement (mm)	Stresses (Von-Mises)		Stresses (Shear) (Mpa)		Total Displacement (mm)	Stresses (Von-Mises)		Stresses (Shear) (Mpa)	
			Top	Bottom	Top	Bottom		Top	Bottom	Top	Bottom		Top	Bottom	Top	Bottom
42	SL-42	0.021	3.87	2.35	0.94	1.01	0.002	0.946	0.852	0.034	0.0309	0.005	0.421	2.213	-0.003	0.83
43	SL-43	0.019	3.65	1.81	0.86	0.43	3E-07	3E-04	4E-04	1E-05	-8E-05	1E-04	0.004	0.024	0.0006	0
44	SL-44	0.02	3.8	2.1	1.06	0.43	9E-06	0.007	0.004	1E-05	-2E-04	2E-04	0.007	0.042	0.0004	0.01
45	SL-45	0.02	3.6	2.06	0.98	0.58	1E-04	0.182	0.085	0.0012	-0.006	0.01	0.853	2.007	0.0243	0.45
46	SL-46	0.02	3.71	2.06	1.17	0.54	0.001	0.9	0.394	0.0494	-0.004	0.001	0.031	0.337	0.0008	0.08
47	SL-47	0.02	3.59	1.91	1.03	0.88	0.001	0.648	0.498	0.0622	0.0116	7E-05	0.001	0.024	8E-06	0.01
48	SL-48	0.021	3.79	2	1.02	0.45	5E-04	0.285	0.186	-7E-04	-0.011	0.002	0.046	0.438	0.0022	0.1
49	SL-49	0.019	3.65	1.81	0.87	0.45	3E-07	3E-04	4E-04	1E-05	-8E-05	7E-05	0.005	0.015	0.0007	0
50	SL-50	0.021	3.95	2.66	1.16	1.33	0.003	2.261	0.936	0.0641	-0.046	0.007	0.664	2.778	-3E-04	0.99
51	SL-51	0.02	3.79	1.82	0.94	0.43	4E-07	7E-04	3E-04	2E-05	-7E-05	2E-04	0.008	0.028	0.0013	0

The results in table 4-1 show the static results from FEM. The same procedure used in validation was followed in simulations. The total deformation, equivalent stress and shear stress were recorded by considering the critical part on a sleeper like rail seat, center section and end section. Probe tool in ANSYS Workbench was used and the deformation results are shown in table 4-1. Pick deformations at sleeper 26, 18 at sleeper rail seat; sleeper 40 and 45 at sleeper end and sleeper 41 and 51 at sleeper center section were reported. Rectangular sleeper sections have lower deformation compared to other shape section as the top and bottom width of rectangular section is higher than the other selected sleeper cases.

The high equivalent stress values were found on sleeper 5, 18 and 26 at top rail seat section; 50, 41, 40 and 29 at top center and 19, 37, 45 and 11 at top end sections. The sleeper 13, 12, 4 and 3 at top rail seat section and 2, 3, 6, 10, 13, 18, 20, 21, 22, 23, 33, 34, 38, 39, 43, 44, 49, 51 at top center and top end sections are having the minimum values. Whereas, the high peak equivalent stress at bottom rail seat are located at sleeper 50, 19 and 1. Sleeper 50, 40, 29, 42 had maximum equivalent stress at the bottom center sections while were sleeper 18, 49, 36, 10, 39 and 28 had higher equivalent stress at bottom end section. Both sleeper 13, 4, 5, 13 at bottom rail seat and 5, 12, 19, 20, 21, 22, 23, 33, 35, 38, 43 at bottom center and end sections had small values of equivalent stress.

4.1.1.4 Bending stress

Bending stress is the normal stress that is induced at a point in a body subjected to loads that cause it to bend. The bending stress is a more specific type of normal stress. Like the shear stress, the bending stress also varies across the cross-sectional area. Equation 3-14 was used to compute the bending stresses that were shown in table 4-2.

Table 4-2 Bending stress for static results

S/N	Sleeper Case	Sleeper Name	Rail seat Bending stress (Mpa)		Center Bending stress (Mpa)		End Bending stress (Mpa)	
			Top	Bottom	Top	Bottom	Top	Bottom
1	SL-1	SI-1	3.34	2.49	0.34	0.15	0.15	0.69
2	SL-2	SI-2	3.47	2.29	0.00	0.00	0.00	0.03
3	SL-3	SI-4	2.22	2.08	0.00	0.10	0.00	0.02
4	SL-4	SI-5	2.18	1.54	0.45	0.15	0.00	0.21
5	SL-5	SI-6	3.75	1.90	0.10	0.04	0.04	0.61
6	SL-6	SI-7	3.42	1.83	0.00	0.00	0.00	0.02
7	SL-7	SI-8	3.25	1.88	0.01	0.01	0.24	0.93
8	SL-8	SI-10	3.11	1.43	0.18	0.09	0.15	0.76
9	SL-9	SI-11	3.30	1.43	0.81	0.39	0.01	0.05
10	SL-10	SII-1	3.41	2.27	0.00	0.00	0.00	0.02
11	SL-11	SII-3	3.20	1.54	1.02	0.43	0.80	1.84
12	SL-12	SII-4	2.03	1.55	0.00	0.01	0.08	0.30
13	SL-13	SII-5	1.98	1.62	0.00	0.00	0.00	0.01
14	SL-14	SII-6	3.55	1.96	0.32	0.58	0.23	1.50
15	SL-15	SII-7	3.42	0.80	0.49	0.31	0.01	0.08
16	SL-16	SII-8	3.30	1.81	0.00	0.00	0.00	0.02
17	SL-17	SII-9	3.30	0.84	0.84	0.33	0.09	0.48
18	SL-18	SII-10	3.66	1.89	0.03	0.02	0.02	0.18
19	SL-19	SIII-1	3.24	2.67	0.02	0.01	1.15	2.50
20	SL-20	SIII-3	3.33	2.19	0.00	0.00	0.01	0.03
21	SL-21	SIII-4	3.59	1.54	0.00	0.00	0.01	0.03
22	SL-22	SIII-5	3.41	1.60	0.00	0.00	0.00	0.03
23	SL-23	SIII-6	3.42	1.66	0.00	0.00	0.01	0.03
24	SL-24	SIII-7	3.38	1.31	0.27	0.13	0.01	0.07
25	SL-25	SIII-8	3.31	0.65	1.07	0.48	0.01	0.14
26	SL-26	SIII-9	3.69	1.06	0.32	0.13	0.43	1.21
27	SL-27	SIV-1	3.47	1.49	0.87	0.48	0.01	0.03
28	SL-28	SIV-2	3.31	1.66	0.09	0.04	0.01	0.05
29	SL-29	SIV-3	3.02	1.72	1.34	0.73	0.26	1.92
30	SL-30	SIV-4	3.12	1.04	0.82	0.42	0.01	0.12
31	SL-31	SIV-5	3.20	0.41	1.09	0.39	0.30	1.72
32	SL-32	SIV-6	2.90	1.31	0.86	0.33	0.20	0.64
33	SL-33	SV-1	3.33	1.66	0.00	0.00	0.00	0.01
34	SL-34	SV-2	3.39	1.71	0.00	0.00	0.00	0.03
35	SL-35	SVI-1	3.60	2.39	0.07	0.03	0.60	1.77
36	SL-36	SVI-2	3.34	1.67	0.08	0.02	0.01	0.03

S/N	Sleeper Case	Sleeper Name	Rail seat Bending stress (Mpa)		Center Bending stress (Mpa)		End Bending stress (Mpa)	
			Top	Bottom	Top	Bottom	Top	Bottom
37	SL-37	SVI-3	3.19	1.74	0.94	0.47	0.88	2.14
38	SL-38	SVII-1	3.38	1.68	0.00	0.00	0.01	0.03
39	SL-39	SVII-2	3.55	1.73	0.00	0.00	0.03	0.02
40	SL-40	SVII-3	3.12	0.87	3.10	0.92	0.08	1.20
41	SL-41	SVII-4	3.30	1.00	2.00	0.80	0.15	0.90
42	SL-42	SVII-5	3.51	1.57	0.94	0.85	0.42	1.68
43	SL-43	SVII-6	3.34	1.65	0.00	0.00	0.00	0.02
44	SL-44	SVIII-1	3.33	1.97	0.01	0.00	0.01	0.04
45	SL-45	SVIII-2	3.18	1.80	0.18	0.08	0.85	1.85
46	SL-46	SVIII-3	3.11	1.83	0.90	0.39	0.03	0.31
47	SL-47	SVIII-4	3.11	1.16	0.64	0.50	0.00	0.02
48	SL-48	SVIII-5	3.36	1.84	0.29	0.18	0.05	0.40
49	SL-49	SVIII-6	3.33	1.64	0.00	0.00	0.00	0.02
50	SL-50	SVIII-7	3.41	1.33	2.26	0.93	0.66	2.19
51	SL-51	SVIII-8	3.42	1.66	0.00	0.00	0.01	0.03

The calculation of bending stress from equivalent stress and shear stress were done using equation 3-14. The peak values of bending stress were on sleeper 5, 26, 18, 35, 21 at top rail seat section. Center sections, peak values were on sleeper 50, 41, 40, 29. End sections had peak values occurring on sleeper 19, 37, 45 and 11. As far as the minimum values of the bending stress at top section are concerned, the sleeper 13, 12, 3, 4, 32 at top rail seat and sleeper 2, 3, 6, 10, 16, 18, 20, 21, 22, 23, 33, 34, 38, 39, 43, 44, 49 and 51 at both center and end sections were found. The critical sleepers as far as the bending stresses at bottom sleeper section was concerned were sleeper 19, 35, 40, 50, 42, 37, 29, 31, 14, 11, 9, 1, 5, 7. The sleepers that are having small stress are 25, 15, and 17.

4.1.2 Impact behavior of prestressed concrete sleepers

As discussed in chapter three, the prestressed concrete sleeper was analyzed using ANSYS Workbench explicit dynamic for impact analysis. The impact simulations have been conducted on fifteen among the fifty-one sleepers selected for static through explicit dynamic analysis. In this section, the analysis results of the selected models are presented.

4.1.2.1 Deformation

In ANSYS Workbench; deformation results are generally obtained as either total deformation or directional deformation. The models are composed of sleeper, rail and impactor. Sleepers, of concern in this research, have been analysed to locate deformations. The maximum deformation obtained in the sleeper occurs at rail seat. Critical sections such as the rail seat, center and end sections have been emphasized to record the corresponding deformation.

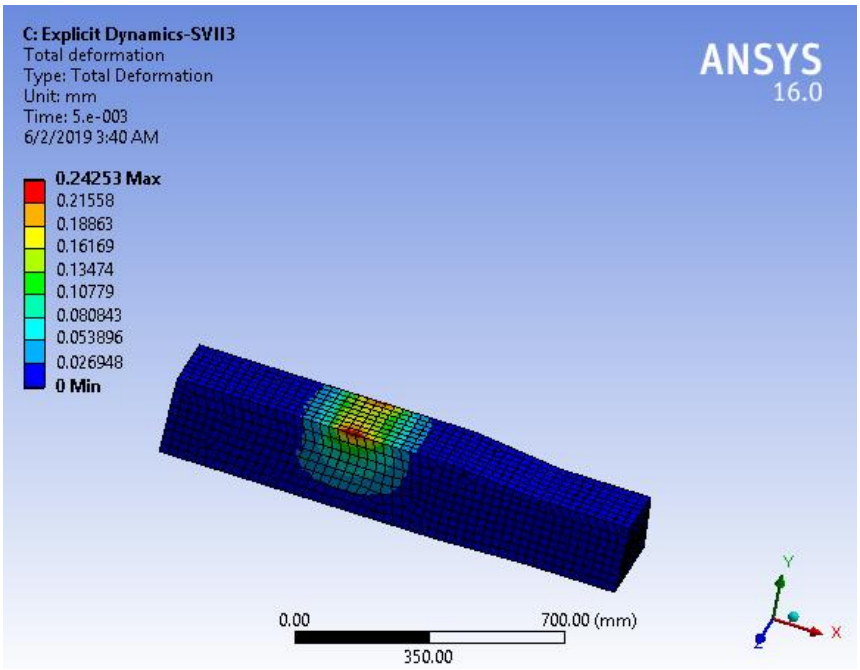

Figure 4-9 Total deformation for SVII3 (SL-40).

4.1.2.2 Equivalent (Von-Mises) stress

The sleeper part of the model has been selected and the stresses, evaluated as shown in figure 4-10 below.

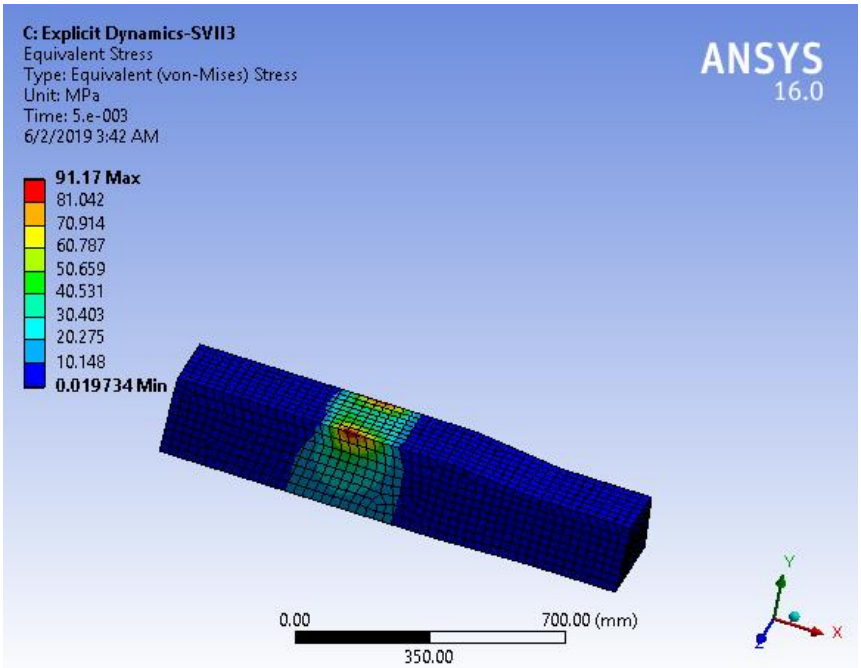

Figure 4-10 Equivalent (von-mises) stress for SVII3 (SL-11)

Deformation and stresses along the sleeper length (SL-40) are shown in figure 4-11 to 4-14.

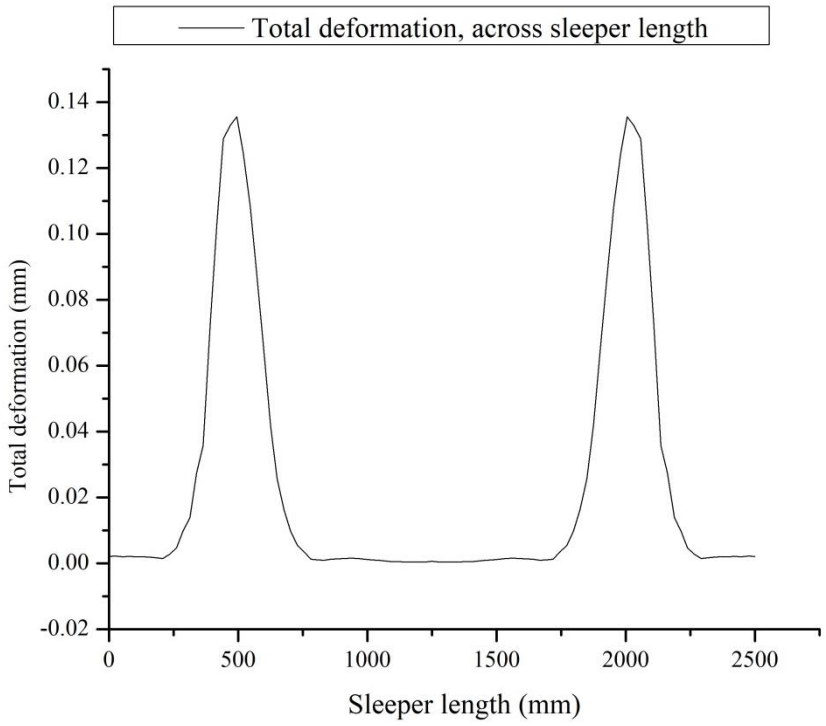

Figure 4-11 Total deformation

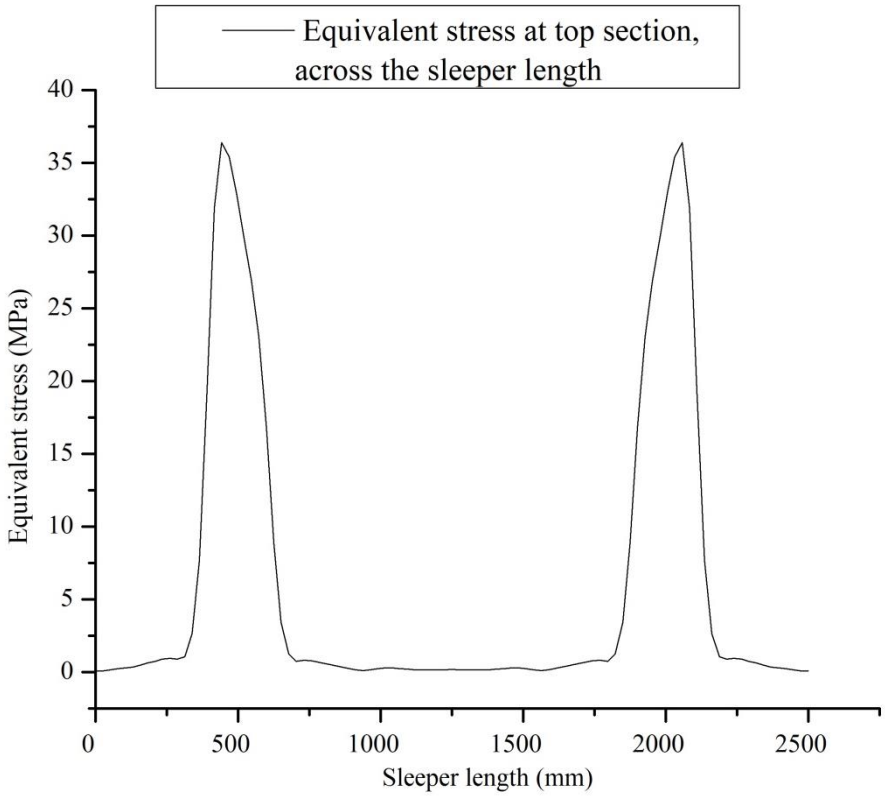

Figure 4-12 Sleeper SVII-3 equivalent stress at top section

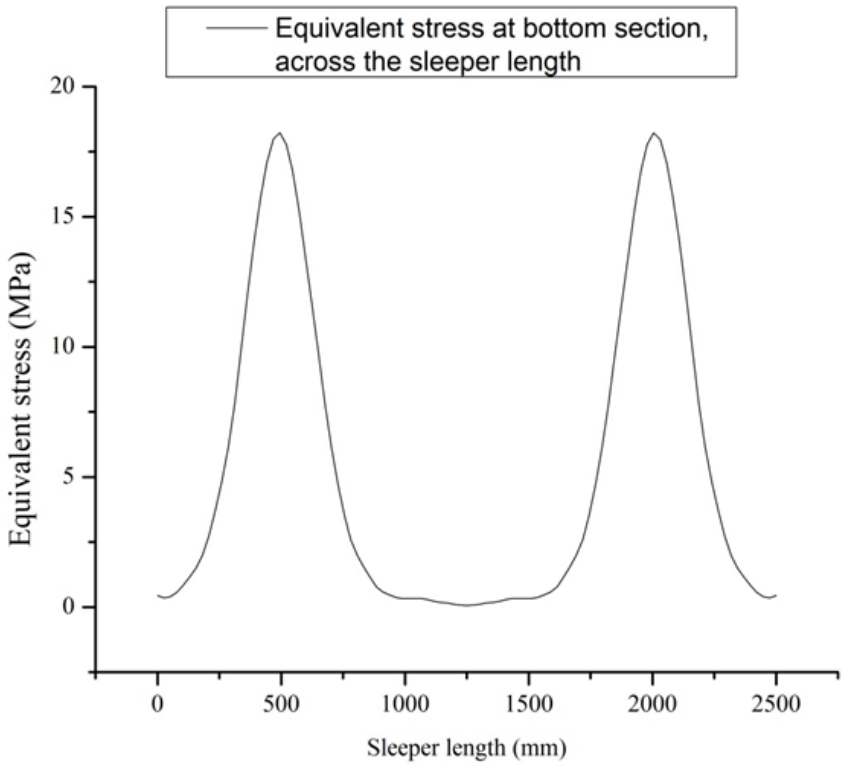

Figure 4-13 Sleeper SVII-3 equivalent stress at bottom section

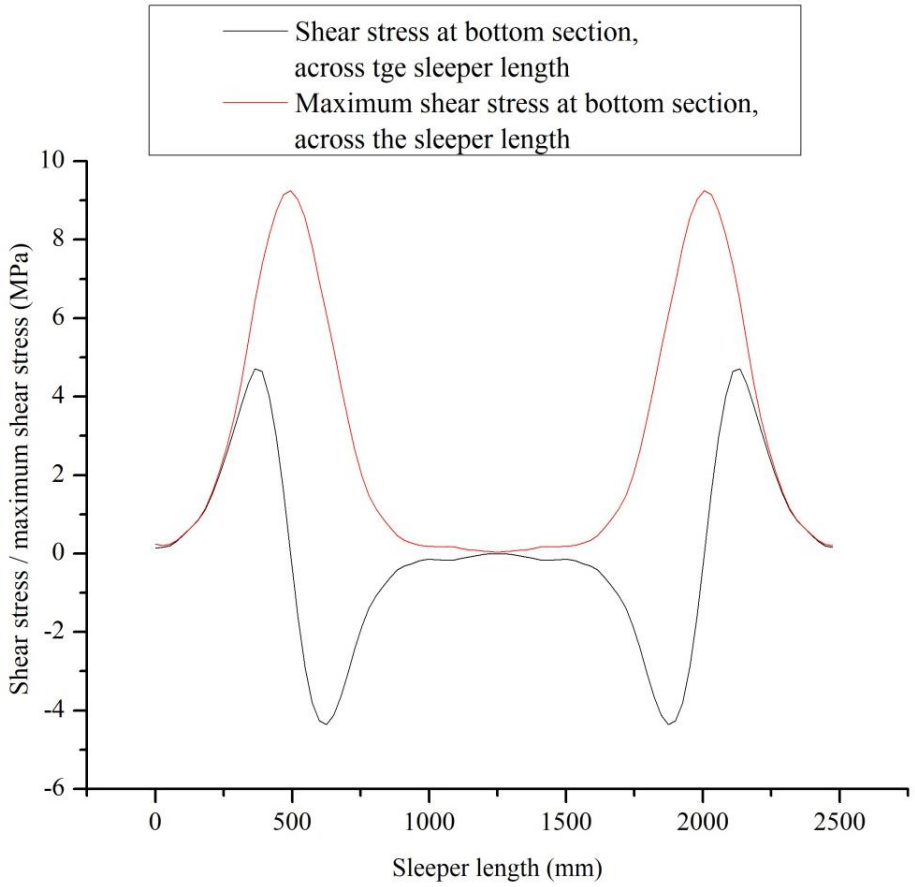

Figure 4-14 Sleeper SVII-3 Shear stress (in black) and maximum shear (in red) stress at bottom section

The figures 4-11 to 4-14, the pick total deformation and stress (both equivalent and maximum shear) values are located at rail seat section and minimum values at center and end section. The maximum values may be located at any point at critical sections shown in figure 4-1 as the considered line was at the centre top section.

The detailed deformations and stresses for the fifteen sleepers were recorded at rail seat, center and end sections of the sleeper as shown in table 4-3. The recording was based on the use of probe tool as it indicates the maximum values at the critical sections shown in figure 4-1. Among the fifteen sleepers modelled, four of them are attached in Appendix G.

Table 4-3 Results from Impact Simulations

S/N	Sleeper Case	RAIL SEAT					CENTER SECTION					END SECTION				
		Deformation (mm)	Equivalent Stresses (Mpa)		Shear Stress (Mpa)		Deformation (mm)	Equivalent Stresses (Mpa)		Shear Stress (Mpa)		Deformation (mm)	Equivalent Stresses (Mpa)		Shear Stress (Mpa)	
			Top	Bottom	Top	Bottom		Top	Bottom	Top	Bottom		Top	Bottom	Top	Bottom
1	SL-8	0.24	92.45	19.61	47.37	10.08	0.0005	0.27	0.10	0.13	0.06	0.0030	0.05	0.66	0.03	0.35
2	SL-11	0.18	51.93	22.98	26.30	11.87	0.0009	0.19	0.19	0.10	0.10	0.0020	0.06	0.54	0.03	0.28
3	SL-17	0.24	91.54	21.36	46.61	10.87	0.0007	0.12	0.20	0.06	0.11	0.0039	0.08	0.49	0.05	0.26
4	SL-18	0.23	84.06	18.29	42.53	9.32	0.0069	0.28	0.16	0.14	0.09	0.0021	0.22	0.42	0.11	0.22
5	SL-19	0.17	55.70	23.34	28.51	12.01	0.0008	0.24	0.15	0.13	0.08	0.0021	0.12	0.39	0.07	0.21
6	SL-23	0.25	90.58	17.06	46.14	8.67	0.0004	0.18	0.11	0.10	0.06	0.0021	0.10	0.51	0.06	0.28
7	SL-25	0.23	85.45	16.70	43.59	8.53	0.0002	0.05	0.03	0.03	0.02	0.0020	0.22	0.42	0.13	0.23
8	SL-30	0.25	114.66	19.03	58.97	9.98	0.0005	0.22	0.10	0.12	0.05	0.0019	0.40	0.30	0.20	0.17
9	SL-33	0.24	88.89	19.19	44.27	10.16	0.0017	0.12	0.38	0.07	0.20	0.0026	0.08	0.57	0.04	0.31
10	SL-35	0.23	80.36	18.36	40.61	9.52	0.0039	0.29	0.33	0.16	0.17	0.0055	0.13	0.66	0.07	0.35
11	SL-36	0.24	86.94	18.60	43.95	9.72	0.0015	0.20	0.23	0.11	0.13	0.0035	0.11	0.51	0.06	0.28
12	SL-37	0.24	93.47	18.78	48.10	9.54	0.0017	0.35	0.15	0.19	0.08	0.0050	0.12	0.78	0.06	0.41
13	SL-40	0.24	91.17	18.43	46.65	9.61	0.0009	0.18	0.17	0.10	0.09	0.0033	0.10	0.54	0.06	0.30
14	SL-41	0.24	88.57	17.98	44.63	9.23	0.0025	0.28	0.48	0.15	0.27	0.0020	0.12	0.39	0.07	0.21
15	SL-45	0.23	83.01	18.03	41.85	9.12	0.0005	0.10	0.13	0.05	0.07	0.0050	0.06	1.12	0.04	0.60

The total deformation, equivalent stress and shear stress have been recorded by considering the critical part on a sleeper like rail seat, center section and end section. The probe tool in ANSYS Workbench has been used and all results are shown in table 4-3. The maximum deformation was located on sleeper 23 and 30. The minimum value was recorded for sleeper 19 and 11. The rectangular sleeper sections that had lower deformations compare to the other shapes as discussed above. It was found that the results such as deformation and stresses at center and end sections are very small compare to the results at rail seat section.

The peak equivalent stress at top rail seat is located in sleeper 30 while the minimum in sleeper 11 and 19. The maximum equivalent stress at bottom rail seat section is located to the sleeper 19, 11, 17 and 8 whereas; the minimum value was on sleeper 25, 23, 45, 41 and 40.

4.1.2.3 Bending stress

The relationship between the equivalent stress, shear stress and bending stress for impact analysis are shown in table 4-4. FEM analysis gave both equivalent stress and shear stress. The equation 3-14 was used to determine the bending stresses.

Table 4-4 Bending stress from impact results

Sleeper Name	Sleeper Case	RAIL SEAT SECTION			CENTER SECTION		END SECTION	
		Total deformation (mm)	Bending Stresses (Mpa)		Bending Stresses (Mpa)		Bending Stresses (Mpa)	
			Top	Bottom	Top	Bottom	Top	Bottom
SI10	SL-8	0.24	42.6001	8.9271	0.1288	0.0002	0.0012	0.2528
SII3	SL-11	0.18	24.9266	10.2500	0.0780	0.0845	0.0255	0.2341
SII8	SL-17	0.24	43.1638	10.0650	0.0482	0.0550	0.0100	0.1685
SII9	SL-18	0.23	40.4888	8.6077	0.1264	0.0469	0.1007	0.1559
SIII1	SL-19	0.17	25.7535	10.5833	0.0399	0.0540	0.0470	0.1485
SIII6	SL-23	0.25	42.6449	8.0999	0.0534	0.0113	0.0028	0.1768
SIII8	SL-25	0.23	40.0332	7.7903	0.0020	0.0055	0.0434	0.1065
SIV4	SL-30	0.25	52.0978	7.9491	0.0510	0.0404	0.1919	0.0714
SV1	SL-33	0.24	44.9521	7.6581	0.0354	0.1302	0.0035	0.2116
SVI1	SL-35	0.23	38.8708	8.0518	0.0992	0.1371	0.0173	0.2646
SVI2	SL-36	0.24	41.9960	7.8962	0.0614	0.0863	0.0329	0.1845
SVI3	SL-37	0.24	42.3994	8.9278	0.1370	0.0150	0.0480	0.3449

Sleeper Name	Sleeper Case	RAIL SEAT SECTION			CENTER SECTION		END SECTION	
		Total deformation (mm)	Bending Stresses (Mpa)		Bending Stresses (Mpa)		Bending Stresses (Mpa)	
			Top	Bottom	Top	Bottom	Top	Bottom
SVII3	SL-40	0.24	42.2391	7.8874	0.0310	0.0459	0.0330	0.1528
SVII4	SL-41	0.24	43.2376	8.2109	0.1041	0.1000	0.0239	0.1726
SVIII2	SL-45	0.23	40.4297	8.6964	0.0416	0.0485	0.0131	0.4284

The results showed in table 4-4 above reveal that the maximum bending stress at top sleeper section was located to the sleeper 30, 17 and 41 while the minimum value was in sleeper 11 and 19. The maximum bending stress at bottom rail seat section on sleeper 19, 11, 17, 8, 37, 45 and 18 while the minimum values were in sleeper 33, 40, 36 and 25.

4.2 Selection of the best geometrical sleeper shape

4.2.1 Static and Impact results

4.2.1.1 Static results

The capacity of the sleeper design has to be checked to ensure that the applied bending stress in compression and tension not to be are above the maximum permissible stresses in compression and tension specified in AS 1085.14-2003. The permissible compressive and tensile stresses were computed according to the equation provided by Australian Standards (AS 1085.14-2003). As shown in table 3-8, the following permissible stresses were computed.

Table 4-5 Permissible stress according to AS 1085.14-2003

Permissible compressive stress	Permissible tensile stress
27 Mpa	3.1 Mpa

From the static results shown in table 4-1 and 4-2, the selected sleepers were safe. The maximum permissible stress in compression and tension was computed as 27 and 3.1 Mpa respectively as shown in table 4-5. Both von mises and bending stress at top rail seat, bottom center and end section were all less than 27 Mpa while the von mises and bending stress at bottom rail seat, top center and top end section were also less than 3.1

Mpa. Therefore, all the selected sleeper shapes were deemed safe as far as static loading was concerned.

4.2.1.2 Impact results

The impact results shown in table 4-4, all top rail seat, bottom center and end sections results were greater than 27 Mpa except the sleeper SII3 (SL-11) and SIII1 (SL-19) having bending stresses of 24.9266 Mpa and 25.7535 Mpa respectively. Considering the bottom bending stress; all values were greater than the permissible stress at tension (3.1 Mpa). Therefore, the selected sleepers were not safe.

The impact simulation conducted on the selected sleepers was high and the sleepers were thus not able to resist those loadings. In fact, when a load was applied to rail in a track system, the load was distributed to other sleepers. When the impact mass of 592 kg was applied to rail, the direct sleeper didn't fully support all load created by the impactor in contact with the rail. A distribution factor was given using figure 3-12 and 3-13. As per AREMA and AS 1085.14-2003, a factor of 0.5 and 0.51 are selected respectively when the sleeper spacing is 600 mm.

In the case of this thesis research, a factor of 0.51 was used. Thus, the modified mass used for one case was equal to 592 kg*0.51 = 309.92 kg. Sleeper SII3 was thus selected. Results from the impact simulations show that the critical part is the rail seat area. Only the rail seat values were thus considered. For the modified impact mass; the results were shown in table 4-6.

Table 4-6 Impact results for sleeper SII3 with both modified and non-modified impact mass

Results with 592 kg impact mass			**Results with a modified impact mass**		
Bending stress at top sleeper (Mpa)	Bending stress at bottom sleeper (Mpa)	Deformation (mm)	Bending stress at top sleeper (Mpa)	Bending stress at bottom sleeper (Mpa)	Deformation (mm)
24.9266	10.25	0.17869	9.34368	3.97372	0.068671

From the values in table 4-6; the factors computed were listed in table 4-7 below.

Table 4-7 Multiplication factor on impact results

Element to consider	Factor
Bending stress at top sleeper (Mpa)	0.37485
Bending stress at bottom sleeper (Mpa)	0.38768
Deformation (mm)	0.3843

Among the above factors in table 4-7, the maximum was taken into account, 0.38768, and multiplied to the values in table 4-4, after which bending stress and deformations were computed. The ratio between the obtained values and actual values was applied to all values in assumption of a linear distribution. Impact results are shown in table 4-8.

Table 4-8 impact results according to the modified impact mass

S/N	Sleeper name	Sleeper case	RAIL SEAT SECTION			CENTER SECTION		END SECTION	
			Deformation (mm)	Bending Stresses (Mpa)		Bending Stresses (Mpa)		Bending Stresses (Mpa)	
				Top	Bottom	Top	Bottom	Top	Bottom
1	SI10	SL-8	0.0926	16.5152	3.4609	0.0500	0.0001	0.0004	0.0980
2	SII3	SL-11	0.0693	9.6635	3.9737	0.0302	0.0328	0.0099	0.0907
3	SII8	SL-17	0.0944	16.7338	3.9020	0.0187	0.0213	0.0039	0.0653
4	SII9	SL-18	0.0908	15.6967	3.3370	0.0490	0.0182	0.0390	0.0604
5	SIII1	SL-19	0.0667	9.9841	4.1029	0.0155	0.0209	0.0182	0.0576
6	SIII6	SL-23	0.0954	16.5326	3.1402	0.0207	0.0044	0.0011	0.0685
7	SIII8	SL-25	0.0881	15.5201	3.0201	0.0008	0.0021	0.0168	0.0413
8	SIV4	SL-30	0.0954	20.1973	3.0817	0.0198	0.0157	0.0744	0.0277
9	SV1	SL-33	0.0923	17.4270	2.9689	0.0137	0.0505	0.0014	0.0820
10	SVI1	SL-35	0.0899	15.0694	3.1215	0.0384	0.0532	0.0067	0.1026
11	SVI2	SL-36	0.0947	16.2810	3.0612	0.0238	0.0335	0.0128	0.0715
12	SVI3	SL-37	0.0945	16.4374	3.4611	0.0531	0.0058	0.0186	0.1337
13	SVII3	SL-40	0.0940	16.3753	3.0578	0.0120	0.0178	0.0128	0.0592
14	SVII4	SL-41	0.0924	16.7623	3.1832	0.0404	0.0388	0.0093	0.0669
15	SVIII2	SL-45	0.0884	15.6738	3.3714	0.0161	0.0188	0.0051	0.1661

The higher bending stresses at top sleeper section were located in sleeper 30, 17, and 41 while the lower value to sleeper 11 and 19. The higher bending stress at bottom rail seat section was located to sleeper 19, 11, 17, 8, 37, 45 and 18 while the lower values to sleeper 33, 40, 36 and 25. The sleeper: SIII8 (SL-25), SIV4 (SL-30), SV1 (SL-33), SVI2 (SL-36) and VII3 (SL-40) was found to be safe when the modified impactor was applied to those models as per table 4-8 when the bending stresses at bottom rail seat section are

compared to the permissible value of 3.1 MPa. The selected sleeper was of rectangular sections, trapezoid sections and irregular hexagon sections. Among those models; the irregular hexagon sections were the safest sleeper shape as far as the impact loading and static loading are concerned.

4.2.1.3 Ranking the sleeper according to safety

Safety ranking was based on bending stress in comparison with the permissible stresses. The total deformation was not considered in the analysis as they are qualifying very small values as shown in table 4-1, 4-3 and 4-8. The bending stress has to be lower than the permissible stresses provided by Australian standards. Therefore, the ratio between the permissible stresses and the bending stresses should be greater than 1. Ratios for the selected five sleepers were computed for the sleepers as shown in table 4-8. Sleeper cases SL-25, SL-30, SL-33, SL-36 and SL-40 were considered and the corresponding rankings are shown in table 4-9 below.

Table 4-9 Ratio of permissible and bending stresses according to impact results

Sleeper Name	Cases	Bending Stresses (Mpa)	Permissible stress at compression (Mpa)	Ratio	Bending Stresses (Mpa)	Permissible stress at compression (Mpa)	Ratio
SIII8	SL-25	15.52	27	**1.74**	3.02	3.1	**1.026**
SIV4	SL-30	20.20	27	**1.34**	3.08	3.1	**1.006**
SV1	SL-33	17.43	27	**1.55**	2.97	3.1	**1.044**
SVI2	SL-36	16.28	27	**1.66**	3.06	3.1	**1.013**
SVII3	SL-40	16.38	27	**1.65**	3.056	3.1	**1.014**

Safety ranking was given to the sleeper according the values shown in table 4-9. To evaluate and rank the consideration of the criteria in theses sleepers; a value of 1 to 5 was assigned to the selected sleeper shown in table 4-9. The ranking was taken as the higher the ratio, the lower the ranking as shown in table 4-10 below.

Table 4-10 Safety ranking per sleeper case

Sleeper Name	Cases	Ratio (Compression)	Ranking	Ratio (Tension)	Ranking
SIII8	SL-25	1.74	**1**	1.026	**2**
SIV4	SL-30	1.34	**5**	1.006	**5**
SV1	SL-33	1.55	**4**	1.044	**1**
SVI2	SL-36	1.66	**2**	1.013	**4**
SVII3	SL-40	1.65	**3**	1.014	**3**

The overall ranking was calculated with the summation of the two values. Rank one was given to the lower value as shown in table 4-11. The sleeper with lowest overall ranking was selected as the safest sleeper to resist impact loadings.

Table 4-11 Overall ranking for impact simulations

S/N	Sleeper Name	Cases	Sum of rankings	Overall Ranking
1	SIII8	SL-25	3	**1**
2	SIV4	SL-30	10	**4**
3	SV1	SL-33	5	**2**
4	SVI2	SL-36	6	**3**
5	SVII3	SL-40	6	**3**

The static results were reviewed against safety for the sleeper shown in table 4-11 above. Respective individual ratios and ranking are shown in table 4-12, and 4-13 respectively.

Table 4-12 Ratio of permissible and bending stress according to static results

Sleeper Code	Cases	Bending Stresses (Mpa)	Permissible stress at compression (Mpa)	Ratio	Bending Stresses (Mpa)	Permissible stress at compression (Mpa)	Ratio
SIII8	SL-25	3.306	27	**8.166**	0.647	3.1	**4.795**
SIV4	SL-30	3.122	27	**8.648**	1.040	3.1	**2.982**
SV1	SL-33	3.333	27	**8.100**	1.660	3.1	**1.868**
SVI2	SL-36	3.336	27	**8.095**	1.672	3.1	**1.854**
SVII3	SL-40	3.117	27	**8.663**	0.872	3.1	**3.553**

Table 4-13 safety ranking and overall ranking as per static results

Sleeper Code	Cases	Ratio (Compression)	Ranking	Ratio (Tension)	Ranking	Sum of rankings	Overall ranking
SIII8	SL-25	8.166	3	4.795	1	4	**2**
SIV4	SL-30	8.648	2	2.982	3	5	**3**
SV1	SL-33	8.100	4	1.868	4	8	**4**
SVI2	SL-33	8.095	5	1.854	5	10	**5**
SVII3	SL-40	8.663	1	3.553	2	3	**1**

The safety ranking combining both static and impact results is shown in table 4-14 below

Table 4-14 Safety ranking according to both static and impact results

Sleeper Code	Cases	Safety ranking as per static results	Safety ranking as per impact results	Sum of rankings	Overall ranking
SIII8	SL-25	2	1	3	**1**
SIV4	SL-30	3	4	7	**4**
SV1	SL-33	4	2	6	**3**
SVI2	SL-33	5	3	8	**5**
SVII3	SL-40	1	3	4	**2**

Investigations made on the sleeper able to resist the applied impact loadings showed that sleeper 25 of irregular hexagon shape with a varying width was the safest compare to the others selected sleeper shapes. Sleeper 40 was the safest when the static loadings were considered. Five models over fifteen sleepers modelled with impact were safe. Generally, from the selected models for impact loadings; the irregular hexagon was safer compare to the other shapes (rectangular and trapezoid).

4.2.2 The total volume of the selected sleeper

In this thesis, the total number of sleepers modelled for static and impact simulations are fifty-one and fifteen respectively. As far as impact results are concerned, five sleepers were selected to be safe. The corresponding total volumes and ranking were shown in table 4-15. It shows that the lower the volume, the lower the ranking number.

Table 4-15 Total volume of the selected sleepers and their ranking

S/N	Sleeper name	Cases	Volume (m^3)	Ranking
1	SIII8	SL-25	0.11419	**4**
2	SIV4	SL-30	0.11421	**5**
3	SV1	SL-33	0.11215	**2**
4	SV12	SL-36	0.11366	**3**
5	SVII3	SL-40	0.11211	**1**

4.2.3 Selection of the best geometrical sleeper shape

Sleeper cases outlined in tables 4-14 and 4-15 above were ranked in regards to safety, and sleeper volume as shown in figure 4-16. For choosing the best geometrical sleeper shape, five models are ranked based on the consideration of each criterion. In other words, the better model satisfies each criterion, the lower rank it gets.

Table 4-16 safety and total volume ranking

Sleeper Name	Sleeper Case	Ranking (Safety)	Ranking (Volume)
II8	SL-25	1	4
SIV4	SL-30	4	5
SV1	SL-33	3	2
SVI2	SL-36	5	3
SVII3	SL-40	2	1

Safety (resistance of the selected sleeper to both static and impact loadings), was awarded the highest percentage followed by total volume. 59% was awarded to sleeper safety [62] and the total volume awarded to 41%.

The overall sleeper safety and volume ranking was computed according to equation 3-8. The objective functions are shown in table 4-16 and the weighting coefficients are given as 0.59 (59%) and 0.41 (41%) for sleeper safety and sleeper volume respectively. The sum of rankings was found by tanking 59% of safety rankings, plus 41 % of volume rankings.

Table 4-17 Best geometrical sleeper shape selection

Sleeper Name	Sleeper Case	Sum of rankings	Overall ranking
SIII8	**SL-25**	**2.23**	**2**
SIV4	SL-30	4.41	5
SV1	SL-33	2.59	3
SVI2	SL-36	4.19	4
SVII3	**SL-40**	**1.59**	**1**

As shown in table 4-17, the sleeper having the lower sum of ratings was considered as the best geometrical sleeper shape since the lower ranking was given to all the three criterions according to the safer, the lower volume and an easier sleeper to construct as per table 4-14, 4-15 and 4-16. Therefore, Sleeper VII3 (SL-40) having a sum of ranking of 1.59 was recommended as the best geometrical sleeper shape, which was characterized by a different width at both the center and rail seat sections. In comparison to the existing sleeper (in the Addis-Djibouti railway track) in Ethiopia; the best geometrical sleeper shape has a 1.75% volume reduction.

The second best geometrical sleeper shape was determined as SIII8 having a sum of ranking of 2.23, constituting of an irregular hexagon shape of varying width. Indeed, the irregular hexagon forms a sleeper that is safe compared to sleepers of other shapes considered in this research.

The detailed geometry with dimensions of the selected best geometrical sleeper shape is clearly shown in figure 4-15 below.

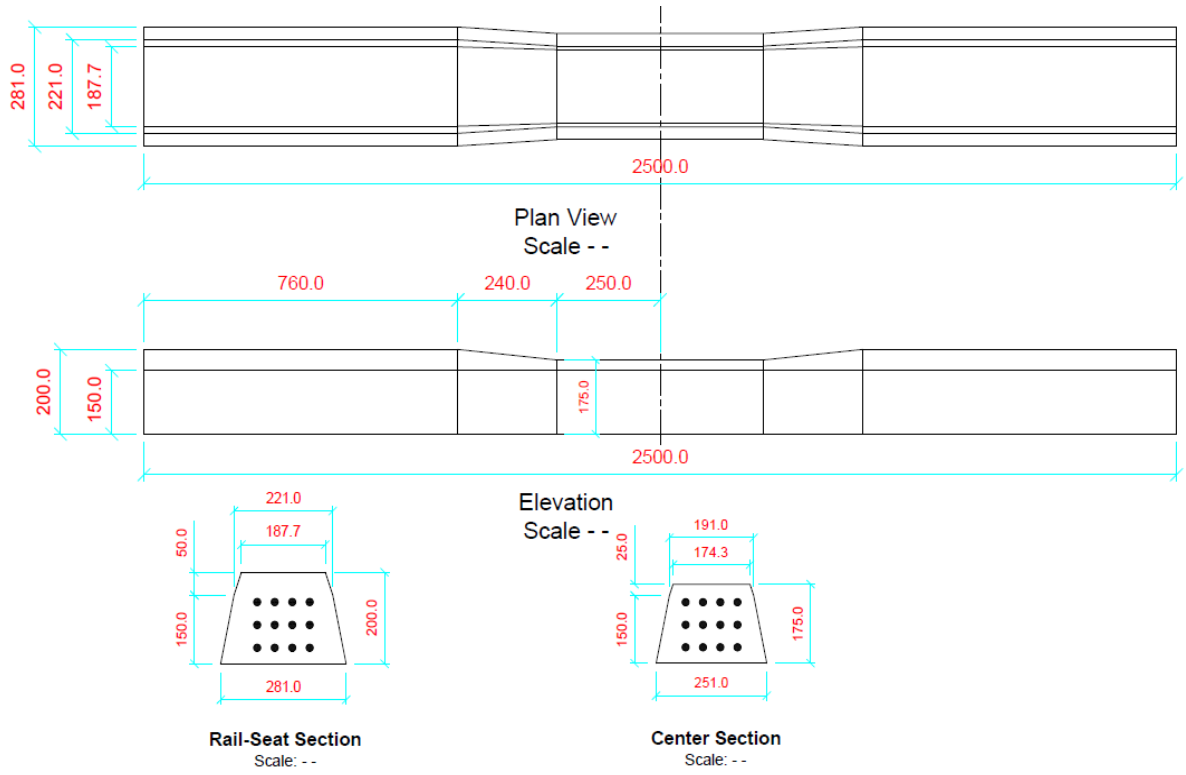

Figure 4-15 Best geometrical sleeper shape

4.3 Effect of prestressing wire spacing on prestressed concrete sleepers

Spacing between the prestressing wires varied from 25 to 45 mm horizontally. In this research, vertical spacing was considered to be constant at 50 mm. The sleeper SVII3 selected as best geometrical sleeper shape was further used to study the effect of the prestressing wire spacing on static results.

Table 4-18 summarizes the static results of sleeper SVII3 with different wire spacing while figures 4-16 to 4-18 for deformations and equivalent stress at top and bottom of sleeper sections.

Table 4-18 Static results with a variation of wire spacing for sleeper SVII3.

S/N	Wire spacing (mm)	RAIL SEAT SECTION					CENTER SECTION					END SECTION				
		Deformation (mm)	Equivalent stress at top (Mpa)	Equivalent stress at bottom (Mpa)	Shear stress at top (Mpa)	Shear stress at bottom (Mpa)	Deformation (mm)	Equivalent stress at top (Mpa)	Equivalent stress at bottom (Mpa)	Shear stress at top (Mpa)	Shear stress at bottom (Mpa)	Deformation (mm)	Equivalent stress at top (Mpa)	Equivalent stress at bottom (Mpa)	Shear stress at top	Shear stress at bottom
1	25.00	0.0205	3.679	2.132	0.990	1.175	0.0015	0.622	0.446	0.036	0.005	0.0004	0.005	0.08	0.0008	0.015
2	27.50	0.0204	3.711	1.860	1.089	0.694	0.0017	0.998	0.803	0.030	0.024	0.0004	0.005	0.09	0.0009	0.018
3	28.75	0.0201	3.687	1.913	1.127	0.669	0.0012	1.015	0.625	0.036	-0.016	0.0021	0.014	0.43	0.0008	0.108
4	33.75	0.0203	3.700	1.832	1.113	0.901	0.0018	1.259	0.667	0.021	0.014	0.0004	0.005	0.08	0.0005	0.017
5	36.25	0.0201	3.595	1.905	0.985	0.520	0.0010	0.811	0.346	0.021	-0.009	0.0019	0.016	0.40	0.0006	0.094
6	38.75	0.0201	3.706	1.951	1.016	0.736	0.0011	0.989	0.492	0.002	-0.025	0.0019	0.015	0.40	-0.0003	0.095
7	42.50	0.0199	3.659	2.228	0.918	0.703	0.0014	0.989	0.525	0.053	0.008	0.0012	0.009	0.26	0.0005	0.057
8	45.00	0.0203	3.624	1.838	0.924	0.734	0.0012	0.707	0.370	0.038	0.005	0.0002	0.005	0.04	0.0007	0.006

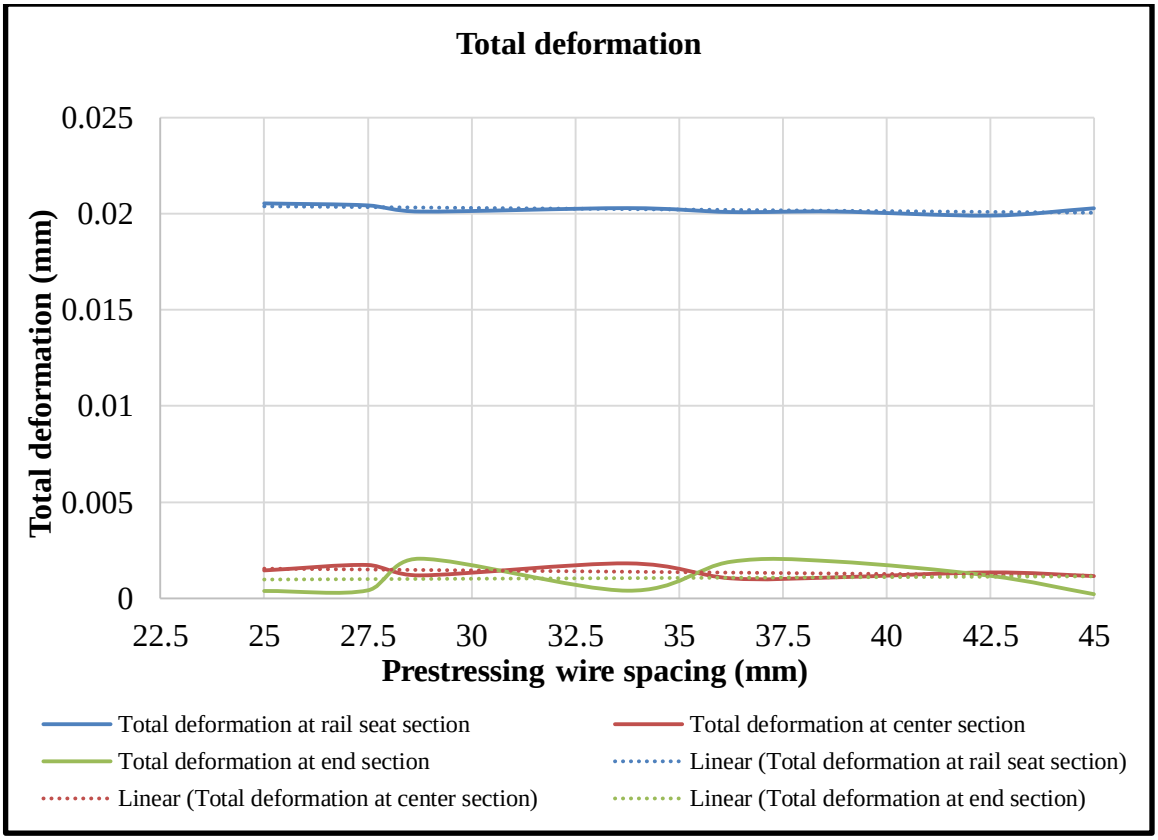

Figure 4-16 Total deformation for SVII3 sleeper with a variation of wire spacing

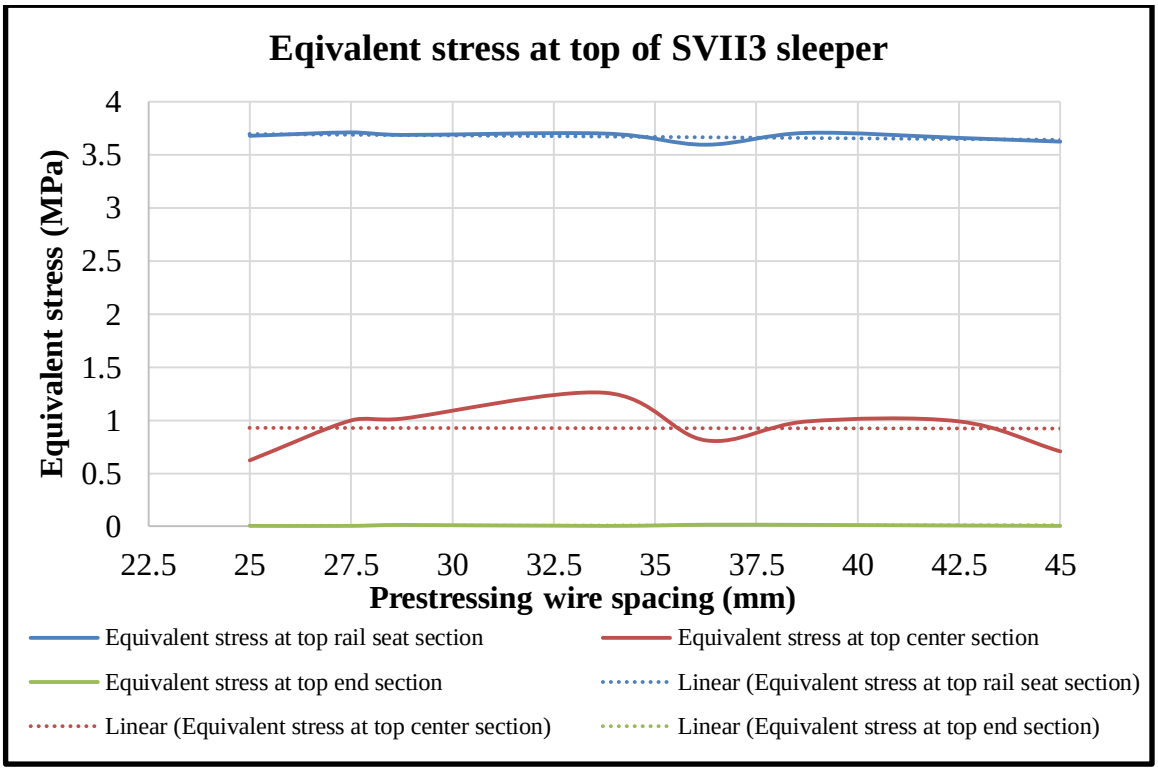

Figure 4-17 Equivalent stress at top of SVII3 sleeper with a variation of the wire spacing

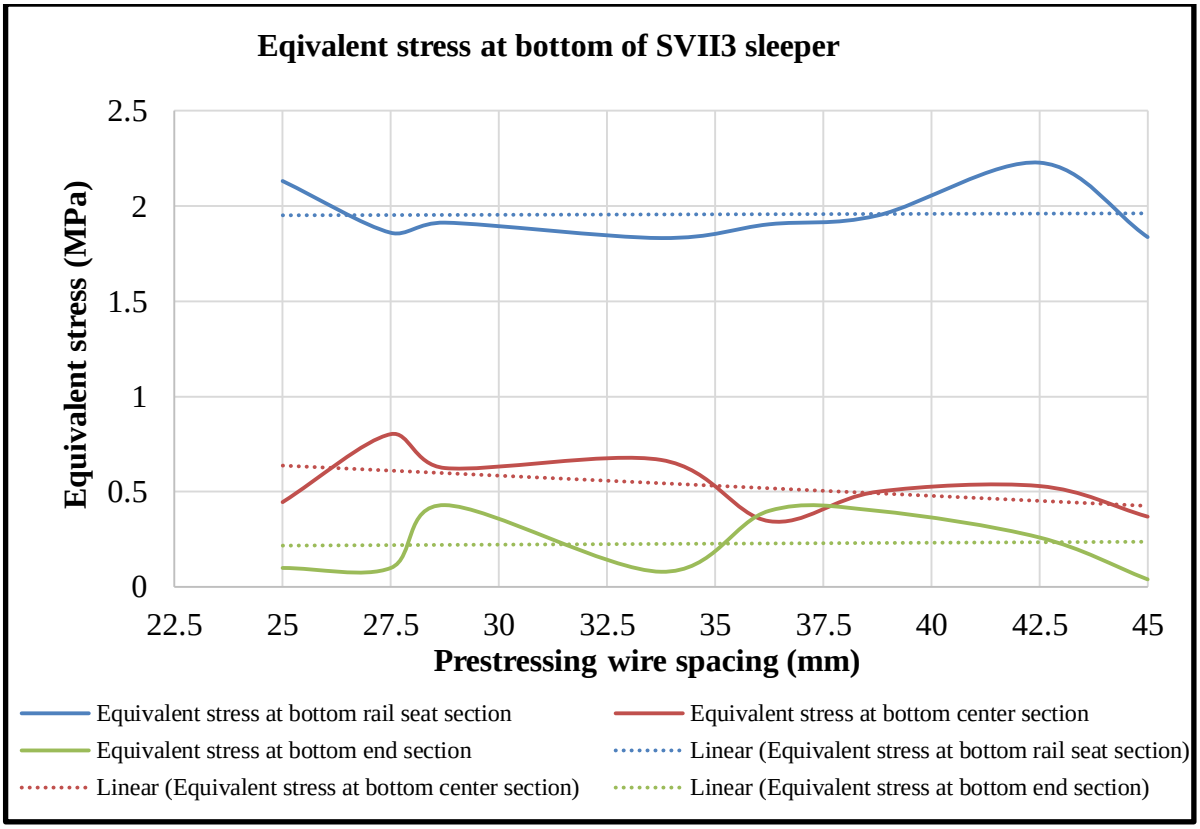

Figure 4-18 Equivalent stress at bottom of SVII3 sleeper with a variation of the wire spacing

Trend line was used to analyze the results in figure 4-16, showing that the sleeper deformation remains constant with an increase in prestressing wire spacing. Increased wire spacing shows no effect whatsoever on the equivalent stress at top of the sleeper as per figure 4-17. The figure 4-18 shows that an increase in prestressing wire spacing results to a very slightly decrease in equivalent stress at bottom center section, but the values of equivalent stress does not affect the bottom equivalent rail seat and end section. Generally, the variation of horizontal prestressing wire spacing does not affect much the behaviour of the concrete sleeper.

The change of horizontal prestressing wire spacing results to no change in stress within any point of the sleeper. The observed behaviour could be explained based on the analytical formula according to AS 1085.14-2005 [39]. Stresses at top and bottom sections are computed based on the following equations:

$$\sigma_t = \frac{-P}{A_g} \pm \frac{Pey_t}{I_g} \pm \frac{My_t}{I_g} \quad \textbf{4-1}$$

$$\sigma_b = \frac{-P}{A_g} \mp \frac{Pey_b}{I_g} \mp \frac{My_b}{I_g} \quad \textbf{4-2}$$

Where;

σ_t = stress at top section

σ_b = stress at bottom section

P = Prestressing force,

e = the effective eccentricity,

M = the bending moment at the rail or center section,

A_g = the gross sectional area;

I_g = the gross moment of inertia of the cross section;

y_t = the distance between top fiber and neutral axis of the cross section and

y_b = the distance between bottom fiber and neutral of cross section.

Using sleeper SVII3 (sleeper 40) with a variation of the horizontal prestressing wire spacing while considering the same number of the prestressing wires; the prestressing force does not chance for all cases. Similar geometry means the I_g, Y_t and y_b do not change but “e” does. The effective eccentricity “e” depends on the vertical wire spacing variation and not the horizontal prestressing wire spacing variations.

For similar vertical spacing of the prestressing wires, there is no change in the value of “e” since the value is computed by taking the distance between bottom fiber and neutral of cross section minus the distance from the centroid of prestressing wires from the bottom of the sleeper. From the equation 4-1 and 4-2, similar values of P; I_g, y_t, y_b, e have been used along with the same loading for all analysis cases thus stress computed by the equations similarly do not change. This is the analytical reasoning used to examine why horizontal wire space variation does not affect the loading capacity of prestressing wires.

CHAPTER 5 CONCLUSION AND RECOMMENDATION

5.1 Conclusion

In this research, optimization of concrete sleeper subjected to static and impact loadings were carried out to determine the optimum sleeper shape. Static and impact simulations were conducted on fifty-nine and fifteen sleeper models respectively. The material properties of the sleeper were of C60 concrete, and prestressing wire spacing of 30.4 mm and 50 mm on the horizontal and vertical respectively. Drop velocity of 1,373 mm/s equivalent to 100 mm was also used for impact simulations.

Results from static simulation revealed that rectangular sleeper shapes are having the lower top stress and higher bottom stress compare to the other sleeper shapes. The trapezoid and irregular hexagon sleeper sections are having lower stress compare to rectangular sections. However, impact simulation's results proved that the irregular hexagon sleeper shapes resisted impact loadings much better compared to the other sleeper shapes.

Optimization of sleeper was based on the criteria of sleeper safety, and sleeper total volume. Analysis results showed that the best geometrical sleeper shape was SVII3 (SL-40) of an irregular hexagon with different widths at rail seat and center sections; 251 mm center width, 281 mm end and rail seat width, 175 mm height at center section and 200 mm height at end and rail seat sections. As per this research, the sum of rankings that included sleeper safety, cost in times of total volume for the best geometrical sleeper shape was 1.59. Sleeper SIII8 (SL-25) was the next best geometrical sleeper shape with a similar ranking sum of 2.23. The shape of sleeper SIII8 (SL-25) was an irregular hexagon with a varying width from center to end sections, having 248 mm as center width, 308 mm on the end section, 171 mm height at center section and 207.8 mm height at end and rail seat sections.

Effect of prestressing wire spacing was investigated on the optimized sleeper. Horizontal wire spacing ranging 25 to 45 mm was considered and the results revealed the no effect on concrete sleeper in terms of its deformation and stresses at top sections and bottom sections. Analytical equations 4-1 and 4-2, illustrate this finding in detail as the stress values at both top and bottom sleeper have to change if the vertical wire spacing changes.

5.2 Recommendation

The following are recommended areas for future research in regards to concrete sleeper optimization:

1. This research provides a static model of the sleeper itself and impact model inclusive of the sleeper, rail and impact mass. However, other track components such as rail pads, ballast bed and subgrade affect the sleeper behaviour under different loadings and their effect was not examined in this research due to time and resource constraints. Therefore, this research further recommends that future analysis for concrete sleeper optimization include all track components such as rail, rail pad, ballast and subgrade as part of railway track system in order to better comprehend the effect of these factors to the sleeper.
2. Railway track route might be straight or curved or transition between the two. The lack of lateral resistance in curved railway track can produce misalignment problems caused by centrifugal forces. In this research, only the vertical wheel load was considered. The effect of other track loads such lateral and longitudinal loads on sleeper optimization were not considered. Therefore, to ensure proper lateral stability of the track is enhanced, future research that includes both lateral and longitudinal loads on sleeper optimization is recommended.
3. The irregular hexagon sleeper shape was found to be the optimum shape among selected sleeper shapes considered in this research. This research further recommends that both the cross sectional dimensions and slopes of sleepers be varied in future analysis so as to better improve on concrete sleeper optimization. Furthermore, sleeper cost may need the front view dimensions optimized to ensure both safety and fair sleeper manufacturing and material cost thus future analysis on this element of dimension is recommended.
4. The laboratory investigations are recommended to be conducted on the selected sleeper to validate the numerical results.
5. An impact simulation requires material properties of concrete and prestressing wires. In this thesis, the same properties were taken the same for both static and impact simulations. The use of dynamic concrete and prestressing wires properties are recommended to be used in future research.

REFERENCES

[1] D. Li, S. Kaewunruen and P. Robery, "Creep and shrinkage effects on Railway Prestressed concrete sleepers.," in *First international conference on rail transportation-ICRT 2017*, Chengdu, China., 2017.

[2] S. Kaewunruen and A. Remennikov, "Impact capacity of railway prestressed concrete sleepers.," *Engineering Failure Analysis,* pp. 1520-1532, 2009.

[3] S. Kaewunruen and A. Remennikov, "On the residual energy toughness of prestressed concrete sleepers In railway track structures subjected to repeated impact loads.," *Electron. J. Struct. Eng.,* pp. 41-61, 2013.

[4] S. Kaewunruen and A. Remennikov, "Experimental and Numerical Studies of Railway Prestressed Concrete Sleepers Under Static and Impact Loads.," *Civ. Comput.,* pp. 25-28, 2007.

[5] W. Ferdous, A. Manalo, T. Aravinthan and A. Remennikov, "Review of Failures of railway sleepers and its consequences.," in *First International Conference on Infrastructure Failures and Consequences.*, 2014.

[6] H. G. Michel, "Numerical analysis of prestressed concrete sleeper with different supports.," Master's Thesis in School of Civil Engineering and Environmental Engineering, Addis Ababa Institute of Technology, Addis Ababa University, Addis Ababa, Ethiopia, 2016.

[7] F. Desalew, "Analysis and Design of Prestressed Concrete Sleeper.," Master's Thesis in Civil Engineering in the Graduate Studies, Addis Ababa Institute of Technology, Addis Ababa University, Addis Ababa , Ethiopia., Addis Ababa , Ethiopia., 2014.

[8] B. L. Gebeyeliu, "Capacity Analysis of Railway Concrete Sleeper.," *Civil and Environmental Research, Vol.9., College of Engineering, Wolaita Sodo University;*

PO.box.138, Wohaito sodo, Ethiopia., 2017.

[9] J. Sadeghi and A. Babaee, "Structural Optimization of B70 railway prestressed concrete sleepers.," *Iranian Journal of Science & Technology, Vol.30.,No.B4 School of Railway Engineering, Iran University of Science and Technology, Tehran, LR of Iran.,* 2006.

[10] S. Minoura, T. Wantanabe, M. Sogabe and K. Gato, "Analytical Study on Loading Capacity of Prestressed Concrete Sleeper," in *Procedia Engineering*, 2017.

[11] A. Remennikov and S. Kaewunruen, "A review on loading conditions for railway track structures due to wheel/rail vertical interaction.," *Struct. Eng. Mater. Inc. Struct. Control Heal. Monit.,* 2007.

[12] A. Manalo, "Behaviour of fiber composite sandwich structures: a case study on railway sleeper application.," PhD Thesis in Faculty of Engineering and Surveying, University of Southern Queensland, Toowoomba, Queensland, Australia, Queensland, Australia., 2011.

[13] E. Selig and J. Waters, Track Geotechnology and Substructure Management., London.: Thomas Telford Publications,, 1994.

[14] T. Paulos, "Structural response evaluation of concrete sleeper under increasing train speed and axle load,," master's thesis, school of civil and environmental engineering, Addis Ababa Institute of Technology, Addis Ababa University, Addis Ababa,, Addis Ababa, 2016.

[15] A. Alexander, B. Hanna, B. Johan and Y. Oscar, "The Influence of Stiffness Variations in Railway Tracks: A Study on Design, Construction, Monitoring and Maintenance procedures to obtain suitable support conditions for railway sleepers," Bachelar Thesis in Civil Engineeing, Department of Applied Mechanics, Chalmer University of Technology, Sweden., Sweden., 2013.

[16] Y. Fong, "The effect of Thin-Layer Elements in Structural Modeling of Rail-Track

Supporting System.," Master's thesis, University of Putra Malaysia., 2006.

[17] S. Saxena and S. Arora, A Text Book of Railway Engineering., New Delhi: Dhanpat Rai publishing Co. Pvt Ltd, 2011.

[18] E. Tutumluer, H. Huang, Y. Hashash and J. Ghabousi, "Aggregate Shape on Ballast Tamping and Railroad Track Lateral Stability.," Final Manuscript, Civil and Environmental Engineering Department, University of IllinoisCivil and Environmental Engineering Department, University of Illinois, Urbana., 2006.

[19] B. Aursudkij, " A Laboratory Study of Railway Ballast Behaviour under Traffic Loading and Tamping Maintenance.," PhD's thesis, University of Nottingham, 2007.

[20] Taufan Abadi, "Effect of sleeper and ballast interventions on rail track performance.," PhD's thesis, Faculty of engineering and the environment, university of Southampton., 2015.

[21] B. Indraratna, B. Salim and C. Rujikiatkamjorn, Advanced rail Geotechnology-ballasted track., Leiden, The Netherlands,: CRC. Press / Balkema, 2011.

[22] J. Leong and M. Murray, "Probabilistic analysis of train-track vertical impact forces.," in *Proceeding of the institution of Civil Engineers, Transport 161,* 2008.

[23] J. Priest and W. Powrie, "Determination of dynamic track modulus from measurement of track velocity during train passage.," *Journal of Geotechnical and geoenvironmental engineering,*, pp. vol. 135, 1732-1740., 2009.

[24] L. Shan, "Railway Sleeper Modelling with Deterministic and Non-deterministic Support Conditions.," Master Degree Project., 2012.

[25] R. Lutch, "Capacity Optimization of a Prestressed Concrete Railroad Tie.," Master's thesis, Michigan Technological University, 2009.

[26] C. Huang, C. Chen, L. Lee, L. Bui and H. Hsieh, "The material and mechanical

property of heavy-duty prestressed concrete sleeper.," in *2011 Int. Conf. Civ. Eng. Transp. ICCET*, 2011.

[27] H. Wolf, "FLEXURAL BEHAVIOR OF PRESTRESSED CONCRETE MONOBLOCK CROSSTIE," Master thesis, Civil Engineering in the Graduate College of the University of Illinois at Urbana-Champaign., Urbana, 2015.

[28] BSI, "Design of concrete structures : Part 1-1: General Rules and Rules for Building,," British Standars Institution, Eurocode 2, London, 2004.

[29] S.A. Popovics, "A Numerical Approach to the Complete Stress-Strain Curve of Concrete," *Cement and Concrete Research*, vol. Vol 3, no. 5, pp. 583-599, 1973.

[30] A. Remennikov and S. Kaewunruen, "Experimental determination of energy absorption capacity for prestressed concrete sleepers under impact loads.," *Innov. Struct. Eng. Constr. Vols 12.*, 2008.

[31] H. Thun, S. Utsi and L. Elfgren, "Load Carrying Capacity of Cracked Concrete Railway Sleepers," *Struct. Concr.*, 2008.

[32] B. Van Dyk, J. Eduards, C. Ruppet and C. Barkan, "Considerations for Mechanistic Design of Concrete Sleepers and Elastic Fastening Systems in North America.," in *IHHA Conference*, 2013.

[33] V. Ungureanu and A. Maris, "Y Shape Railway Sleepers From Fiber Reinforced Foamed.," *Bulletin of the Transilvania University of Braşov, vol. 6, no. 1.,* pp. pp.191-198, 2013.

[34] Y. Koike, T. Nakamura, K. Hayano and Y. Momoya, "Numerical method for evaluating the lateral resistance of sleepers in ballasted tracks.," *Soils and Foundations.*, p. 54(3):502–514, 2014.

[35] AREMA, "AREMA Manual for Railway Engineering Part 4 Chapter 30 Concrete Ties.," 2003.

[36] T. Jeffs and G. Tew, "SLEEPERS AND BALLAST', A REVIEW OF TRACK DESIGN PROCEDURE.," 1991.

[37] Z. Cai, P. Raymond and R. Bathurst, "Estimation of Static Track Modulus Using Elastic Foundation Models.," *Transportation Research Record 1470, TRB, National Research Council, Washington, D.C,*, pp. pp. 65-72., 1994.

[38] B. Jian, "FLEXURAL BEHAVIOR OF PRESTRESSED CONCRETE MONOBLOCK CROSSTIES.," PhD's Thesis, School of Chemistry, Physics and Mchanical Engineering, Science and Engineering Faculty, Queensland University of Technology., 2012.

[39] AS, " Australian Standard, AS 1085.14 "Railway track materials", Part 14: "Prestressed Concrete Sleepers"." 2003.

[40] K. L. Knothe and S. L. Grassie, "Modelling of railway track vehicle/track interaction at high frequency," *Vehicle System Dynamics 22,* pp. pp. 209-262, 1993.

[41] Timoshenko, "Method of analysis of statical and dynamical stresses in rail.," in *International Congress for Applied Mechanics -- Proceedings, .*, 1926.

[42] G. Xie and S. Iwnicki, "Simulation of wear on a rough rail using a time-domain wheel-track interaction model.," pp. V 265, n 11-12, p 1572-83., 2008.

[43] S. Grassie, "Dynamic Modelling of concrete railway sleepers.," *Journal of Sound Vibration, v 187,*, pp. p 799-813., 1995.

[44] K. Knothe, "Benchmark Test of Models of Railway Track and of Vehicle/Track Interaction in the Low Frequency Range.," *Vehicle System Dynamics Supplement, v 24,*, pp. pp. 363-379, 1995.

[45] S. Grassie, "Models of Railway Track and Vehicle/Track Interaction at High Frequencies: Results of Benchmark Test,," *Vehicle System Dynamics supplement, 25.*, pp. pp. 243-262., 1996.

[46] A. Remennikov and S. Kaewunruen, "Resistance of Railway Concrete Sleepers to Impact Loading.," in *The 7th International Conference on Shock and Impact Loads on Structures, vol. 158, October,*, 2007.

[47] S. Kaewunruen, "Experimental and numerical studies for evaluating dynamic behaviour of prestressed concrete sleepers subject to severe impact loading,," PhD thesis, UoW, Aust.,, 2007.

[48] C. Hong Lim, S. Kaewunruen and N. Mlilo, "Performance of Railway Sleepers with Holes under Impact Loading.," *IOP Conference Series: Materials Science and Engineering 280.*, pp. pp 1-6, 2017.

[49] J. Taherinezhad, P. Mendis, T. Ngo and M. Sofi, "Behaviour of Pre-Stressed High Strength Concrete Sleepers.," in *Second Int. Conf. Performance-based Lifecycle Struct. Eng.,*, 2015.

[50] S. Kaewunruen and A. Remennikov, "Low-velocity impact analysis of railway prestressed concrete sleepers.," in *Proceedings of the 23rd Biennial Conference of the Concrete Institute of Australia: Design, Materials, and Construction, Adelaide, Australia*, Adelaide, Australia, 18-20 October 2007, 2007.

[51] S. Kaewunruen and A. M. Remennikov, " Progressive failure of prestressed concrete sleepers under multiple high-intensity impact loads," *Engineering Structures 31(10):*, pp. pp. 2460-2473, 2009.

[52] J. Sadeghi and P. Barati, "Evaluation of conventional methods in analysis and design of railway track system.," *International journal of Civil Engineering, Vol. 8, No. 1.*, 2010.

[53] Z. Jabbar Ali and M. Seyed Ali, "Study of ballast layer stiffness in railway tracks," pp. pp. 311-318, 2016.

[54] W. Zhai, K. Wang and J. Lin, "Modelling and experiment of railway ballast vibrations," *Journal of sound and vibration, 270 (2004) 4-5*, pp. pp. 673-683., 2004.

[55] D. Ahlebeck, H. Meacham and R. Prause, "The development of Analytical models fro railroad track.," in *Proc., Symposium on Railroad Track Mechanics (A. D. Kerr, ed.),*, 1975.

[56] J. Bowles, Foundation Analysis and Design., New York.: Fourth edition, McGraw-Hill Book Company, , 1988.

[57] H. E. Stewart, "Measurement and Prediction of Vertical Track Modulus.," *Transportation Research Record 1022, TRB, National Research Council, Washington, D.C.*, , pp. pp. 65-71. , 1985.

[58] J. Alan, "Soil Mechanics of High Speed Rail Tracks.," in *Civil and Environmental Engineering Student Conference (1st), Imperial College Conference.*, 2012.

[59] W. C. Peter and k. Anders, An introduction to structural optimization,, waterloo, Ontario, Canada: Department of civil engineering, university of Waterloo, waterloo, Ontario, Canada, N2L 3GI, 2009.

[60] X.-S. Yang, Engineering optimization, an introduction with Metaheuristic applications,, United Kingdom: University of Cambridge, Department of engineering, Cambridge, A JOHN WILEY & SONS, INC.,PUBLICATION, 2010.

[61] W. Steve, "Network rail safe by design: building and civils working group," in *proceedings of the institution of civil engineers-forecasting engineering; ISSN 2043-9903/E-ISSN 2043-9911; , pp 3-11. Volume 171.*, 2018.

[62] B. Johan, "Railway Safety-Risk and economics,," PhD's thesis, Department of infrastructure and planning, Royal Institute of Technology, ISSN 1651-0216, 2002.

[63] G. Rikard, "Static and dynamic finite element analysis of concrete sleepers.," Licentiate Thesis, Department of structural engineering, Chalmers University of Technology, Göteborg, Sweden,, Göteborg, Sweden, 2000.

[64] ANSYS 16, "Help Manual.".

[65] N. Doyle, Railway Track Design: A review of current Practice., 1980.

[66] R. M. Kartik, D. Marcus and K. Ryan, "Vertical load path under static and dynamic loads in concrete crosstie and fastening systems.," in *Proceedings of the 2014 Joint Rail Conference JRC2014; April 2-4,*, Colorado Springs, CO, USA., 2014.

[67] C. Satish and M. Agarwal, Railway Engineering, Jai Road, New Dehli: OXFORD UNIVERSITY PRESS, YMCA Library Building, ISBN-13:978-0-19-568779-8, 2007.

[68] ERC, "Ethiopian Railways Corporation: Ethiopia/Sebeta-Djibouti/Nagad Railway Feasibility Study, Part I General Specification, Executive Edition.," 2012.

[69] S. Chinese, "National Standard of People's Republic of China: Code of Design of Concrete Structures. GB50010-2002.," 2002.

[70] I. Ivanov and B. Corves, "Fatigue testing of flexure hinges for the purpose of the development of high-precision micro manipulator.," *"Mechanical Sciences; department of mechanism theory and dynamics of machines (IGM), RWTH Aachen University, Aachen, Germany,* pp. pp.59-66, 2014.

APPENDICES

Appendix A: Sketch of sleeper type A9P

Appendix B: Excel sheet used to determine the existing sleeper volume and soffit area.

Appendix C: Excel sheet used to determine the volume and soffit area for the sleeper to model.

Appendix D: Sleeper ballast stiffness

Appendix E: Maximum number of cycles

Appendix F: Static analysis results

Appendix G: Explicit dynamics results

Appendix A: Sketch of Sleeper Type A9P

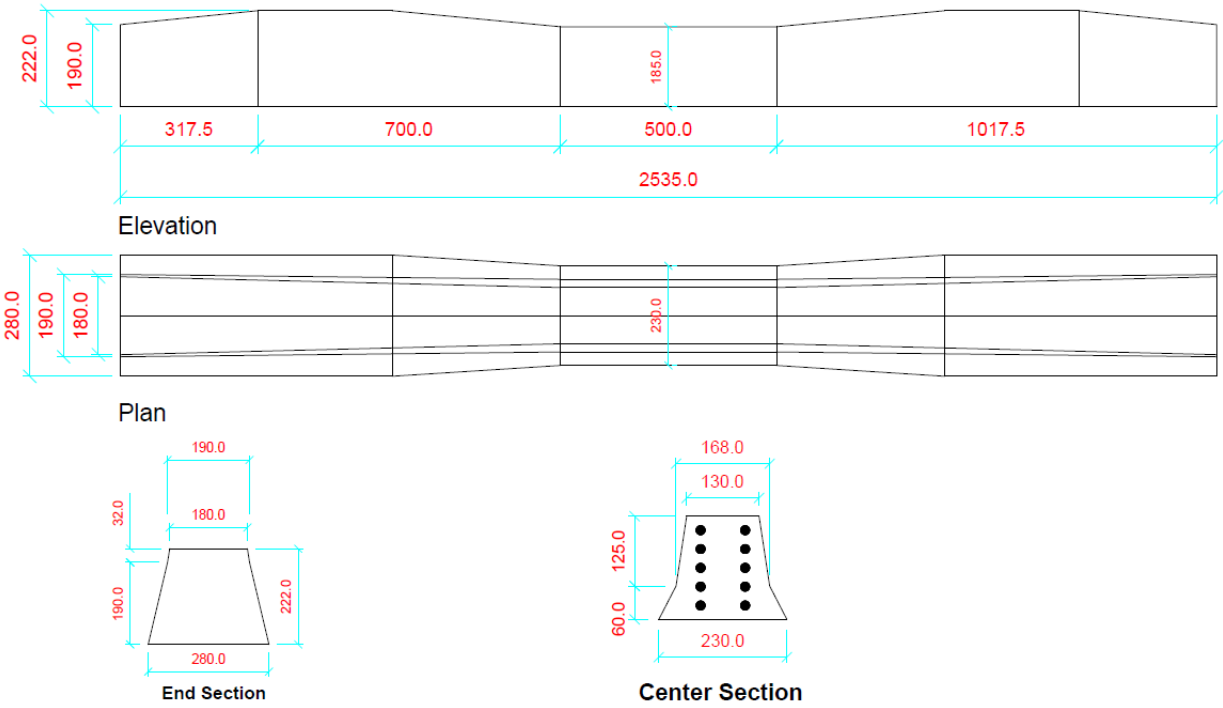

Figure A-1 Sketch of sleeper type A9P, Rikard (2000)

Appendix B: Excel sheet used to determine the existing sleeper volume and soffit area

Table B-1 Existing sleeper volume calculation

Figure section	Width (m)	Length (m)	Area (m^2)	Height (m)	Volume (m^3)	No.	Total
Trapezoids at the centre	0.2465	0.19	0.038	0.25	0.0095		
Trapezoids							
up to 175 mm							
for 150 mm	0.3065	0.2585	0.0424				
up to 25 mm	0.2585	0.2251	0.006				
A1			0.0484				
area at centre	0.2465	0.19	0.0382				
Average area up to 175mm			0.0403	1	0.0403		
The following 60 mm at the end and 48 mm at 760 mm							
end side							
A2 (h=30mm)	0.2251	0.185	0.0062				
Figure section	**Width (m)**	**Length (m)**	**Area (m^2)**	**Height (m)**	**Volume (m^3)**	**No.**	**Total**
A3 (h=30mm)	0.185	0.1463	0.005				
A2&A3 (A4)			0.0111				
at 760 mm							
A5 (h=48 mm)	0.2064	0.1345	0.0082				
Average A4&A5			0.0097	0.76	0.0073		
Area aside the centre			0.0041	0.24	0.001		
TOTAL					**0.0582**		
Deduct the area for rail seat							
A6	0.168	0.1435	0.0035				
	0.168	0.1345	0.0034				
			0.0035	0.3079	0.0011		
A7	0.05	0.03	0.0008	0.1643	0.0001		
Total deduct					**0.0012**		
NET VOLUME (Total - deduct)					**0.057**	2	**0.1139 m^3**

Table B-2 Existing sleeper soffit area calculation

Figure	End width(m)	Centre width (m)	length (m)	Area (m2)	No.	Total (m2)
Trapezoid	0.3065	0.2465	1	0.28		
Rectangular		0.2465	0.25	0.06		
Total (m2)				**0.34**	2	**0.68 m^2**

Appendix C: Excel sheet used to determine the volume and soffit area for the sleeper to model.

Table C-1 Rectangular sections with or without different width at rail seat and center section

B4	0.05	Variable
B1	0.25	Fixed
B2	0.24	Fixed
HC	0.15	Variable
h2	0.01	Variable
B	0.2	Variable
Bc	0.22	Variable

Sub-sections	**B (m)**	**b (m)**	**H (m)**	**Area (m^2)**	**W (m)**	**Volume (m^3)**	**No.**	**Volume (m^3)**	**Soffit Area (m^2)**
	0.22	0.22	0.15	0.033	0.76	0.0251			0.1672
	0.2	0.2	0.15	0.03	0.25	0.0080			0.05
	0.76	0.71	0.01	0.00735	0.22	0.0016			
	0.22	0.2	0.24	0.0504	0.15	0.0076			0.0504
	0.24		0.01	0.0012	0.2	0.0002			
	0.24		0.01	0.0024	0.01	0.00001			
Total						0.0420	2	**0.0842**	**0.5352**

Table C-2 Rectangular sections with a varying width, from center section to end section.

B4	0.05	Variable
B1	0.25	Fixed
B2	0.24	Fixed
H1	0.15	Variable
h2	0.02	Variable
Bc	0.25	Variable

Sub-sections	**B (m)**	**b (m)**	**H (m)**	**Area (m^2)**	**W (m)**	**Volume (m^3)**	**No.**	**Volume (m^3)**	**Soffit Area (m^2)**
Rectangular	0.25	0.25	0.15	0.0375	0.25	0.0094			0.125
Trapezoid	0.264	0.25	0.24	0.0617	0.15	0.0093			
	0.24		0.02	0.0024	0.25	0.0006			
	0.24		0.01	0.0017	0.01	0.0000			
	0.264	0.31	0.71	0.2028	0.17	0.0345			
	0.307	0.31	0.05	0.0154	0.15	0.0023			
	0.05		0.02	0.0005	0.31	0.0002			0.56
Total						0.05620	2	**0.1124**	**0.685**

In Table C-1 and C-2; the dimensions are in m, m^2 (for area) and m^3 (for volume). As shown in table C-1; the difference in width between the rail seat section and center section on both sides varies. The values of 10 mm, 15 mm and 20 mm have been considered for one side. Then after, the value of Be = B+2*10 mm (or 15 mm 0r 20 mm). In table C-2, the horizontal slope used is 3 in 100; in this case Be = Bc + 2*30 mm.

Table C-3 Rectangular sections with wing sections

B	0.2	Variable
H	0.16	Variable
b	0.1	Variable
A	0.2	Variable
a	0.2	Variable

Sub section	**B (m)**	**b (m)**	**H (m)**	**Area (m^2)**	**W (m)**	**Volume (m^3)**	**No.**	**Volume (m^3)**	**Soffit Area (m^2)**
Full Rectangular	0.2	0.2	0.16	0.032	1.25	0.04			0.5
Wing	0.2	0.2	0.16	0.032	0.2	0.0064			0.08
Total						0.0464	2	**0.0928**	**0.58**

N.B: For rectangular with a rectangular winged section, A = a; and for trapezoidal winged section A is not equal to a. Dimensions are in m, m^2 (for area) and m^3 (for volume).

Table C-4 Trapezoid and Irregular hexagon sections with or without different width

1	S1			5 in 1	Variable				
2	S2			3 in 1	Variable				
3	Bc	0.25	Variable						
4	H1	0.15	Variable						
5	h1	0.025	Variable						
6	h2	0.025	Variable						
7	Be	0.281	Variable						
8	B1	0.25	Fixed						
9	B2	0.24	Fixed						
S/N	**B (m)**	**b (m)**	**Height (m)**	**Area (m^2)**	**Width (m)**	**Volume (m^3)**	**No.**	**Volume (m^3)**	**Soffit Area (m^2)**
1	0.251	0.19	0.15	0.033					0.06275
2	0.191	0.17	0.025	0.005					
1&2				0.038	0.25	0.0094			
3	0.281	0.25	0.24	0.064					
4	0.221	0.19	0.24	0.049					
3&4				0.057	0.15	0.0085			0.06384
5	0.221	0.2	0.025	0.005					
6	0.191	0.17	0.025	0.005					
5&6				0.005	0.24	0.0012			
7	0.24		0.025	0.003	0.25	0.0008			
8	0.24		0.015	0.004	0.01	5E-05			
9	0.281	0.22	0.15	0.038	0.76	0.0286			0.21356
10	0.221	0.17	0.05	0.01	0.76	0.0074			
						0.056	2	**0.11194**	**0.6803**

For trapezoid sections, the value of h1 is taken as 0 and for irregular hexagon it is different from 0. As shown in table C-4; the difference in width between the rail seat section and center section on both sides varies.

The values of 10 mm, 15 mm and 20 mm have been considered for one side. Then after, the value of Be = B+2*10 mm (or 15 mm 0r 20 mm). Dimensions are in m, m^2 (for area) and m^3 (for volume).

Table C-5 Trapezoid and Irregular hexagon sections with a varying width

1	S1			5 in 1		Variable			
2	S2			3 in 1		Fixed			
3	Bc	0.25	Variable						
4	H1	0.135	Variable						
5	h1	0.04	Variable						
6	h2	0.0242	Variable						
7	B1	0.25	Fixed						
8	B2	0.24	Fixed						
S/N	**B (m)**	**b (m)**	**Height (m)**	**Area (m^2)**	**Width (m)**	**Volume (m^3)**	**No.**	**Volume (m^3)**	**Soffit Area (m^2)**
1	0.25	0.196	0.135	0.0301					0.125
2	0.196	0.164	0.04	0.007					
1&2				0.0373	0.25	0.0093			
3	0.2644	0.25	0.24	0.0617					
4	0.2104	0.196	0.24	0.0488					
3&4				0.0553	0.15	0.0083			0.56
5	0.2104	0.1784	0.04	0.0078					
6	0.196	0.164	0.04	0.007					
5&6				0.0075	0.24	0.0018			
7	0.24		0.0242	0.003	0.25	0.0007			
8	0.2644	0.31	0.76	0.2183					
9	0.2104	0.256	0.76	0.1772					
8&9				0.1978	0.135	0.0267			
10	0.2104	0.256	0.76	0.1772					
11	0.15904	0.20464	0.76	0.138					
10&11				0.1577	0.0642	0.0101			
						0.05696	2	**0.11392**	**0.685**

For trapezoid, the value of h1 is taken as 0 and for irregular hexagon it is different from 0. As shown in table C-5, the horizontal slope used is 3 in 100; in this case Be = Bc + 2*30 mm. Dimensions are in m, m^2 (for area) and m^3 (for volume).

Appendix D: Sleeper ballast stiffness

Table D-1: Selected sleeper ballast stiffness

S/N	Selection criteria	Sleeper name	Sleeper number	Sleeper length	Stiffness		Equivalent stiffness for the support layer underneath the sleeper
					Stiffness, K1	Stiffness, K2	
				(mm)	(N/mm)	(N/mm)	(N/mm)
1	Same volume as existing sleeper	SI-1	SL-1	2500	79197	-808960	87791
2		SI-2	SL-2	2500	79704	-814880	88345
3		SI-4	SL-3	2500	98177	-1060928	108188
4		SI-5	SL-4	2500	93160	-988642	102851
5		SI-6	SL-5	2500	79513	-812646	88137
6		SI-7	SL-6	2500	80649	-826047	89375
7		SI-8	SL-7	2500	81581	-837210	90389
8		SI-10	SL-8	2500	81553	-836876	90358
9		SI-11	SL-9	2500	81117	-831629	89884
10	Soffit area as the existing sleeper	SII-1	SL-10	2500	80339	-822362	89037
11		SII-3	SL-11	2500	80339	-822362	89037
12		SII-4	SL-12	2500	95570	-1022904	105420
13		SII-5	SL-13	2500	95261	-1018455	105090
14		SII-6	SL-14	2500	80339	-822362	89037
15		SII-7	SL-15	2500	80930	-829396	89681
16		SII-8	SL-16	2500	81182	-832411	89955
17		SII-9	SL-17	2500	80930	-829396	89681
18		SII-10	SL-18	2500	81089	-831294	89854
19	Volume and area	SIII-1	SL-19	2500	80339	-822362	89037
20		SIII-3	SL-20	2500	81182	-832411	89955
21		SIII-4	SL-21	2500	80339	-822362	89037
22		SIII-5	SL-22	2500	81460	-835759	90258
23		SIII-6	SL-23	2500	80930	-829396	89681
24		SIII-7	SL-24	2500	81182	-832411	89955
25		SIII-8	SL-25	2500	80930	-829396	89681
26		SIII-9	SL-26	2500	81275	-833527	90056
27	Volume and Heights	SIV-1	SL-27	2500	80621	-825712	89345
28		SIV-2	SL-28	2500	81368	-834643	90157
29		SIV-3	SL-29	2500	81562	-836987	90368
30		SIV-4	SL-30	2500	81331	-834197	90117
31		SIV-5	SL-31	2500	82170	-844353	91028
32		SIV-6	SL-32	2500	83736	-863655	92727
33	Heights	SV-1	SL-33	2500	81460	-835759	90258

S/N	Selection criteria	Sleeper name	Sleeper number	Sleeper length	Stiffness		Equivalent stiffness for the support layer underneath the sleeper
					Stiffness, K1	Stiffness, K2	
				(mm)	(N/mm)	(N/mm)	(N/mm)
34	Heights	SV-2	SL-34	2500	80921	-829285	89671
35		SVI-1	SL-35	2500	80150	-820129	88831
36		SVI-2	SL-36	2500	81117	-831629	89884
37		SVI-3	SL-37	2500	82926	-853615	91849
38	Area and Heights	SVII-1	SL-38	2500	80930	-829396	89681
39		SVII-2	SL-39	2500	80339	-822362	89037
40		SVII-3	SL-40	2500	81182	-832411	89955
41		SVII-4	SL-41	2500	80930	-829396	89681
42		SVII-5	SL-42	2500	81368	-834643	90157
43		SVII-6	SL-43	2500	80150	-820129	88831
44	Any volume	SVIII-1	SL-44	2500	80930	-829396	89681
45		SVIII-2	SL-45	2500	81182	-832411	89955
46		SVIII-3	SL-46	2500	81117	-831629	89884
47		SVIII-4	SL-47	2500	81553	-836876	90358
48		SVIII-5	SL-48	2500	80930	-829396	89681
49		SVIII-6	SL-49	2500	81460	-835759	90258
50		SVIII-7	SL-50	2500	80930	-829396	89681
51		SVIII-8	SL-51	2500	80930	-829396	89681

K1= the ballast layer stiffness

K2 = the sub-ballast layer stiffness

K= the equivalent stiffness for the support layer underneath the sleeper

Appendix E: Maximum number of cycles

Table E-1 Maximum number of cycles

		Trains/day	**Locomotives**	**Wagons**
Passenger	No	2	1	12
	No of bogies		2	2
	No of axles per bogie		3	2
	Wheels per axle		2	2
	Total No of wheels		**24**	**192**
Freight	No	3	1	54
	No of bogies		2	2
	No of axles per bogie		3	2
	Wheels per axle		2	2
	Total No of wheels		**36**	**1296**
	Total	**5**	**60**	**1488**
Total No of wheels/day				1548
Design life (yrs)	40			22600800
	No of Cycles/rail seat			**11300400**
1 year	No of Cycles/rail seat			30960

Appendix F: Static analysis results

Among the fifty-one sleepers modelled in static structural analysis, numerical results of four of them are attached from figure F-1 to F-4.

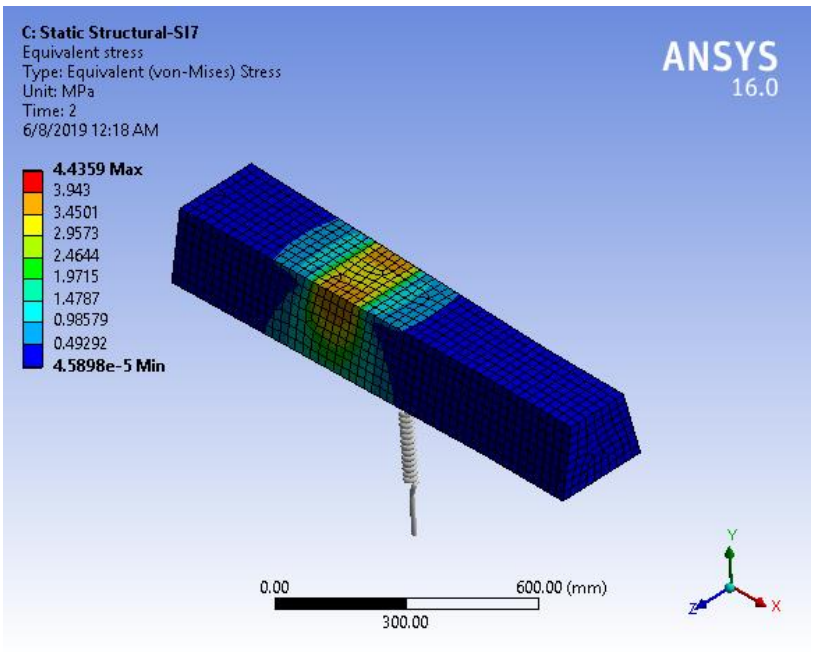

(a)

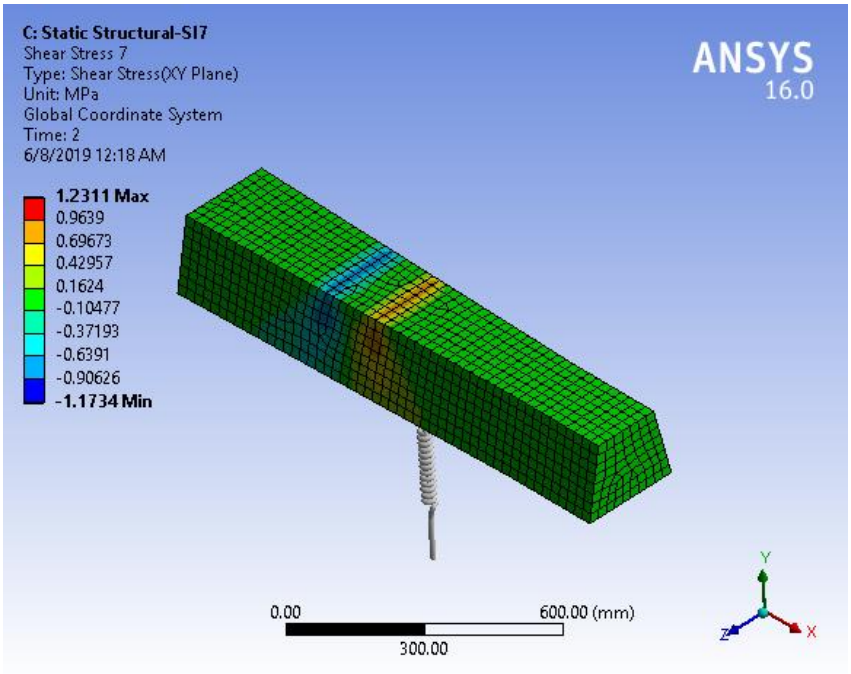

(b)

Figure F-1 Static results for sleeper SI7 (a) equivalent stress (b) shear stress

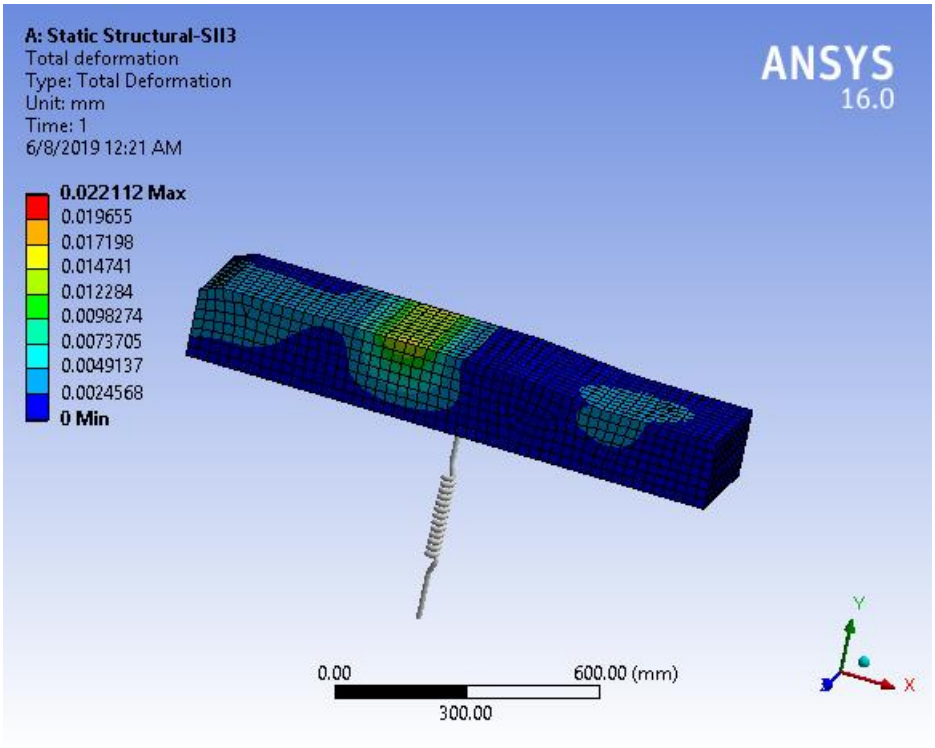

(a)

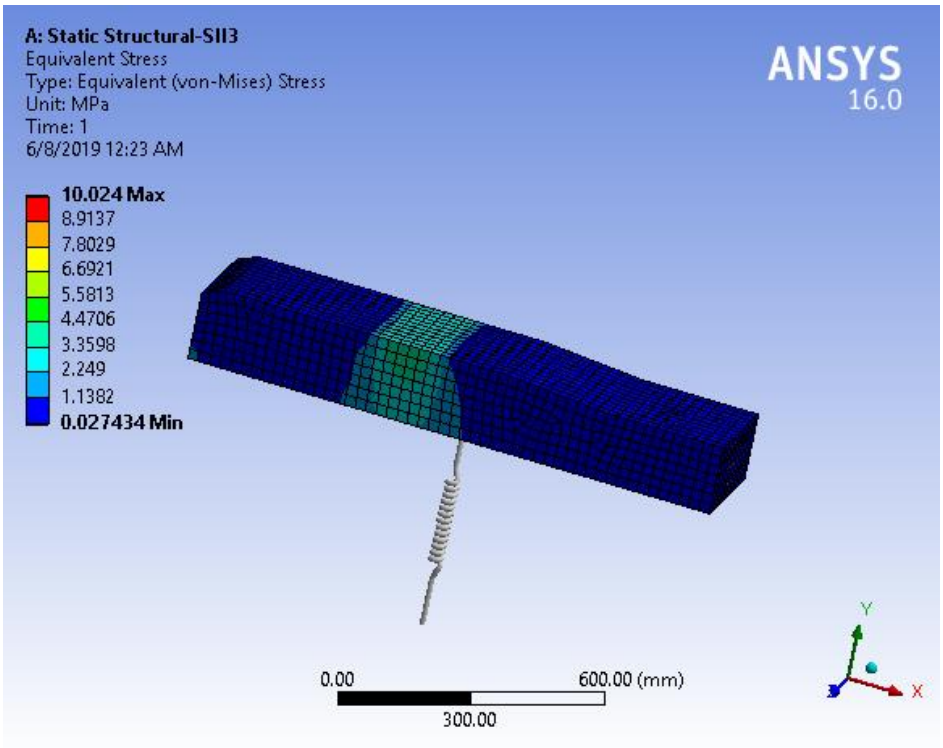

(b)

Figure F-2 Static results for sleeper SII3 (a) deformation (b) equivalent stress

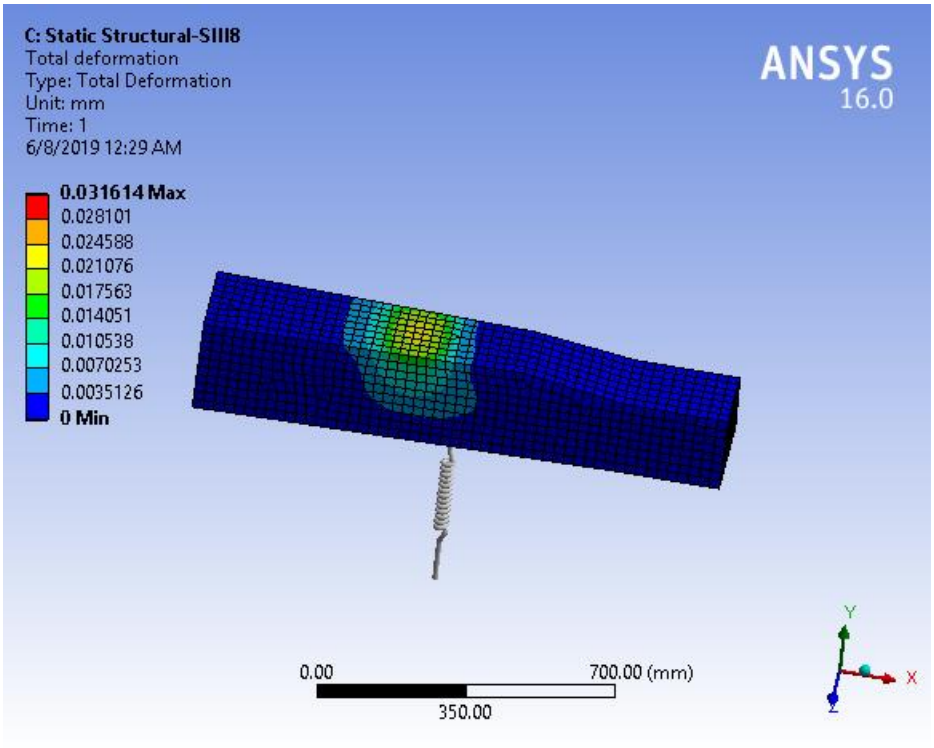

(a)

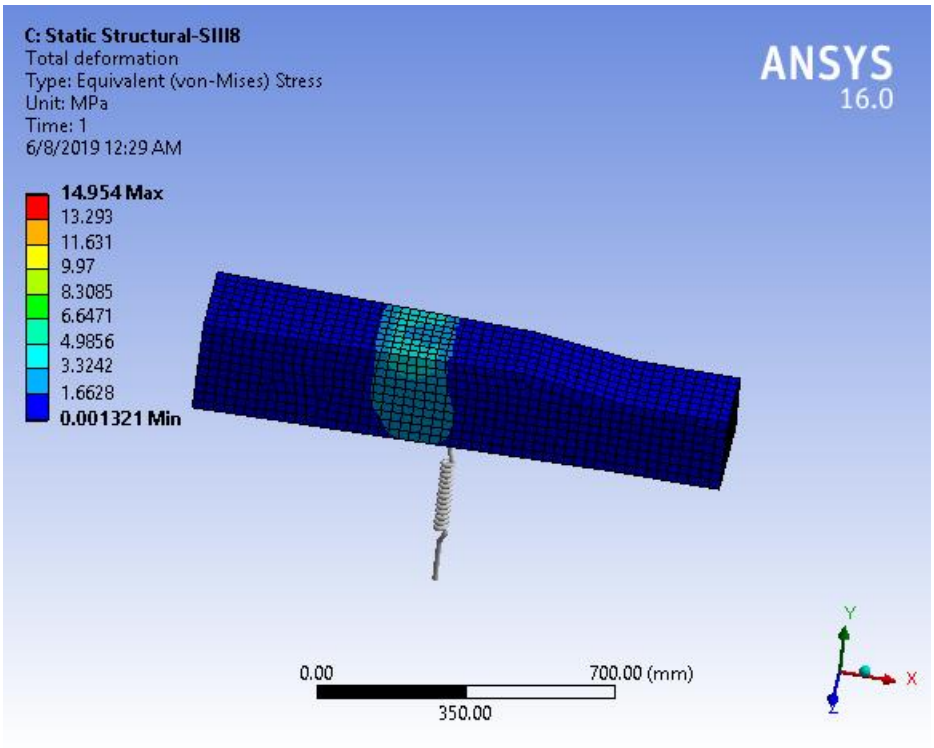

(b)

Figure F-3 Static results for sleeper SIII8 (a) deformation (b) equivalent stress

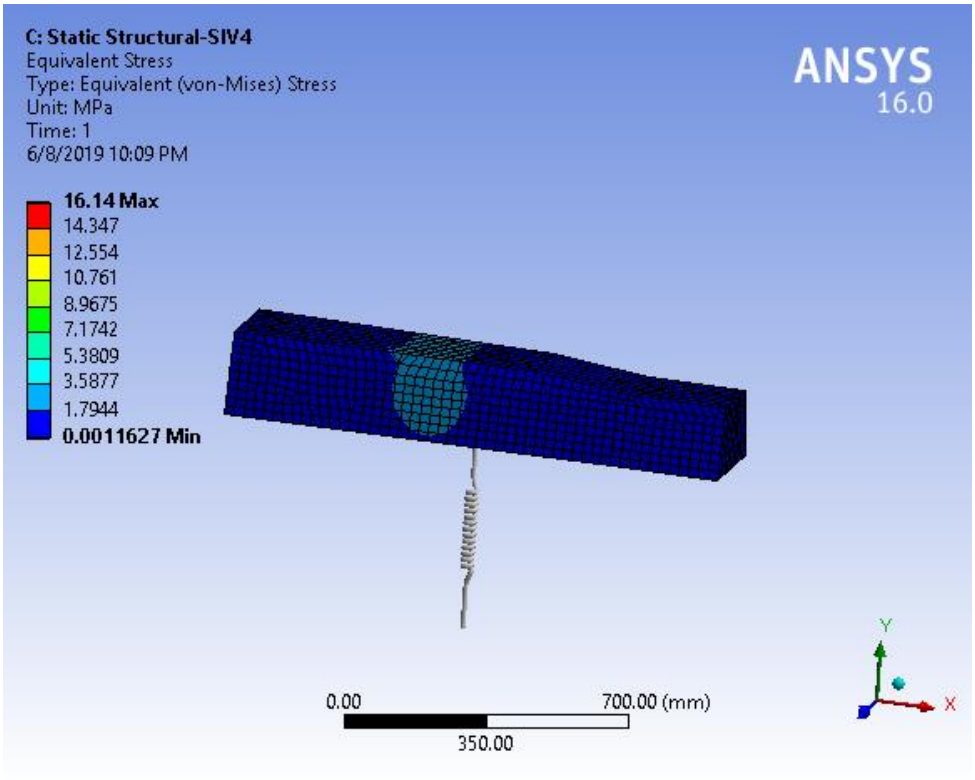

(a)

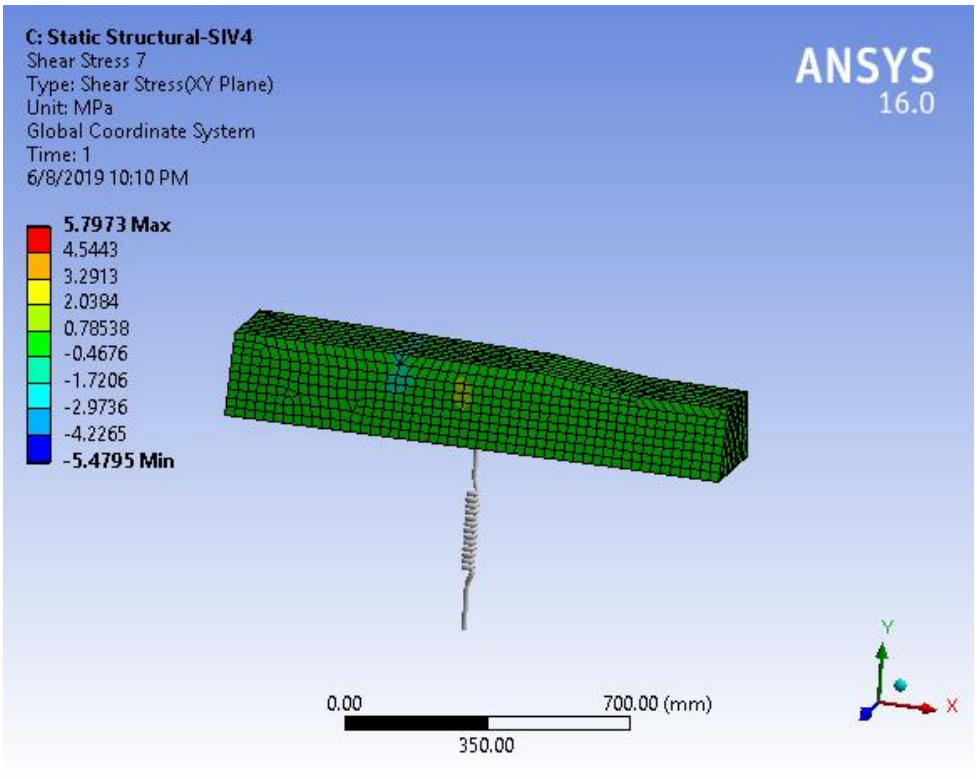

(b)

Figure F-4 Static results for sleeper SIV4 (a) equivalent stress (b) shear stress

APPENDIX G: Explicit dynamics results

Among the fifteen sleepers modelled in explicit dynamics, numerical results of four of them are attached from figure G-1 to G-4.

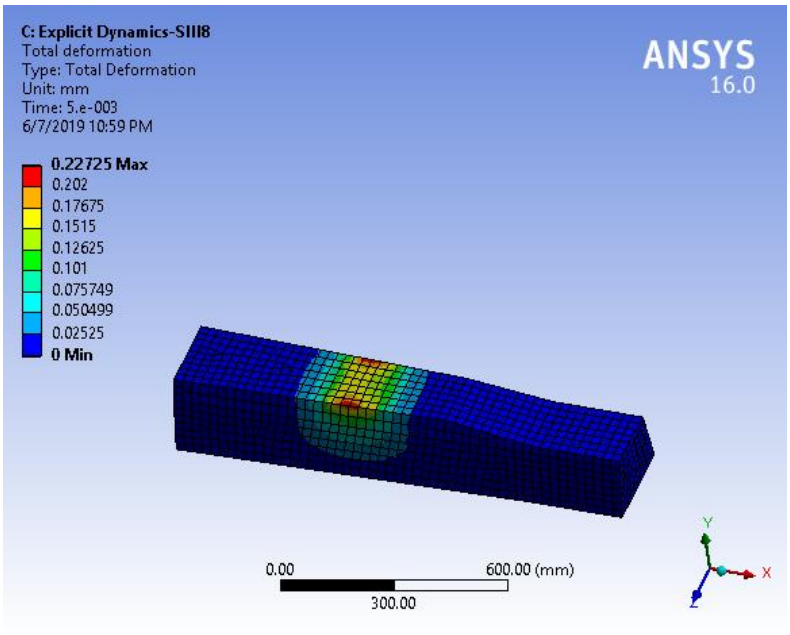

(a)

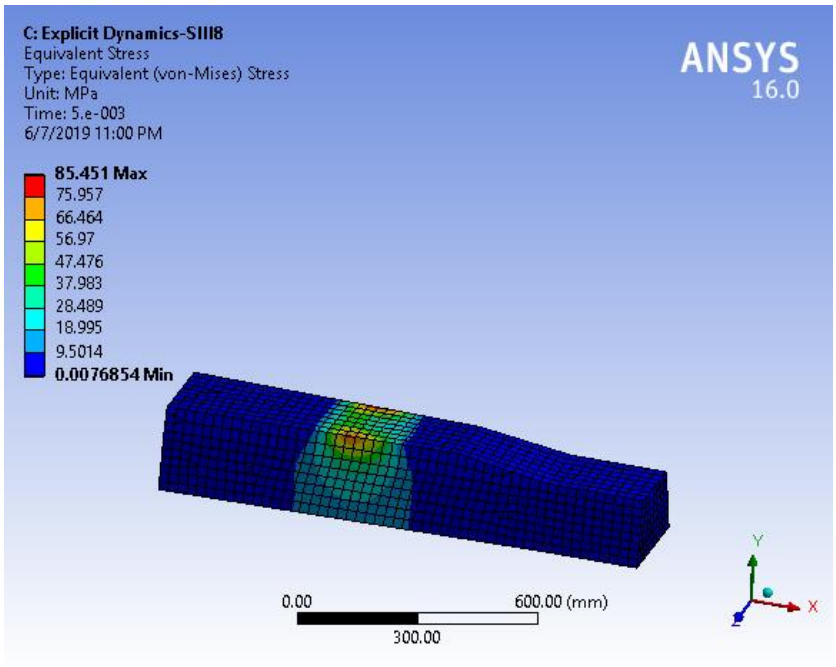

(b)

Figure G-1 Impact results for sleeper SIII8 (a) deformation (b) equivalent stress

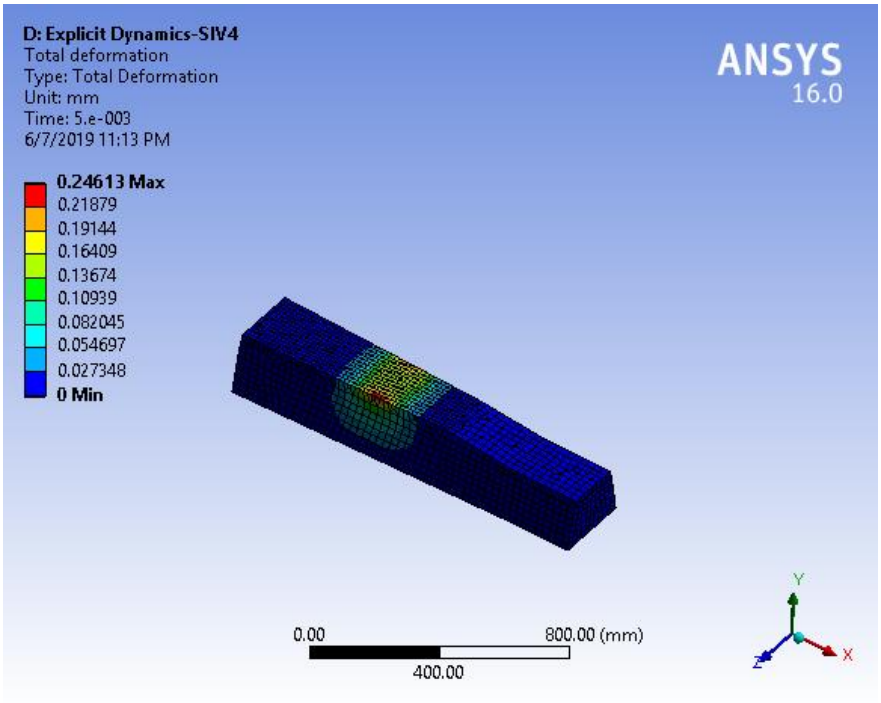

(a)

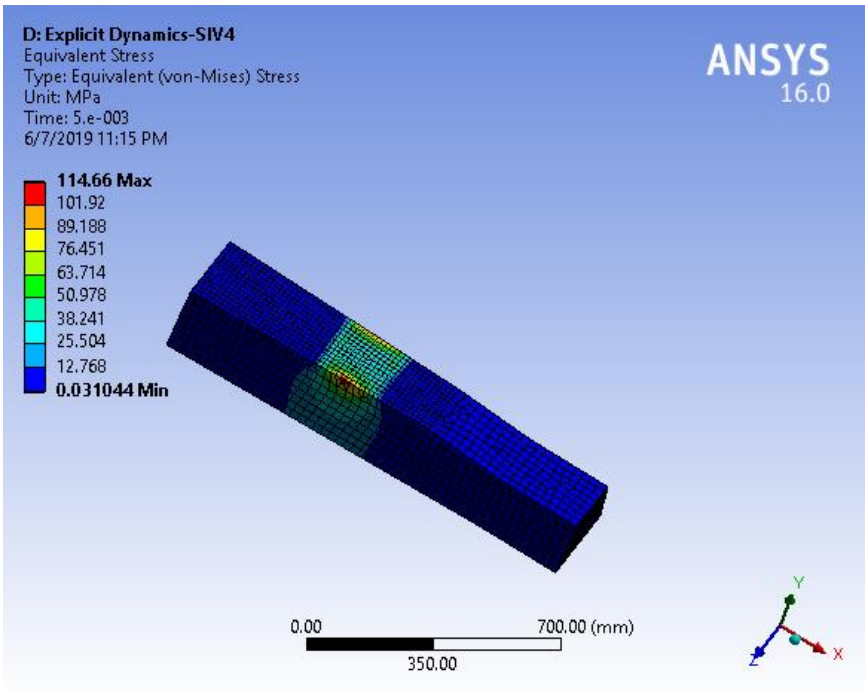

(b)

Figure G-2 Impact results for sleeper SIV4 (a) deformation (b) equivalent stress

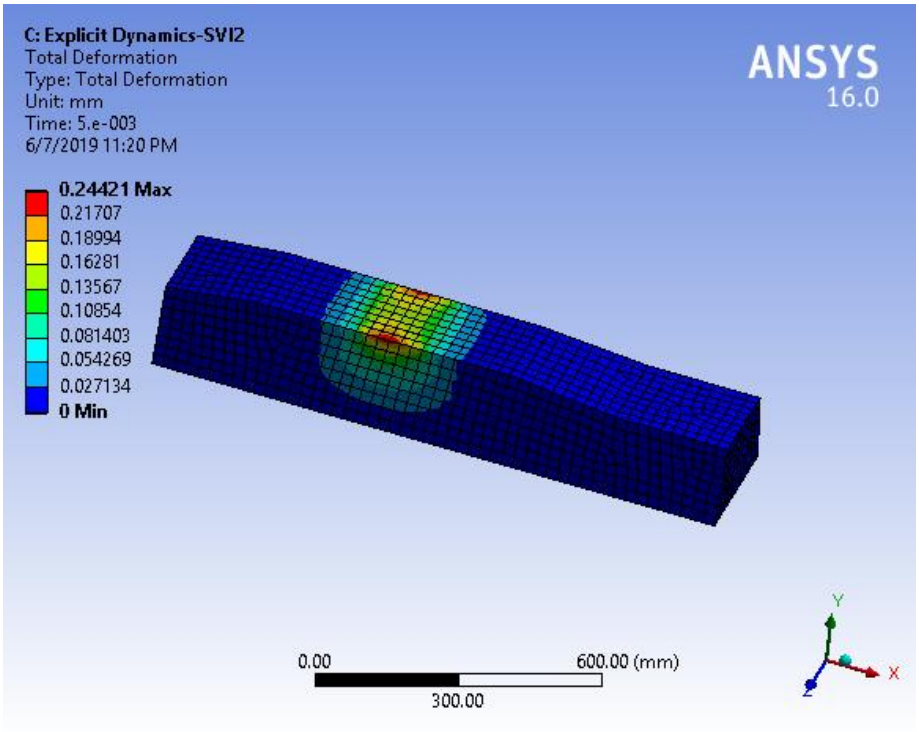

(a)

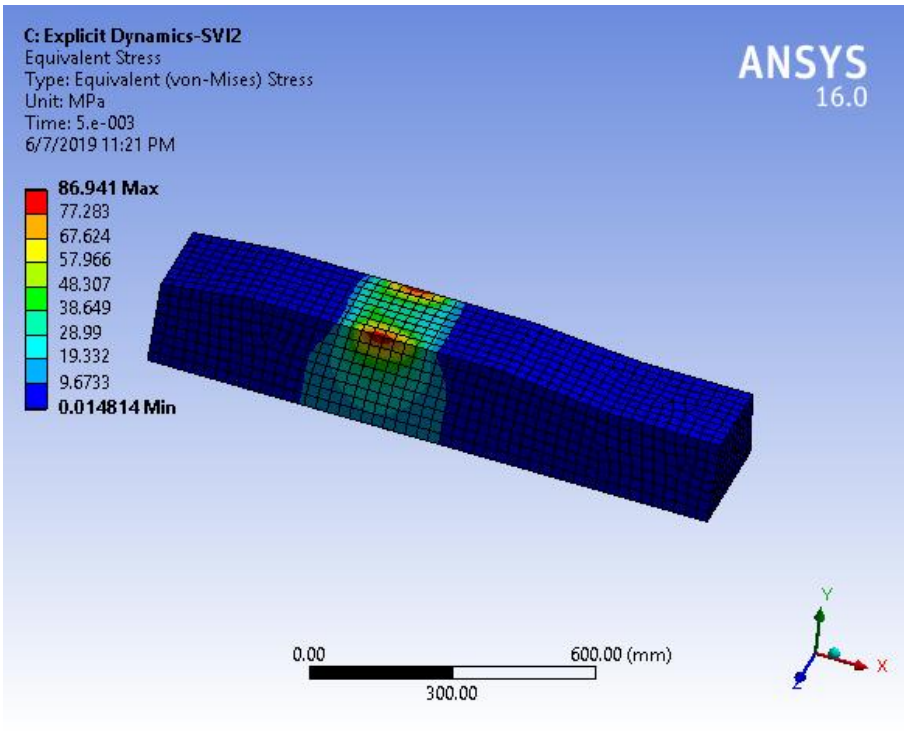

(b)

Figure G-3 Impact results for sleeper SVI2 (a) deformation (b) equivalent stress

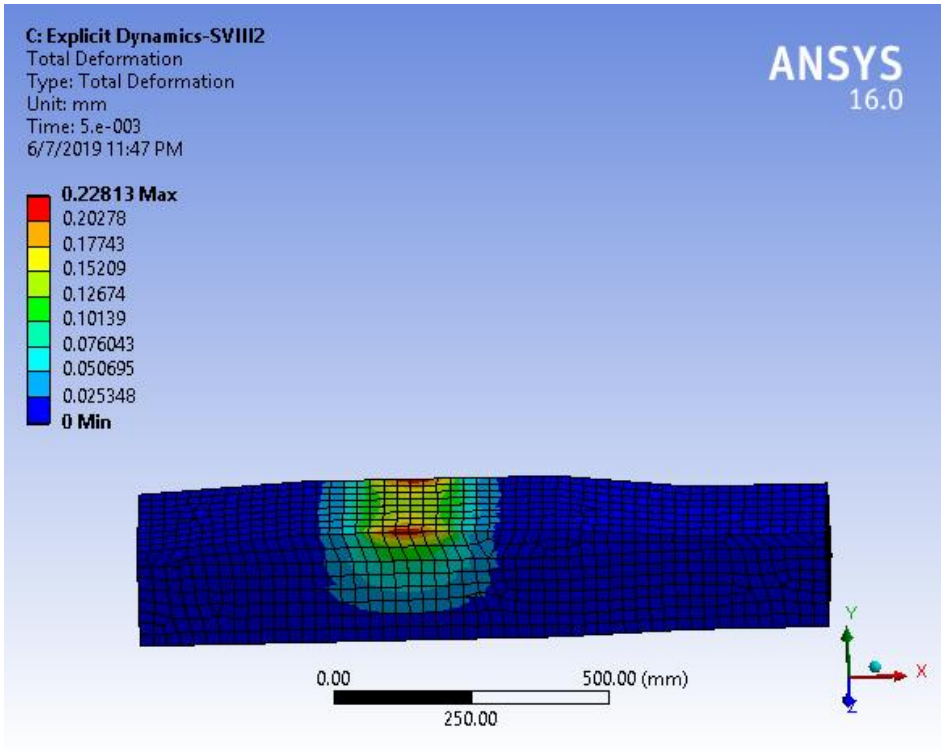

(a)

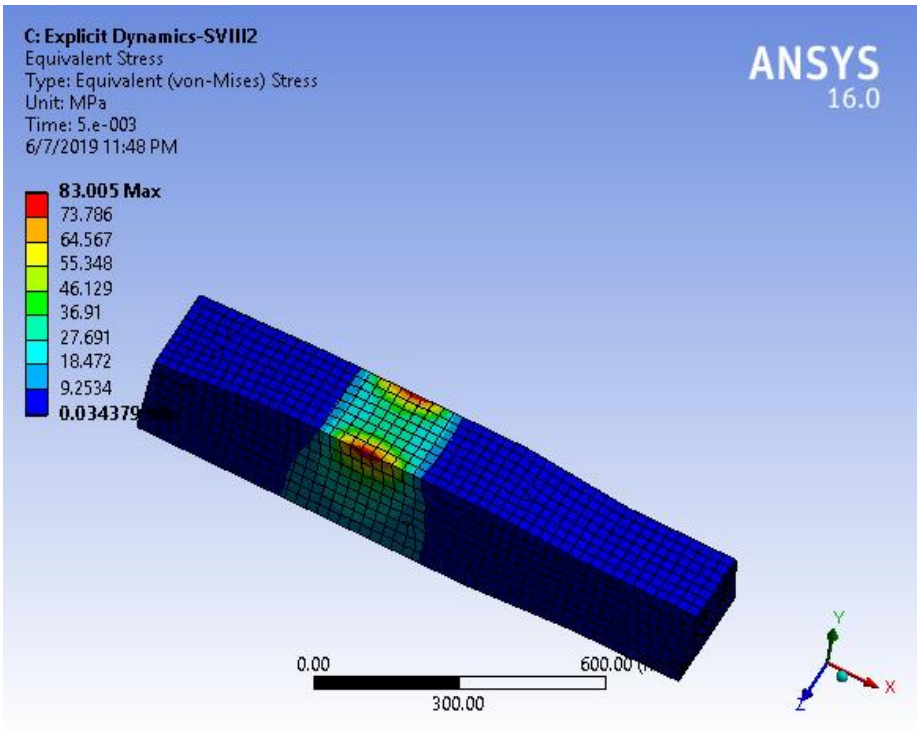

(b)

Figure G-4 Impact results for sleeper SVIII2 (a) deformation (b) equivalent stress